University of Alberta

Ceramic Fuel Cell Anode Enhancement by Polarized Electrochemical Vapour Deposition

by

Mark Haldane ©

A thesis submitted to the Faculty of Graduate Studies and Research in partial fulfillment of the requirements for the degree Master of Science

in

Materials Engineering

Department of Chemical and Materials Engineering

Edmonton, Alberta

Spring 2004

Library and
Archives Canada

Published Heritage
Branch

395 Wellington Street
Ottawa ON K1A 0N4
Canada

Bibliothèque et
Archives Canada

Direction du
Patrimoine de l'édition

395, rue Wellington
Ottawa ON K1A 0N4
Canada

Your file Votre référence
ISBN: 0-612-96480-9
Our file Notre référence
ISBN: 0-612-96480-9

The author has granted a non-exclusive license allowing the Library and Archives Canada to reproduce, loan, distribute or sell copies of this thesis in microform, paper or electronic formats.

L'auteur a accordé une licence non exclusive permettant à la Bibliothèque et Archives Canada de reproduire, prêter, distribuer ou vendre des copies de cette thèse sous la forme de microfiche/film, de reproduction sur papier ou sur format électronique.

The author retains ownership of the copyright in this thesis. Neither the thesis nor substantial extracts from it may be printed or otherwise reproduced without the author's permission.

L'auteur conserve la propriété du droit d'auteur qui protège cette thèse. Ni la thèse ni des extraits substantiels de celle-ci ne doivent être imprimés ou aturement reproduits sans son autorisation.

In compliance with the Canadian Privacy Act some supporting forms may have been removed from this thesis.

Conformément à la loi canadienne sur la protection de la vie privée, quelques formulaires secondaires ont été enlevés de cette thèse.

While these forms may be included in the document page count, their removal does not represent any loss of content from the thesis.

Bien que ces formulaires aient inclus dans la pagination, il n'y aura aucun contenu manquant.

Canada

Abstract

Experiments were conducted to determine the effect of deposition conditions on the performance of solid oxide fuel cell anodes manufactured by polarized electrochemical vapour deposition (PEVD). The effect of deposition time, deposition temperature and bias voltage were investigated. To determine the effects of these variable on anode performance polarization measurements were conducted on the cells, and the resulting anode structure was examined using scanning electron microscopy, and energy dispersive x-ray spectroscopy. It was found that by maintaining a deposition temperature of 900 to 950°C it was possible to avoid electrode densification, and get an overall increase in anode performance if the bias voltage was sufficient. At low bias voltages the deposition process was too slow to have a significant effect, and at higher deposition temperatures densification of the electrode occurred before a deposit could be formed.

Acknowledgements

I would like to thank Dr. T.H. Etsell for his guidance throughout this project and for his contagious enthusiasm for the project.

I would also like to thank the staff in the department, without whom nothing would ever get done. In particular I would like to thank Ms. T. Barker for her many hours helping me with the SEM, Mr. S. Merali for his help with the analytical work and Mr. J. Young for his valuable advice and understanding.

To my friends and family whose patience and support made this fun, thank you.

Contents

Chapter 1 Introduction 1
- 1.1 Solid Oxide Fuel Cells 3
  - 1.1.1 Traditional Cell Materials 4
  - 1.1.2 Operating Temperature 5
  - 1.1.3 Polarization 6
  - 1.1.4 How the SOFC Works 7
  - 1.1.5 Cell Designs 10

Chapter 2 Cell Components 15
- 2.1 Electrolyte Materials 15
  - 2.1.1 Zirconia Electrolytes 16
  - 2.1.2 Ceria Based Electrolytes 19
  - 2.1.3 Doped Lanthanum Gallate 22
- 2.2 Cathodes 24
  - 2.2.1 Cathode Structure 25
  - 2.2.2 Cathode Materials 31
    - 2.2.2.1 Platinum 31
    - 2.2.2.2 Doped Lanthanum Manganite 31
    - 2.2.2.3 Doped Lanthanum Cobaltite 33
    - 2.2.2.4 LSCF Cathodes 34
    - 2.2.2.5 YSZ - LSM Cathodes 35
- 2.3 Anode Materials 36
  - 2.3.1 Ni-YSZ anodes 37
  - 2.3.2 Perovskite Anodes 41
  - 2.3.3 Ni-Ceria Anodes 42
  - 2.3.4 LSGM-Ni Anodes 43
- 2.4 Interconnect Materials 43
  - 2.4.1 Perovskite Interconnects 44
  - 2.4.2 ODS Alloy Interconnects 44
  - 2.4.3 Nickel and Iron Based Chromia Formers 46
- 2.5 Sealing Materials 46

Chapter 3 Manufacturing Techniques 48
- 3.1 Electrolyte Manufacturing 49
  - 3.1.1 Chemical Vapour Deposition 49
  - 3.1.2 Physical Vapour Deposition 52
  - 3.1.3 Tape Casting 56
  - 3.1.4 Sol-Gel Electrolytes 57
  - 3.1.5 Electrophoretic Deposition 60
  - 3.1.6 Other Electrolyte Systems 62
- 3.2 Electrode Manufacturing 63
  - 3.2.1 Pressing and Sintering 64
  - 3.2.2 Tape Casting 65
  - 3.2.3 Extrusion 66
  - 3.2.4 Screen Printing 66

3.2.5 Powder Spray Techniques ... 67
3.2.6 EVD ... 67
3.2.7 PEVD ... 69
Chapter 4 Experimental ... 71
4.1 PEVD Processing ... 71
4.2 Electrochemical Investigation ... 74
4.3 Microstructural Examination ... 76
4.4 Materials ... 76
4.5 Engineered Porosity Samples ... 78
Chapter 5 Results and Discussion ... 79
5.1 Deposition ... 79
5.2 Deposition at 1050 °C and -300mV ... 84
5.3 Effect of Deposition Voltage ... 106
5.4 Deposition Temperature ... 124
5.5 Effect of Deposition Time and Temperature ... 143
5.6 Pore Forming Agent Samples ... 147
Chapter 6 Conclusions ... 149
Suggestions for Future Work ... 151
References ... 154

List of Tables

Table 1: Analysis of YSZ electrolytes 77
Table 2: Analysis of YCl_3 powder 77
Table 3: Analysis of $ZrCl_4$ powder 77
Table 4: Deposition statistics for cells deposited at 1050°C and -300mV 85
Table 5: Deposition conditions for cells deposited at 1050°C 107
Table 6: Deposition conditions for cells deposited at less than 1050°C 124

List of Figures

Figure 1: Schematic of a fuel cell (a) proton conducting electrolyte (b) oxide ion conducting electrolyte 2
Figure 2: (a) Bulk Cathode reaction pathway (b) surface cathode reaction pathway 8
Figure 3: Schematic of segmented cell in series design 12
Figure 4: Schematic of sealless tubular design 12
Figure 5: Co-flow monolithic design 13
Figure 6: Flat plate cell 14
Figure 7: Fluorite crystal structure 16
Figure 8: Perovskite structure centered on the B cation 23
Figure 9: Cathode reaction processes 26
Figure 10: Composite electrode 30
Figure 11: (A) Pore closure by CVD (B) Film growth by EVD 52
Figure 12: Tape casting apparatus 57
Figure 13: Cermet growth by EVD 68
Figure 14: Support tube/electrolyte setup 72
Figure 15: PEVD reactor schematic 73
Figure 16: Schematic of setup for polarization measurements 75
Figure 17: Molar evaporation rates for zirconium (a) and yttrium (b) chlorides from two different data sources 82
Figure 18: I-V characteristics of cells deposited at 1050 °C and -300mV 86
Figure 19: Power density for cells deposited at 1050°C and -300mV 88
Figure 20: I-V curve for cell 500-20 at 950°C showing two distinct slope regimes... 91
Figure 21: Intermediate magnification SE images of cells deposited at 1050°C and -300 mV 92
Figure 22: Cross sectional SE images of cells deposited at 1050°C and -300 mV..... 96
Figure 23: High magnification SE (a) and BSE (b) images of cell 500-19 99
Figure 24: EDX spectrum for dark surface phase seen in figure 23 (b) 100
Figure 25: EDX spectrum for cured cement 101
Figure 26:EDX spectrum for uncoated platinum electrode 102
Figure 27: EDX spectrum for uncoated, unmounted platinum electrode 102
Figure 28: I-V curves for cell 500-39 at 1050°C 105
Figure 29: Area Specific Resistance (ASR) of cell processes as a function of deposition time 106

Figure 30: I-V curves for cells deposited at 1050°C and deposition voltages other than -300mV 108
Figure 31: Power density curves for cells deposited at 1050°C and voltages other than -300mV 110
Figure 32: Selected SE images of cells deposited at 1050°C, and voltages other than -300mV 115
Figure 33: Cross sections of cells deposited at 1050°C and -300mV 118
Figure 34: SE(a) and BSE (b) images of the electrode surface of cell 500-24 121
Figure 35: EDX spectrum for point 1 in figure 34 (b) 122
Figure 36: EDX spectrum for the entire electrode of cell 500-24 122
Figure 37: EDX spectrum for dark phase in pores of the cross section 123
Figure 38: I-V curves for cells deposited at less than 1050°C 125
Figure 39: Power density for cells deposited at less than 1050°C 127
Figure 40: I-V curves for three best performing cells at 750°C 130
Figure 41: Plan view of anodes of cells deposited at less than 1050°C 131
Figure 42: Cross section of cells deposited at less than 1050°C 135
Figure 43: Close up of electrode cross section for cell 500-33 (BSE mode) 138
Figure 44: EDX spectrum for point 1 in figure 43 138
Figure 45: XRD pattern for anode of cell 500-34 139
Figure 46: WDX spectrum for cell 500-34 140
Figure 47: Cross section of cell 500-38 141
Figure 48: Complex impedance plots before (a) and after (b) deposition 142
Figure 49: I-V curves during deposition for cell 500-40 143
Figure 50: Power density of cell 500-40 during deposition 144
Figure 51: a) cell 500-39 b) cell 500-40 145
Figure 52: a) BSE cross section of cell 500-39 b) BSE cross section of cell 500-40 . 146
Figure 53: I-V curve for cells made by coated pore forming agent process 147

List of Equations

Equation 1: Nernst equation 7
Equation 2: Incorporation reaction for yttria into zirconia 17
Equation 3: Incorporation reaction for calcia into zirconia 17
Equation 4: Incorporation reaction for M_2O_3 into ceria 19
Equation 5: Incorporation reaction for MO into ceria 20
Equation 6: Oxygen vacancy equilibrium 20
Equation 7: Nernst equation modified for electronic leakage current 21
Equation 8: Incorporation of SrO into lanthanum gallate 22
Equation 9: Incorporation of MgO into lanthanum gallate 22
Equation 10: Incorporation of adsorbed oxygen into the electrolyte 27
Equation 11: CVD of yttria 50
Equation 12: CVD of zirconia 50
Equation 13: Hertz-Knudsen molar evaporation rate 51
Equation 14: EVD of yttria 52
Equation 15: EVD of zirconia 52

Equation 16: Sol-gel active precursor formation **58**
Equation 17: Condensation polymerization reaction **58**

Chapter 1 Introduction

A fuel cell is an electrochemical device for the conversion of chemical energy directly to electrical energy. The underlying principle of electrochemically combining fuel and oxidant to make electricity was first demonstrated by Sir William Grove in 1839 [1]. Compared to conventional techniques for the generation of electricity, fuel cells do not require intermediate conversion of chemical to thermal or kinetic energy; therefore, the efficiency of fuel cells is theoretically higher than traditional power plants [2]. To achieve this conversion, a species present in both inlet gases must be ionized. For electrolytes that transport protons, the hydrogen atom is stripped of its electron at the anode. The proton then passes through the electrolyte to the cathode, where it reacts with oxygen. The electron meanwhile passes through an external electrical circuit, creating a DC current. Eventually the electron is returned to the cathode, where it participates in the reduction of oxygen atoms to oxide ions. These oxide ions are what react with the protons, forming water.

In the alternate case where the electrolyte transports oxide ions, the fuel is again oxidized at the anode, and the electrons released by this process migrate through the external circuit to the cathode. At the cathode they are used to form O^{2-} ions, which are then transported back through the electrolyte to the anode. Here they can react with the fuel, which need not be hydrogen, releasing more electrons and forming an exhaust gas. This process is illustrated in figure 1. In general the processes shown in figure 1 are common to all fuel cells; however, the actual mechanisms involved in the various steps of the reaction vary among cell types.

There are five main types of fuel cells that have been developed for various energy generation applications. These cells are typically identified by the electrolyte material used. There are three types of low temperature fuel cells, which operate below 200°C [3]. These are the phosphoric acid fuel cell (PAFC), polymer electrolyte fuel cell (PEFC), and the alkaline fuel cell (AFC). Of these cells, the PAFC and the PEFC both use proton conducting electrolytes, while the AFC electrolyte conducts hydroxide ions. All of these cells require hydrogen as the fuel, with the PEFC and, especially the AFC, being very sensitive to CO poisoning of the anode catalyst [3].

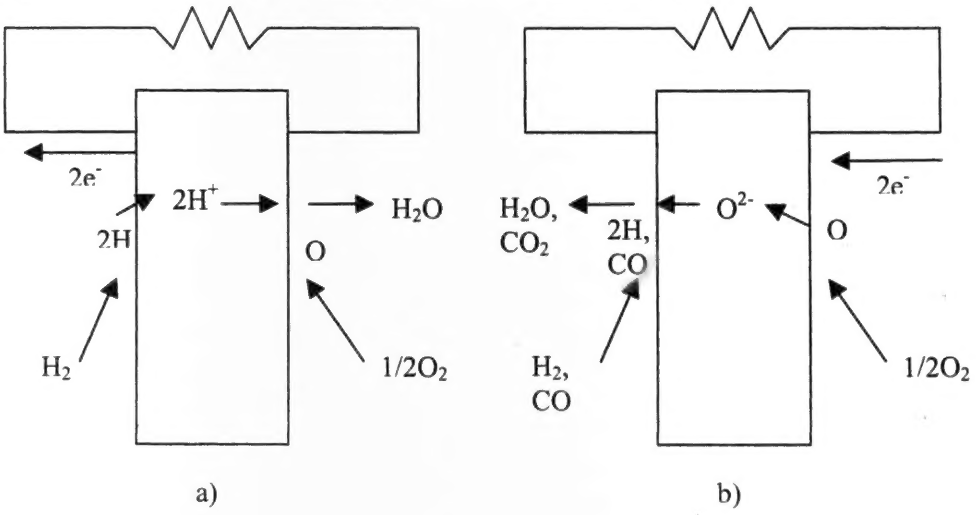

Figure 1: Schematic of a fuel cell (a) proton conducting electrolyte (b) oxide ion conducting electrolyte

Because of the low operating temperature, precious metal catalysts must be used to give sufficient performance for commercial applications. On the reverse side the low operating temperatures allow for rapid startup and simplify design.

The other two types of fuel cells under investigation are the high temperature solid oxide (SOFC) and molten carbonate fuel cells (MCFC). Both types operate at temperatures above 500°C and use oxide ion conducting electrolytes, although in the MCFC it is actually a carbonate ion that is transported through the electrolyte [3]. Because the high temperatures lead to rapid reaction kinetics, no precious metal catalysts are required, and both types of cells are capable of producing electricity from CO-based fuels since the electrolytes conduct O^{2-} ions. However the high operating temperature creates numerous materials problems when designing commercial cells. The following two chapters focus on the materials and manufacturing techniques used to fabricate SOFC's, for operation at 1000°C as well as at reduced temperatures.

1.1 Solid Oxide Fuel Cells

Like all fuel cells the solid oxide fuel cell consists of three main components. The electrolyte is a ceramic oxide layer that usually conducts oxygen ions. The primary function of the electrolyte is to conduct a single ionic species from one electrode to the other, while blocking gas diffusion and electronic current. Most ceramic electrolytes do not attain sufficient ionic conductivity for use in a fuel cell at temperatures in the 500-1000°C range. For this reason cells were initially designed to operate at 1000°C. The anode provides a site for oxidation of the fuel, and, therefore must have good stability in the highly reducing anode atmosphere, as well as exhibit good electronic conductivity and catalytic activity for fuel oxidation. The cathode, on the other hand, must be stable in a highly oxidizing atmosphere, have good electronic conductivity and show good catalytic activity for the reduction of oxygen.

Each cell, consisting of the three layer anode/electrolyte/cathode structure, is capable of producing about 1 volt; thus in order to obtain higher voltages individual cells are joined together in series to form what is known as a stack. Electrical connection is made by a so-called interconnect. The interconnect makes electrical contact between the anode of one cell and the cathode of the next; therefore, it needs to be stable in both the anode and cathode environments. Additionally, it must have high electronic conductivity, and be fully dense to prevent mixing of fuel and oxidant gases.

Apart from these functional requirements, each cell component must be stable with respect to the other components it contacts, and not degrade over the lifetime of the cell, which is targeted at over 50 000 hours [4]. At 1000°C there are very few materials that meet these strict requirements, and those that do tend to be expensive. For these reasons there has been a significant amount of research done over the past decade with the goal of lowering the operating temperature to 850°C or less. While this solves a lot of materials problems it leads to reduced performance of the cell. In order to counteract this loss of performance it is important to optimize the electrode behaviour and minimize ohmic losses in the cell. This has led to a vast amount of literature on novel materials for all cell components, as well as numerous techniques to obtain the optimum structure at minimal cost.

1.1.1 Traditional Cell Materials

As a starting point to understanding how SOFC's work, it is good to have an idea of the materials used in their fabrication. This section gives a brief introduction into the materials that make solid oxide fuel cells work. More detail on the materials listed here will be given in the appropriate section on cell materials later on. The current state-of-the-art SOFC uses an electrolyte of yttrium oxide doped zirconia. This is a highly stable material which exhibits primarily ionic conductivity for the oxygen partial pressure range of 1 to 10^{-18} atm [5]. In other words, the material does not develop electronic conductivity in either the oxidizing cathode atmosphere or the reducing anode atmosphere, which is important for attaining maximum performance. One drawback to YSZ as an electrolyte material is its aging behaviour at temperatures around 1000°C. It is believed that this is due to ordering of defects, and the possible formation of a pyrochlore phase, which cause an increase in the resistivity of the electrolyte. The other drawback of YSZ as an electrolyte material its low ionic conductivity, which requires cell operation at 1000°C, or the use of thin, dense films of YSZ in order to sufficiently reduce ohmic losses in the cell during operation.

Because traditional thick film YSZ electrolytes require such a high operating temperature, there are very few options available for the other cell components. The most common cathode material used is strontium doped lanthanum manganite (LSM), a perovskite type oxide (ABO_3), which exhibits p-type electronic conductivity. The charge is carried by a small polaron hopping mechanism among the B site cations [6]. This material is relatively stable in contact with both the oxidizing atmosphere, as well as with the YSZ electrolyte.

The anode is exposed to a highly reducing fuel atmosphere, so nickel, which provides high electronic conductivity as well as catalytic activity for fuel oxidation, can be used. In order to prevent sintering of the nickel over the target cell lifetime and to improve the thermal expansion match with the electrolyte, YSZ is mixed with the nickel forming a cermet structure. The Ni-YSZ anode is quite stable with respect to the electrolyte.

The most demanding requirements in the fuel cell stack are placed on the interconnect, which contacts both the anode and cathode atmospheres. Since they rapidly oxidize in the cathode environment, non-precious metals cannot be used as the interconnect at 1000°C, while there are very few ceramic electronic conductors that can survive the harsh reducing conditions in the anode chamber. One material that meets these requirements is strontium doped lanthanum chromite (LSC), which like LSM is a p-type perovskite oxide. This oxide has been extensively used as the interconnect in SOFC stacks designed to operate at 1000°C [7].

1.1.2 Operating Temperature

Among the numerous advantages of lowering the operating temperature of SOFC's are lower thermal stresses in the stack, lower cell material and fabrication costs, and less long term degradation [8, 9, 10]. On the down side, at lower temperatures the conductivity of the electrolyte is lower, and polarization losses in the electrodes are greatly increased [11]. Therefore, in order to attain the desired power output at temperatures at or below 800°C it is necessary to have a high conductivity electrolyte and high performance electrodes [11]. Additionally, operation at near 1000°C is advantageous for SOFC power plants fed by coal gas [12].

1.1.3 Polarization

When current is drawn from a cell, non-reversible reactions occur which lead to a deviation from 100% efficiency. These losses are manifested as electrode polarization and tend to take on one of two forms, concentration polarization and activation polarization. Activation polarization corresponds to a potential shift in the electrode in order to stimulate the electrode reaction, whether it be oxidation or reduction [13]. This type of polarization affects all electrodes, and is strongly influenced by temperature. At higher temperatures reaction kinetics tend to be much faster; therefore, as the cell operating temperature is reduced activation polarization becomes more severe. This is the major cause of losses in modern reduced temperature cells. In order to lower this effect it is important to design electrodes with a high catalytic activity and maximum active electrode area. This is best accomplished with a fine, porous electrode structure.

Concentration polarization is a shift in electrode potential caused by mass transfer limitations [13]. This occurs because reacting species must diffuse through the gas phase to the active electrode sites. Although it does not affect all electrodes, in cases where a high enough current density can be achieved it becomes a limiting factor [13]. Concentration polarization is dependent on the diffusion coefficient of the active species but, because the fuel and oxidant are gaseous, temperature has less of an effect than the electrode structure and gas flow rates. By increasing gas flow rates, the thickness of the depleted layer that the active species must diffuse through can be reduced. Large well connected pores in the structure allow for easy gas migration to and from the active sites. Therefore a compromise must be made between a maximum active area and an electrode that allows rapid diffusion of reactant and product gases to and away from those active sites.

A third form of polarization is resistance polarization, which in the case of SOFC's is primarily associated with the electrolyte resistance, but also includes contact resistances. Resistance polarization is caused by the ohmic losses of passing a current through the electrolyte or electrodes [13]. Generally, the conductivities of the electrodes are orders of magnitude larger than that of the electrolyte; however, in cell configurations where the current paths through the electrodes are quite long, it can be important to maximize electrode conductivity. Because the ionic conductivity of ceramic electrolytes strongly decreases with temperature, it is vital to make a low resistance electrolyte for cell operation at reduced temperatures. This can be done by finding an electrolyte material with a high conductivity at the desired operating temperature, or by shortening the current path through the electrolyte by using a thinner material.

1.1.4 How the SOFC Works

In the simplest sense an SOFC is an oxygen concentration cell, in which a ceramic electrolyte separates an oxidizing atmosphere at the cathode from a reducing atmosphere at the anode. The open circuit potential of this cell is determined by the oxygen pressure difference between the electrodes and is given by the Nernst equation (equation 1)[14].

$$E = \frac{RT}{nF} \ln \frac{P_{O_2 cathode}}{P_{O_2 anode}}$$

Equation 1: Nernst equation

Here R is the universal gas constant, T the absolute temperature, F is the Faraday constant, and n the number of electronic charges exchanged [13]. In a hydrogen fuel cell this voltage is approximately one volt. In this section the individual steps of the reaction process of an SOFC will be examined.

For the cathode reaction there are two possible reaction pathways [15], the surface reaction pathway and the bulk reaction pathway. These are illustrated in figure 2. The reaction steps are as follows [16]: i)diffusion of gaseous oxygen to the surface of the electrode, ii)dissociative adsorption of oxygen molecules to O_{ads}. After this point the next step depends on the electrode properties. If the electrode material is a pure electronic conductor (does not conduct ions), the oxygen atom is transferred via surface diffusion to the three phase boundary (3PB); that is, the point where the electronic conductor, ionic conductor and the gas phase are in contact. At the 3PB all of the products and reactants can co-exist, allowing the oxygen atoms to be reduced to O^{2-} and transported through the electrolyte to the anode. If the electrode conducts both ions and electrons to an appreciable extent (i.e., a mixed ionic-electronic conductor - MIEC), the oxygen can be ionized and incorporated into the bulk of the electrode. From here the O^{2-} ion migrates to the electrode/electrolyte interface, and is transferred to the electrolyte.

The 3PB, which is the active area of the electronic conducting electrode [17], exists directly on the electrolyte, at the pore surfaces. Therefore by having a finer pore structure it is possible to increase the active area, and improve the electrode performance. Taking this concept a step further by adding an ionic conducting phase to the cathode itself, the 3PB can be extended from the two dimensional electrode-electrolyte interface to the three dimensional cathode volume [17]. This is the same effect as seen in the bulk reaction pathway for mixed conducting electrodes.

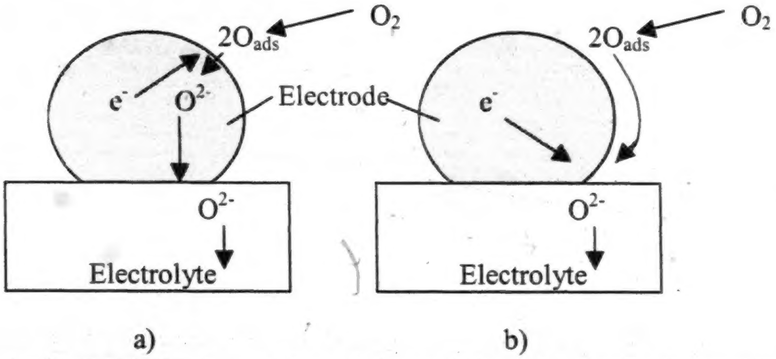

Figure 2: (a) Bulk Cathode reaction pathway (b) surface cathode reaction pathway

By doing this it is possible to greatly increase the number of active sites in the electrode, which serves to reduce the activation polarization [15]. Further reductions in activation polarization can be obtained by using a cathode material that has good catalytic activity for reduction of the oxygen [15]. Additionally, the cathode must be chemically stable with respect to the atmosphere, the electrolyte and the interconnect, with which it is in intimate contact.

The primary function of the electrolyte is to separate the anode and cathode gases, and to pass current via a single ionic species. Most ceramic electrolytes that have been investigated for fuel cell use are oxygen ion conductors, which allows for the consumption of fuels other than hydrogen [18]. Fluorite-type electrolytes conduct oxygen ions by a vacancy diffusion mechanism. An excess of oxygen vacancies is created by aliovalent doping. To reduce the resistance of the electrolyte even further, it should be made as thin as possible while maintaining near theoretical density. This prevents direct mixing of the anode and cathode gases and improves the open circuit voltage (OCV). Additionally, the electrolyte should be an electronic insulator in both reducing and oxidizing atmospheres. This prevents short circuiting of the cell through the electrolyte, which lowers OCV and decreases efficiency [19]. Because of its requirement to be crack free, it is very important to match the coefficient of thermal expansion (CTE) of other cell components to that of the electrolyte. This allows the cell to go through multiple thermal cycles, such as startup and shutdown, without damage.

The functional requirements of the anode are very similar to those of the cathode. Its primary job is to provide reaction sites for the oxidation of fuel, and like the reduction of oxygen, this takes place at the 3PB between the electrolyte, electrode and gas phase. Because the anode atmosphere is a reducing one, it is possible to use metals to provide electronic conduction as well as catalytic activity for fuel oxidation. However, at fuel cell operating temperatures, most metals tend to sinter quite rapidly which destroys the fine structure required to maximize active area [20,21]. Metals also tend to have higher CTE's than the electrolyte material; therefore, during thermal cycles cracking of cell components or delamination of the layers can occur. The most common solution to these problems is to use a ceramic-metal composite, or cermet, electrode. In these types of anode a ceramic material, usually the same material as the electrolyte, is added to the electrode, which gives several advantages. As well as improving the CTE match between the electrode and electrolyte, the ceramic phase supports the metal, preventing it from sintering and closing off pores. And because the ceramic phase is usually the same material as the electrolyte, it allows for extension of the 3PB into the electrode. In order for a 3PB site to be active, it must be on a percolation path for ions, electrons and the gas phase.

The interconnect is used to pass electrons from the anode of one cell to the cathode of the next, which means it must have good electronic conductivity in both anode and cathode environments, and must prevent gas leakage. At 1000°C only a few ceramic materials are suited to this task; however, at lower temperatures some heat resistant metal alloys can be used [22]. The savings in cost by using metallic interconnects is one of the major reasons for the drive to lower the SOFC operating temperature.

1.1.5 Cell Designs

Apart from various cell materials, there are also different cell designs with their own advantages and limitations [23]. There are two basic types of cell design being considered, the tubular design and the planar configuration [2]. The difference is that, in tubular designs the cells are in the form of tubes, with one gas flowing inside the tube and the other on the outside while, in planar designs, the fuel and oxidant gases are separated by cell components that are arranged as a series of plates. Each of these types of cells has two main variants. The tubular cells are divided into the sealless tubular design, and the segmented cell in series design. The most common types of planar cells are the flat plate cells and monolithic cells [2]. Cell designs can be further broken down in terms of the major structural component, i.e., anode supported, cathode supported or electrolyte supported designs [24].

In 1962 Westinghouse began developing solid oxide fuel cell technology with the ultimate objective of creating a fuel cell power plant capable of running on coal derived fuel [14]. Their original design was a tubular stack of cells that came to be known as the segmented cell in series design. Individual cells are deposited in bands around a porous ceramic support tube. Adjacent to the calcia stabilized zirconia support tube is the anode, which is then covered with the interconnect material and the electrolyte. Finally the cathode is deposited on the surface. This arrangement is shown in figure 3. An alternative arrangement for the segmented cell in series design is known as the bell and spigot arrangement [23]. In this design a self-supporting electrolyte is used, which reduces gas transfer losses due to the support tube; however, the increased thickness of the electrolyte increases resistive losses. Individual cells must be tapered to allow them to be fitted together to make a stack in the bell and spigot arrangement. The main advantage of the segmented cell in series design is improved efficiency compared to the sealless tubular design due to the series gas flow. Because the first cell in this arrangement will have higher output voltage, the resistive losses of the cell will be lower. However, this advantage is lost if the stacks contain more than about five or six cells [23].

In 1980 Westinghouse developed the sealless tubular cell design in order to address some practical problems with the segmented cell in series design and to take full advantage of a new manufacturing process [14]. In this design each cell consists of a single tube with one closed end [23]. The heart of this is a support tube made of the cathode material. The porous cathode tube has an inner diameter of about 12 mm, over which is deposited a thin, dense layer of YSZ, save for a strip about 9 mm wide, running the entire active cell length, which can be up to 150 cm [25]. The exposed strip of cathode is then coated with the interconnect material, LSM. Finally the anode is deposited on the outer surface of the electrolyte, leaving the interconnect exposed. This design requires that the fuel be passed over the outside of the tube, rather than through the tube. Because of this it is possible to use inexpensive metallic electrical contacts, rather than thick ceramic conductors or precious metals as required for the segmented cell in series design [14]. When the cells are bundled to make stacks, they are connected in parallel as well as series to allow the stack to continue working should any individual cells fail [23]. One drawback to this design, shown in figure 4, is the long path the current must travel through the electrodes, allowing electrode resistance to make an appreciable contribution to power losses. For this reason it is important that the electrodes, especially the thinner anode, have a very high electronic conductivity.

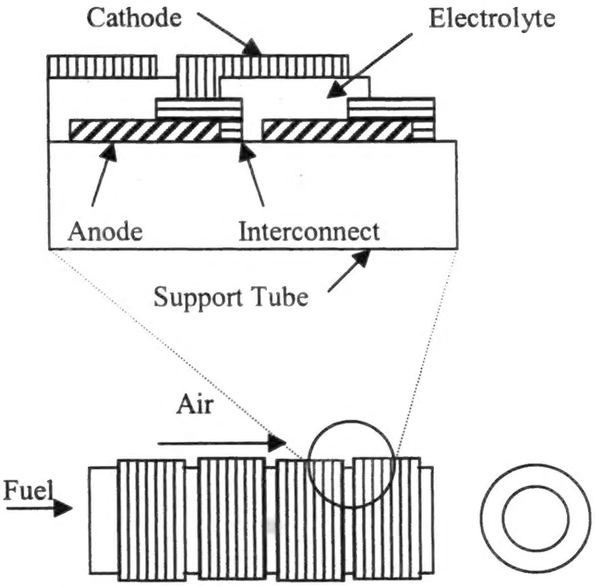
Cathode
Electrolyte
Anode
Interconnect
Support Tube
Air
Fuel

Figure 3: Schematic of segmented cell in series design

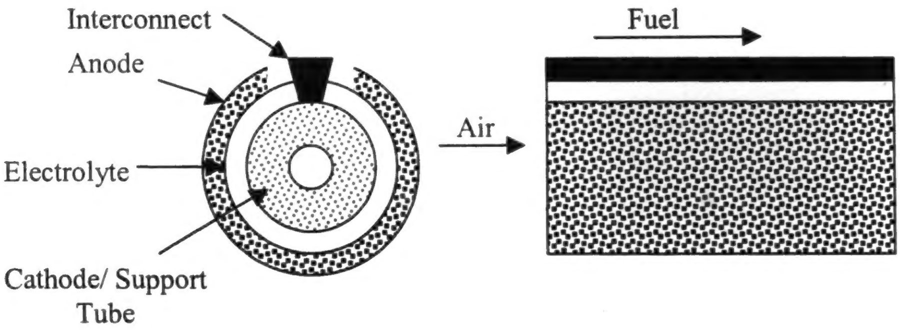
Interconnect
Anode
Electrolyte
Cathode/ Support Tube
Air
Fuel

Figure 4: Schematic of sealless tubular design

The alternative to the tubular type of fuel cell is the planar design, where the anode, electrolyte and cathode are a series of plates. This arrangement allows for higher power densities than can be achieved with the tubular designs, but also requires high temperature sealing to prevent mixing of the fuel and oxidant gases [23]. Like the tubular cell designs, planar cells are divided into two categories, the monolithic type and the flat plate type.

The monolithic design calls for two sets of multilayered ceramics, which incorporate corrugations to allow gas flow over the electrodes. The corrugations can be configured to allow for co-flow or cross-flow of the fuel and oxidant gasses, the co-flow arrangement giving higher power densities and the cross-flow making for simplified gas manifolding. This arrangement allows for small cell size and large active area which both contribute to the high power densities that can be achieved. Additionally, current paths are much shorter than in the tubular design, so resistive losses are reduced. The co-flow arrangement of a monolithic cell is shown in figure 5. As can be seen, this type of cell requires the fabrication of some fairly complex ceramic parts, which can be difficult and expensive.

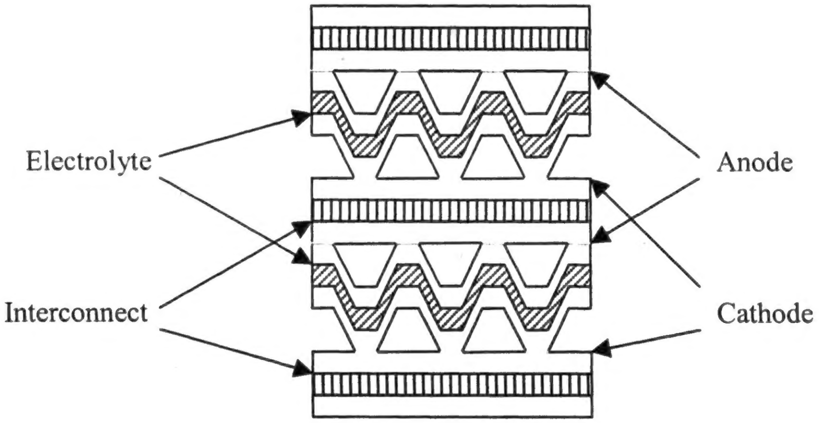

Figure 5: Co-flow monolithic design

The flat plate design reduces the complexity of the anode and cathode required for the cell. In this design the anode, electrolyte and cathode are a series of flat layers, sandwiched together. Traditionally, the electrolyte has been the structural component and, therefore, a thickness of greater than 200 μm was required. In recent years this has changed in order to lower resistive losses in the cell, so that state-of-the-art flat plate cells are electrode supported. The gas distribution in the cell is attained by using a ribbed interconnect as shown in figure 6. Because of the need for gas flow channels, it can be difficult to fabricate the interconnect from ceramic materials, but this is partially offset by the fact that the electrode/electrolyte structure and the interconnect do not need to be co-fired [23]. As cell operating temperatures are lowered, it becomes possible to use metallic materials, which are much easier to form, as interconnects. The primary advantages of this arrangement are ease of fabrication and increased power density when compared to tubular cell designs. The major drawback is the requirement for high temperature sealing of the plate edges. To date no entirely satisfactory sealing mechanism has been reported.

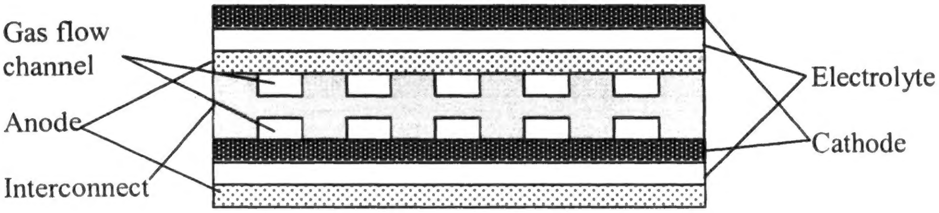

Figure 6: Flat plate cell

Chapter 2 Cell Components

2.1 Electrolyte Materials

There have been a large number of electrolyte materials proposed for use in SOFC's in the past several years [26, 27, 28, 29]. Of these the fluorite-type materials, YSZ and doped ceria, and the perovskite, doped lanthanum gallate show the most promise for commercial applications. In order for a material to be useful as an electrolyte, it should have an ionic transference number (t_{ion}) of at least 0.99 over the entire range of operating conditions [30]. That is 99% of the charge passed through the electrolyte should be carried by ions, with only 1% carried by electronic charge carriers (i.e., electrons or holes). Additionally, the electrolyte should not react with the oxidizing and reducing atmospheres present in the cathode and anode, respectively, nor with the anode and cathode materials themselves. It should also have good thermo-mechanical stability to avoid damage to the cell during thermal cycling, and ideally will be easy and inexpensive to manufacture into thin, dense layers. Any gas leakage across the electrolyte will lead to a lowering of the open circuit voltage, as will any electronic leakage. In this section some of the aspects of three different types of electrolytes will be discussed; these are zirconia-based electrolytes, ceria-based electrolytes and perovskite electrolytes. There are several other electrolyte materials; however, most development has focused on these three materials.

2.1.1 Zirconia Electrolytes

The structure of zirconia is monoclinic at room temperature, transforming to tetragonal above 1200°C, and finally to a cubic fluorite structure from 2300°C to its melting temperature [31]. Addition of certain aliovalent oxides, such as yttria, stabilizes the high temperature fluorite structure, in which the cations occupy face centered cubic sites, and the oxygen ions fill in the tetrahedral sites (figure 7). At yttria levels of about 7 mol%, the cubic structure becomes fully stabilized [31] which allows for thermal cycling of the cell without inducing phase transformations, which usually have a volume change associated with them.

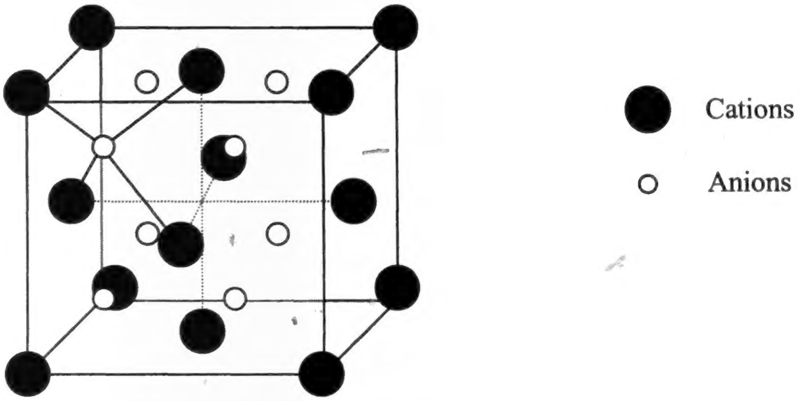

Figure 7: Fluorite crystal structure

In addition to stabilizing the fluorite structure, aliovalent dopants, such as Y^{3+}, cause formation of oxygen ion vacancies in order to compensate for the charge differences on the cation sublattice. The incorporation reaction for yttria into zirconia is shown in equation 2 [2], and for calcia into zirconia in equation 3 [32]. The fluorite structure has relatively low activation energies for anionic migration, and the ability to dope them so as to form large concentrations of anion vacancies makes them highly useful as electrolytes [32].

$$Y_2O_3 \xrightarrow{2ZrO_2} 2Y'_{Zr} + V_O^{\bullet\bullet} + 3O_O^x$$

Equation 2: Incorporation reaction for yttria into zirconia

$$CaO \xrightarrow{ZrO_2} Ca''_{Zr} + V_O^{\bullet\bullet} + O_O^x$$

Equation 3: Incorporation reaction for calcia into zirconia

As would be predicted from equations 2 and 3, the conductivity of doped zirconia increases with an increase in the dopant concentration; however, when conductivity is plotted as a function of dopant concentration a maximum is exhibited. This maximum has been attributed to interactions between the large number of defects in highly doped zirconia. It is found that for any of the common aliovalent dopants these maxima fall near the minimum dopant concentration required to fully stabilize the fluorite structure [32]. Above this dopant level it is believed that coulombic attraction between the dopant cations and oxygen ion vacancies leads to short range ordering of the vacancies, reducing conductivity [33]. The size ratio of the dopant cations to the host cation also plays a role in determining ionic conductivity. Sc^{3+}, which is 1.03 times larger than Zr^{4+}, gives a conductivity two and a half times that of YSZ, which has a cation size ratio of 1.18 [34, 35]. Unfortunately, scandia stabilized zirconia (SSZ) undergoes chemical aging at high temperatures and is much more expensive than YSZ [2]. Currently, YSZ is the most commonly used zirconia-based electrolyte due to its combination of excellent electrical and mechanical properties, having higher conductivity than calcia stabilized zirconia due to weaker defect interactions [31, 35]

In ceramic fuel cells the typical composition of a YSZ electrolyte is 8-10 mol% yttria. This is denoted, in the case of 8 mol% yttria stabilized zirconia, as 8YSZ. This composition is at the low yttria end of the fully stabilized cubic structure domain, and is very close to the maximum conductivity attainable in YSZ. At this composition a conductivity of 10^{-1} S/cm is attained at about 1000°C [36], which allows for use of electrolytes up to about 200 μm thick. This is important for the planar cell designs because at this thickness the electrolyte can be the supporting member of the cell structure. In other words the cells can be electrolyte supported. When the temperature is reduced to 800°C the conductivity in turn drops to about 10^{-2} S/cm. Thus, if YSZ is to be used as an effective electrolyte at temperatures of 800°C or less, its thickness must be reduced to the order of 50 μm [2]. In order to achieve this some other component must be made the supporting element. For the planar design, anode supported cells are most commonly used, so the thin, dense electrolyte must be deposited onto a porous anode substrate.

The chief drawbacks of YSZ as an electrolyte are its low conductivity at temperatures below 1000°C and its aging behavior. According to one investigation the resistivity of 8YSZ increased from 18 to 32 Ωcm after annealing in hydrogen for three days at 1000°C [31]. Studies of the effect of aging various compositions of YSZ at various temperatures show that, as the aging temperature decreases, the effect of aging increases [33], and above a certain temperature no aging is observed. The value of this critical temperature decreases as the yttria content of the ceramic rises; however, at a composition of 8 mol% Y_2O_3 the critical temperature is on the order of 1200°C, much higher than the SOFC operating temperature. Explanations put forth for the aging behaviour of stabilized zirconia include phase transformation, precipitation of second phases, segregation of a glassy phase to the grain boundaries, and short range ordering of oxygen ion vacancies [37].

YSZ with less than 8 mol% yttria exists in a two-phase field and is, therefore, expected to decompose, from fully cubic after sintering, to a mixture of cubic and tetragonal zirconia. The tetragonal phase has much lower conductivity than the cubic, and this definitely contributes to loss of conductivity in partially stabilized zirconia. Tetragonal zirconia has also been detected in small amounts in 8YSZ [37]; however, it does not seem to be the cause of the loss of conductivity here. A detailed study of various aspects of aging of YSZ [33, 37, 38] showed that aging was also not likely due to formation of long range ordered second phases such as $Y_2Zr_2O_7$, as cation migration at lower temperatures, where aging is most severe, is too slow. Nor was it found that a glassy phase at the grain boundaries was contributing significantly to aging. Therefore, the prime suspect is short range ordering of oxygen ion vacancies. This can occur for one of two reasons. Firstly, the coulombic attraction between dopant cations with a net negative charge, and O^{2-} vacancies, with a net positive charge, can lead to trapping of the vacancies. Secondly, it is possible that the vacancies are trapped by zirconium cations, in order to reduce the anisotropy of the lattice distortion in YSZ. Extended x-ray absorption fine structure (EXAFS) analysis showed that indeed, with aging time, there was a decrease in the coordination number of Zr ions. This suggests that trapping of oxygen ion vacancies is the most likely cause of the loss of conductivity of YSZ over time at intermediate temperatures (800-1000°C).

Currently YSZ is the best choice for use as the electrolyte in the SOFC, in part due to the large amount of research that has gone into optimizing the performance of electrodes that are compatible with YSZ. The search for alternative electrolyte materials has focused primarily on finding electrolytes that have a higher conductivity than YSZ, allowing them to be used at lower operating temperatures without sacrificing performance.

2.1.2 Ceria Based Electrolytes

Ceria (CeO_2) is a fluorite-type oxide that, like zirconia, can be doped to give high ionic conductivity. Common dopants include samaria (Sm_2O_3), gadolinia (Gd_2O_3), calcia (CaO), and yttria (Y_2O_3) [39, 40, 41]. All of these aliovalent dopants create oxygen ion vacancies in order to maintain charge neutrality according to one of the following incorporation reactions, depending on the valency of the cation dopant.

$$M_2O_3 \xrightarrow{2CeO_2} 2M'_{Ce} + V_O^{\bullet\bullet} + 3O_O^x$$

Equation 4: Incorporation reaction for M_2O_3 into ceria

$$MO \xrightarrow{CeO_2} M''_{Ce} + V_O^{\bullet\bullet} + O_O^x$$

Equation 5: Incorporation reaction for MO into ceria

The conductivity of these doped ceria electrolytes is significantly higher than the conductivity of YSZ, particularly at reduced temperatures [39], and as is the case for zirconia electrolytes the maximum attainable conductivity is dependent on the nature of the dopant. It has been shown [42] that the conductivity increases with the radius of the dopant cation up to a point, then falls off again. The best dopant in terms of attaining maximum ionic conductivity is samaria, 10 mol% gives a peak oxide ion conductivity at 800°C comparable to that of YSZ at 1000°C [39]. This should allow for operation of SOFC's at temperatures down to around 700°C. This combined with the CTE of ceria, which is comparable to that of ferritic stainless steels at high temperature, would allow the use these relatively low cost alloys as the cell interconnect, greatly reducing costs [43, 44].

The primary weakness of doped ceria as an electrolyte for SOFC's is its narrow electrolytic range. Under reducing conditions ceria becomes nonstoichiometric(i.e. CeO_{2-x}) according to:

$$O_O^x \rightarrow \tfrac{1}{2}O_2(g) + V_O^{\bullet\bullet} + 2e'$$

Equation 6: Oxygen vacancy equilibrium

The electronic defects created by this reaction, although less plentiful than the total number of ionic defects (oxygen vacancies), have a much higher mobility and, therefore, make a significant contribution to the total conductivity of the material [40]. Under conditions where this happens, ceria becomes a mixed ionic-electronic conductor (MIEC). It has been estimated [40] that, at a temperature of 800°C, the ionic domain of ceria (i.e., t_{ion}=0.99) does not extend below a P_{O2} of about 10^{-5} atm; however as the temperature is lowered the electrolytic domain extends to much lower oxygen activities.

Doping ceria with aliovalent oxides is known to reduce the effects of n-type conductivity in reducing atmospheres, partly because of its effect of increasing the material's ionic conductivity. The dopant used also has an effect on the reducibility of ceria electrolytes, as has been shown by thermogravimetric analysis [39, 42]. Samarium oxide dopants give the lowest weight loss as a function of oxygen partial pressure, particularly in the range of 10^{-9} to 10^{-12} atm; however, at lower oxygen pressures, as experienced in the anode of the fuel cell, this advantage appears to vanish [42].

Because of the mixed conducting nature of ceria electrolytes there are some additional design considerations for its successful use as the electrolyte of an SOFC. The cell voltage becomes dependent on the properties of the electrolyte at the given operating conditions, and can no longer be predicted by the Nernst equation (equation 1). The equation must be modified to account for the leakage current according to:

$$E = \frac{RT}{nF} \ln\left(\frac{1 + p_{O2}^{*\,1/4}}{p_{O2}^{1/4} + p_{O2}^{*\,1/4}} \right)$$

Equation 7: Nernst equation modified for electronic leakage current

where p_{O2}^{*} is the oxygen partial pressure where the ionic transference number of the MIEC is 0.5 [41]. The leakage current tends to increase as the electrolyte thickness is lowered since the electronic conductivity increases, as does the relative thickness of the reduced portion of the electrolyte. This is in stark contrast to purely ionic conducting electrolytes where the performance is optimized by minimizing electrolyte thickness. In order to attain the optimum combination of efficiency and power density, a procedure has been suggested by Godickemeier and Gauckler [19]. The procedure takes into account various aspects of cell operation, including the electrochemical properties of the electrodes.

One approach used to overcome the limitations incurred when using a MIEC as the electrolyte for SOFC's has been to employ a two-layer electrolyte. Tsai and Barnett [45] deposited a very thin layer of YSZ onto the anode side of a ceria electrolyte and were able to attain near theoretical OCV, and high power densities at temperatures as low as 550°C. This may lead to a problem for long term operation, since it provides one more interface to degrade over long times at the operating temperature. Because of the drawbacks of zirconia and ceria electrolytes new electrolyte materials have been sought. One class of materials that shows promise is the perovskite type electrolyte.

2.1.3 Doped Lanthanum Gallate

A large number of oxides crystallize in the perovskite structure, which takes on the general formula ABO_3. In this structure (figure 8) the oxide ions and the A cations take on a cubic close packed arrangement [34]. Lanthanum gallate ($LaGaO_3$) has a distorted perovskite structure, and like the fluorite structure electrolytes, high oxide ion vacancy concentrations can be introduced by doping with lower valence cations. Ishihara et al. [46] showed that the maximum ionic conductivity for the lanthanum gallate system was obtained by substituting strontium for lanthanum on the A site, and magnesium for gallium on the B site. The substitution reaction for these dopants is shown in reactions 8 and 9.

$$2SrO \xrightarrow{LaGaO_3} 2Sr'_{La} + 2O_O^x + V_O^{\bullet\bullet}$$

Equation 8: Incorporation of SrO into lanthanum gallate

$$2MgO \xrightarrow{LaGaO_3} 2Mg'_{Ga} + 2O_O^x + V_O^{\bullet\bullet}$$

Equation 9: Incorporation of MgO into lanthanum gallate

From these equations it is apparent that the conductivity should increase with the dopant concentration. When SrO is added to $LaGaO_3$ to form the compound $La_{1-x}Sr_xGaO_{3-x/2}$, it was found that secondary phases began to appear above x values of 0.1 [46], which have low conductivity, and, therefore limit the extent to which doping can be used to increase conductivity. In order to further improve conductivity it is possible to dope the B site as well. Mg^{2+} is soluble on the B site of $La_{0.9}Sr_{0.1}Ga_{1-x}Mg_xO_{2.95-x/2}$ up to an x value of about 0.2, at which point the conductivity of the material becomes a maximum. Thus the composition that gives the optimum performance as an electrolyte is $La_{0.9}Sr_{0.1}Ga_{0.8}Mg_{0.2}O_{2.85}$ (LSGM9182). The electrolytic domain of this material at 1000°C extends from a P_{O_2} of 1 atm down to 10^{-20} atm, more than sufficient for use as an electrolyte in SOFC's [46]. In addition to a wide electrolytic range, the conductivity of LSGM at 800°C (~0.1 S/cm)is comparable to that of 8YSZ at 1000°C [28].

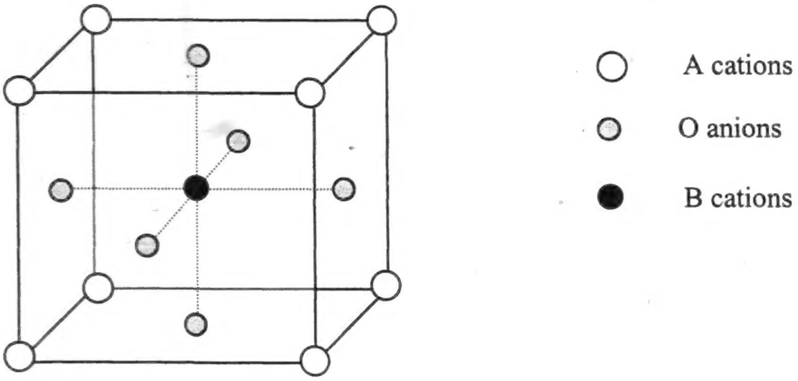

Figure 8: Perovskite structure centered on the B cation

The reason for the exceptionally high ionic conductivity is not immediately apparent, since the activation energy for ionic conduction (~1.07 eV) is slightly higher than it is for YSZ(~0.98 eV), and much higher compared to Ceria electrolytes (~0.76 eV) [28, 39, 40]. It has been seen that the pre-exponential factor of the Arrhenius equation for conductivity is about 20 times greater for LSGM than it is for YSZ. It is thought that the large pre-exponential factor is due to a temperature dependent component of the activation energy related to an order-disorder transition which leads to short range ordering of oxygen vacancies below 600°C [28]. The properties of LSGM discussed so far make it an almost ideal candidate for SOFC's operating at or below 800°C; however, there are some questions as to its stability in the fuel cell operating environment and with respect to other cell components.

Feng and Goodenough showed that no loss of conductivity was found over a period of 140 h at 650°C [28], but other studies have raised concerns about the stability of LSGM in an operational fuel cell [47, 48]. Yamaji et al reported roughening of the electrolyte surface in both the anode and cathode environment, and found second phases on the anode side that contained silicon, likely from the Pyrex seal used [48]. Depletion of gallium and magnesium from the anode side was also observed. The loss of gallium has been attributed to the high vapour pressures of Ga and Ga_2O in the anode atmosphere, as well as reaction with other cell components. Other tests have shown a significant reduction in cell performance after only 20 hours; however, some of this loss may be due to electrode degradation [47].

An examination of the stability of LSGM in reducing atmospheres [49] found that evaporation of Ga was a concern at elevated temperatures. Strontium additions increased the rate of Ga loss, while Mg additions reduced the effect of Sr. Tests on an electrolyte material without Sr doping on the A site showed that Ga loss could be significantly reduced at elevated temperatures, with only a slight decrease in conductivity. This could be useful for an electrolyte used in the 800°C range. At temperatures below 750°C no gallium loss was found after a 10 h test for LSGM9182, so cells designed to operate at such low temperatures may be able to employ this material without incurring critical shortfalls in cell lifetime.

LSGM as an electrolyte for reduced temperature solid oxide fuel cells shows significant promise; however, there are some problems that must be worked out. Development of suitable electrode materials for use with LSGM electrolytes, and ceria electrolytes for that matter, is well behind that for zirconia electrolytes. In order to develop a commercial fuel cell that uses an alternative electrolyte material, it is important to develop electrodes, interconnects and sealant materials that are compatible with the electrolyte and have good performance. The next two chapters focus on the electrodes that have been tried in conjunction with these three electrolyte materials and optimization of their structures.

2.2 Cathodes

As we have already seen, the active cathode area is the three phase boundary (3PB) where the electronically conducting electrode, ionically conducting electrolyte and the gas phase are all in contact. In order to maximize the 3PB area, the cathode should have high electronic as well as high ionic conductivity. Additionally, it needs to have high catalytic activity for oxygen reduction, good chemical and thermal stability with the atmosphere and other cell components, and ideally should be easy to manufacture inexpensively, with a processing temperature as near as possible to other cell components [15]. Because of these requirements, suitable cathode materials depend on the properties of the electrolyte, and to a large extent the performance of any cathode is determined by its structure, which is dependent on the manufacturing route used. In the next section we will discuss the idealized structure for a cathode. The manufacturing techniques used to attempt to achieve this structure will be discussed later.

2.2.1 Cathode Structure

The purpose of the cathode is to provide a reaction site for reduction of oxygen. In order to design a cathode that does this efficiently, it is important to understand the steps involved in this reaction. However these reaction steps depend on the electrical nature of the cathode. That is, whether it is an electronic conductor, a MIEC, or a composite electronic/ionic conducting electrode. In this section the reaction paths and the resulting ideal structure for each of these types of cathode will be discussed.

The following processes have been identified as possible rate determining steps in the reduction of oxygen at the cathode of an SOFC [50]:

1) Migration of oxygen ion vacancies in the electrolyte
2) Oxygen diffusion in the gas phase or the pores of the electrode
3) Oxygen chemisorption and dissociation at the electrode surface
4) Oxygen diffusion at the electrode surface, the electrode grain boundaries or along the electrolyte surface
5) Dissolution and diffusion of oxygen into the electrode phase
6) Oxygen chemisorption and dissociation at the electrolyte surface followed by diffusion
7) Dissolution and diffusion of oxygen in the electrolyte
8) Migration of electrons in the electrolyte

9) Electrochemical reaction, consisting of the transfer of electrons across the electrode/electrolyte phase boundary

These steps are shown in figure 9 [50], which illustrates the possible reaction pathways at the cathode.

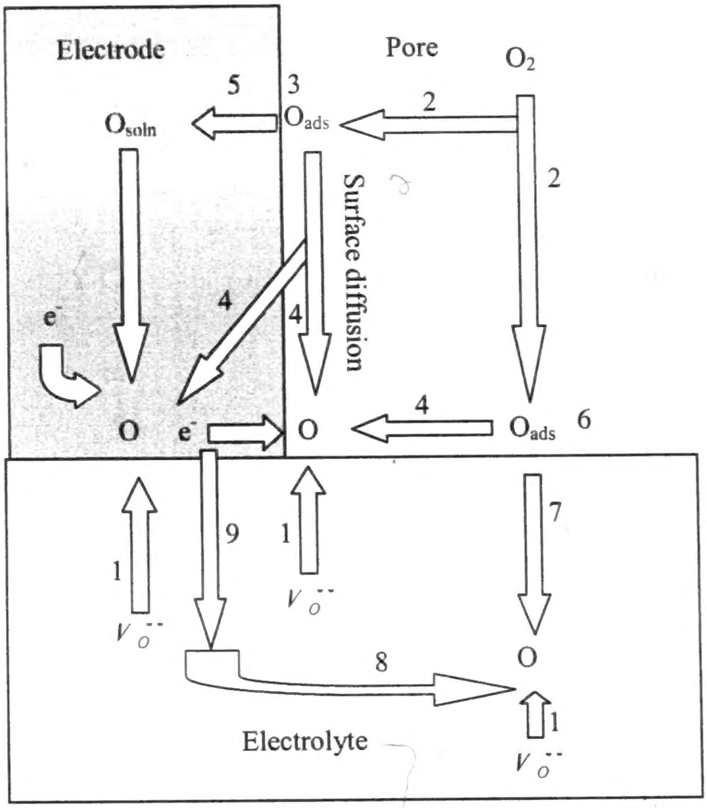

Electrode
Pore
O_2
5
3
O_{ads}
2
O_{soln}
2
Surface diffusion
4
4
e^-
4
O
e^-
O
O_{ads}
6
7
9
1
1
$V_O^{\cdot\cdot}$
$V_O^{\cdot\cdot}$
8
O
1
Electrolyte
$V_O^{\cdot\cdot}$

Figure 9: Cathode reaction processes

These reaction pathways are broken down into the bulk reaction path, which is active when there is appreciable oxygen mobility in the electrode, the surface path, and the direct reaction path. In the direct reaction path, oxygen reacts directly on the surface of the electrolyte, and is reduced to form oxygen ions. Because all of the electrolytes that are commonly used for SOFC's have negligible electronic conductivities in the cathode environment this, reaction path will not make a significant contribution to the overall cathode activity.

The surface reaction path can occur on any electrode; however, in electrodes with limited ionic mobility, it will be the dominant reaction path. First the oxygen molecules are dissociatively adsorbed onto the electrode surface forming adsorbed oxygen atoms. Then these atoms diffuse along the surface to the 3PB. Here they are ionized and incorporated into the electrolyte according to the following reaction:

$$O_{ads} + 2e' + V_O^{\bullet\bullet} \rightarrow O_O^x$$

Equation 10: Incorporation of adsorbed oxygen into the electrolyte

Therefore, in the case of purely electronic conducting electrodes, the possible rate limiting steps are diffusion in the gas phase(2), dissociative adsorption(3), surface or grain boundary diffusion(4), and vacancy migration through the electrolyte(1). Vacancy migration in the electrolyte will not be considered here, since it should be unaffected by the materials used for the cathode, while diffusion in the gas phase and through the pores is determined by the electrode structure rather than the material. Thus the primary functional concerns of an electronically conducting cathode are that its catalytic activity for the dissociative adsorption of oxygen and its oxygen surface diffusion coefficient be as high as possible. This will allow for rapid supply of oxygen to the 3PB.

From the above it is clear that the optimum structure for an electronic conducting SOFC cathode has a maximum number of 3PB sites, as well as easy gas diffusion paths. Unfortunately, 3PB sites are maximized by having a very fine porous microstructure, while gas diffusion is facilitated by large open pores. The stability of the electrode material must also be taken into account. In finer microstructures the diffusion distances are shorter so, if the material is not stable, densification of the electrode and severe degradation of performance can occur.

For typical porous fuel cell electrodes, which operate at around 1 atm pressure and have pore sizes greater than 1 micron, continuum diffusion is the main contributor to gas flux. Thus concentration polarization effects in the cathode tend to be controlled by the binary diffusion coefficient for a mixture of oxygen and nitrogen [36, 51]. It should be noted that, at the anode side, the diffusion coefficient of interest is that of an H_2/H_2O

mixture, which is higher than for O_2/N_2 mixtures; therefore, concentration polarization is generally less important at the anode. If pore sizes become smaller than a micron, Knudsen diffusion, which is slower, begins to play a role and concentration polarization worsens. For this reason the cathode microstructure should incorporate a large amount of open porosity, with an average pore size greater than 1 μm. Having a pore size as close to this value as possible will result in a maximum number of 3PB sites.

Another consideration in cathode design is thickness. Up to a point increasing the thickness increases the activity of the electrode and decreases ohmic losses in the electrode [52] Above this optimum thickness, losses again tend to increase and concentration overpotential becomes important in electrodes over 100 μm thick [53, 54]. However, in cathode supported cell designs, it is necessary to have a thicker electrode. When this is the case, it is sometimes useful to have a graded porous structure, with coarse porosity in the support layer, then next to the electrolyte a finer active layer. This allows for rapid gas transport through the supporting layer, while having a maximum number of active sites near the electrolyte. Thickness also plays a role in determining the ohmic losses in the cell. A thick electrode will have little effect on the resistance of a planar cell, since the electrode conductivity is generally much higher than that of the electrolyte; however, in tubular designs where the current path through the electrode is much longer, it is important to have a certain minimum thickness. This is done in order to give sufficiently low in plane resistance.

It has also been shown that in order to maximize the performance of the cathode the final structure should be as homogenous as possible [52, 55]. A starting powder with a narrow particle size distribution will lead to a more homogeneous distribution of current through the electrode and a larger number of 3PB contacts. This increases the active area of the cathode, reducing polarization losses and reducing current constriction in the cathode which has the effect of lowering ohmic losses. A uniform microstructure does not mesh well with the concept of a graded electrode structure discussed above; however, the coarse outer layer of the cathode acts as a current collecting layer rather than an active cathode layer and, therefore, needs only good conductivity and large, open porosity. It has been shown that a shorter contact spacing in the current collecting layer also helps to reduce cathodic losses; thus, providing the active layer is uniform and of the optimum thickness, a graded cathode can function effectively.

If the material used for the cathode exhibits both ionic and electronic conductivity then the structural requirements of the electrode may be altered. Instead of ionization occurring at the 3PB, it can occur over the entire free surface depending on the rate determining step (rds), and ions can be transferred to the electrolyte at the two phase boundary (2PB) between the electrode and electrolyte, rather than the 3PB [56] Referring back to figure 9, it is possible for both the surface and bulk reaction paths to be active. This means, in addition to the steps seen above, that ionization of oxygen and incorporation into the electrode, as well as ionic transport through the electrode, can become rate limiting. The factors affecting the surface reaction mechanism remain unchanged from the case of the electronically conducting cathode material, and will not be discussed further here. The bulk path will be affected by the catalytic activity of the electrode material for the adsorption, dissociation and reduction of oxygen from the gas, as well as the ionic conductivity of the electrode. Models of MIEC cathodes [56] have shown that, in the case where the transport of oxygen ions through the cathode is rate limiting, the reaction area is still confined to a very narrow region around the 3PB. Therefore, the same structural guidelines that apply to electronic conducting cathodes should be applied to an MIEC cathode of this type. However, if transport of oxygen ions through the cathode material becomes faster than surface oxygen diffusion, then the entire 2PB becomes active and structural requirements change.

When the 2PB is more active than the 3PB, it is desirable to increase its area as far as possible [57]. This is done by applying a dense layer of the MIEC cathode over the electrolyte. A porous outer layer can be applied over this to act as a current collector. The current collector should have relatively large pores (>10 μm) to avoid gas diffusion limitations, maintain high electronic conductivity and leave as much of the dense MIEC surface exposed as possible In order for this to be effective, it is important that the ionic and electronic conductivity of the cathode are quite high; however, it is often the case with MIEC's that when one type of conductivity is high the other is low. Also, since a dense electrode layer has a much lower surface area, surface reactions (3 and 5 in figure 9) may become rate limiting, in which case a porous electrode again becomes beneficial.

In order to solve this problem, composite electrodes have been proposed [50, 58, 59] in which an electronically conducting phase and an ionically conducting phase are applied as interpenetrating networks. Such an arrangement is shown schematically in figure 10. This arrangement allows for the creation of 3PB sites throughout the electrode. As expected it has been found that the activity of such electrodes increases with the content of ionic conductor up to a point [58]. This gives the maximum number of contacts between ionic conductor, electronic conductor and gas phase. However, these contacts can only be active reaction sites if they lie on percolation paths for electrons, oxygen ions and the gas phase. This means that the ionic conductor must connect to the electrolyte, the electronic conductor to the current collector (or interconnect) and the pores must be open. Additionally, it has been shown that the performance of such an electrode is dependent on the ionic conductivity of the electrolytic phase, with minimum losses corresponding to maximizing the conductivity of the ionic conductor [58]. As the amount of electrolytic phase is increased the electronic conductivity of the electrode will also decrease, leading to power losses.

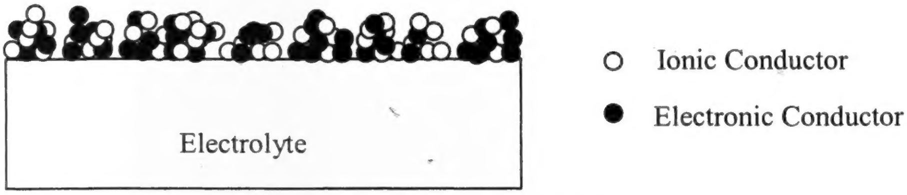

Figure 10: Composite electrode

Mixing particles of ionic conductor with electronic conductor gives a large area for interdiffusion and reactions to occur between the two phases. Therefore, it is important that the two phases be stable with respect to each other at the operating temperature if optimum performance is to be obtained [58]. Proper design of composite electrodes can give significant improvements in cell performance, which has led to their use in several high performance cells [51].

2.2.2 Cathode Materials

2.2.2.1 Platinum

Platinum is one of the few metals that is stable in the harsh cathode environment. As a metal it has very high electronic conductivity and good catalytic activity for the oxygen reduction reaction [2]. Because of this, it is frequently used as a counter electrode or reference electrode in developmental work [61] Platinum is not very useful in commercial high temperature cells due to its high cost, its non-zero evaporation rate and because the high cell operating temperature means platinum is not required as a catalyst.

2.2.2.2 Doped Lanthanum Manganite

As mentioned before, the perovskite type oxide strontium doped lanthanum manganite (LSM) is the most common cathode material for SOFC's based on YSZ electrolytes. In this oxide, divalent strontium replaces trivalent lanthanum on the A site (see figure 8). In its undoped state lanthanum manganite ($LaMnO_3$) exhibits semiconductor type behaviour [30]. By the addition of appropriate dopants, the conductivity can be further increased. An investigation by Kerstesz et al [62] showed that even at only 80% of theoretical density, the composition $La_{0.84}Sr_{0.16}MnO_3$ has a conductivity of 133 S/cm at 1000°C. This is orders of magnitude larger that the conductivity of any of the electrolyte materials being examined, so LSM cathodes have little impact on the overall ohmic losses of the cell.

Strontium additions enhance the intrinsic p-type conductivity of lanthanum manganite by replacing La^{3+}. This leads to the transformation of Mn^{3+} to Mn^{4+} in order to maintain charge neutrality and leads to an electronic reordering, described by Goodenough [63], which creates electron holes. While doping lanthanum manganite gives it very high electronic conductivity, it does not enhance its ionic conductivity. This is because no increase in oxide ion vacancy concentration is associated with doping. The creation of oxide ion vacancies, such as by reducing atmospheres, leads to an overall decrease in conductivity as Mn^{4+} is reduced back to Mn^{3+}, reducing the number of electronic charge carriers. This is not an issue in the cathode environment though.

Because of its lack of ionic conductivity (5.9×10^{-8} S/cm at 800°C) [64], proper electrode design with LSM requires maximization of 3PB sites at the electrode/electrolyte interface.

The electrical conductivity of LSM seems to peak when strontium occupies 30% of the A sites [65], but the chemical and mechanical compatibility of LSM with the YSZ electrolyte must also be considered. For the compound $La_{1-x}Sr_xMnO_3$ the thermal expansion coefficient (TEC) is a function of the value x [66]. In any case the TEC of LSM is greater than that of YSZ; however, this difference is minimized in the strontium doping range of $x = 0.1$-0.2. This puts important constraints on the allowable doping level if the cell is to undergo numerous thermal cycles without delamination. It has also been found that undoped lanthanum manganite can react with YSZ to form poorly conducting $La_2Zr_2O_7$ at the cathode/electrolyte interface [58]. The amount formed is dependent on the sintering temperature, with higher sintering temperatures giving more $La_2Zr_2O_7$ formation. However, even at sintering temperatures as low as 1100°C, there is some evidence of $La_2Zr_2O_7$ in the x-ray diffraction spectrum. One way to avoid the formation of this second phase is to use an A-site deficient perovskite such as $La_{0.85}MnO_3$ [58, 67]. This leads to a reduction in diffusion of lanthanum into the electrolyte, and allows for cofiring of the electrode/electrolyte structure at temperatures up to 1300°C. The behaviour of LSM is similar to that of undoped lanthanum manganite; however, additional reaction products Sr_2ZrO_4 and $SrZrO_3$ exist [53, 67]. The stability of the interface between the electrode and electrolyte materials can still be improved through the use of A site deficient materials [67], and the use of appropriate doping levels. It should also be noted that the conditions in an operating cathode can be quite different than the conditions used in examinations of the chemical compatibility of LSM and YSZ [68].

The activity of LSM for the cathodic reaction seems sufficient. Yamamoto et al [53] compared the performance of cathodes made from several different perovskite-type oxides both with each other and with platinum and found that only lanthanum cobaltite ($LaCoO_3$) and A-site doped lanthanum cobaltite outperformed LSM. Thus, with proper control of the composition of LSM, including doping levels and A-site deficiency, and sufficient attention to electrode morphology, it is a highly suitable cathode material for use in SOFC's.

Numerous other perovskite type materials have been tested as cathodes for solid oxide fuel cells, including lanthanum ferrite and lanthanum chromite [53]. Cathodes have also been made by doping these oxides on the B site as well as the A site. Examples include $La_{0.6}Sr_{0.4}Co_{0.8}Fe_{0.2}O_3$ [69] and $(La_{0.7}Sr_{0.3})_{0.9}Mn_{1-y}Cr_yO_3$ [6]. Other cathodes based on the perovskite structure include manganites with lanthanoids other than La on the A site, such as Pr, Nd and Sm [70]. For various reasons such as performance, reactivity and cost, none of these materials has had the same acceptance as LSM as the cathode for YSZ cells.

2.2.2.3 Doped Lanthanum Cobaltite

Strontium doped lanthanum cobaltite (LSCo) with the formula $La_{1-x}Sr_xCoO_3$ has a very high electrical conductivity, which tends to increase with temperature at low temperatures and low Sr levels. As the Sr dopant concentration increases beyond $x = 0.5$ or the temperature rises above around 500°C, the conductivity of the oxide decreases with temperature [71, 72]. For compositions with $x = 0.1$-0.2 the maximum observed conductivity is around 1500 S/cm. This, combined with high activity for oxygen reduction [73] and high oxygen diffusivity [11], make it a superior cathode material compared to LSM . Cell tests show that the best performance comes from a cathode structure with a fine pore structure and well connected particles [11], which suggests that oxygen transport within the electrode is rate limiting. The TEC of LSCo is in the range of $20\text{x}10^{-6}$/°C [74] which is significantly beyond the suggested acceptable difference in TEC between electrode and electrolyte of 20% [43] (for YSZ, TEC=10-$11\text{x}10^{-6}$/°C) [75] and it is chemically unstable with respect to that electrolyte [2, 27, 76]. It has been shown [75] that when YSZ and lanthanum cobaltite are in contact at high temperature the highly resistive phase $La_2Zr_2O_7$ forms.

Doping of $LaCoO_3$ has been shown to have an effect on the TEC of the material [43, 74, 75], and with proper composition control it may be possible to obtain a material that will be compatible with ceria (TEC = 12.6x10^{-6}/°C) or LSGM (TEC = 11.5x10^{-6}/°C) electrolytes. There has been no observed reaction product between LSCo and ceria electrolytes [2, 15, 77]. There have not been any reports of adverse reactions between LSGM and LSCo either, but the TEC mismatch is still of concern for both ceria and LSGM electrolytes. One solution might be a composite electrode, which should have an overall TEC closer to that of the electrolyte.

2.2.2.4 LSCF Cathodes

A variation on the theme of LSCo is LSCF, $(La_{1-x}Sr_x)(Co_{1-y}Fe_y)O_3$, which has also been investigated recently. Like LSCo it has high conductivity, greater than 100 S/cm at temperatures above 600°C [78], with charge being carried by both electronic and ionic carriers [69]. LSCF also shows good catalytic activity for oxygen reduction in the temperature range of 600-800°C [78]. The reactivity of LSCF with YSZ was evaluated over 120 h at 1100°C by Kostogloudis et al. [79], and it was found that reaction products similar to those for LSCo-YSZ formed. Reactivity tests at lower temperatures [78] showed that at 800°C no reaction products formed over 96 h, but longer reaction times [80] did result in the formation of strontium zirconate ($SrZrO_3$). A final factor that prevents the use of this electrode composition with YSZ is the TEC, which is in the range of 20x10^{-6}/°C [78].

An examination of the compatibility of LSCF with a samaria doped ceria electrolyte showed no reaction between the two at temperatures up to 1200°C [80]. The same study also showed that LSCF has a lower interfacial resistance with ceria electrolytes than either platinum or LSM electrodes. Despite the larger TEC of ceria compared to YSZ, thermal mismatch between electrode and electrolyte is still a potential problem. Another problem that has been identified is sintering of the LSCF structure. Cells running at as little as 500°C with this electrode material, while showing excellent early behaviour, experienced significant losses with time [81]. These losses have been attributed to loss of 3PB area after sintering of the LSCF. In addition to reducing the TEC mismatch, a composite electrode of LSCF and doped ceria would likely inhibit the sintering of LSCF [82].

2.2.2.5 YSZ - LSM Cathodes

In an effort to find a cathode material that will improve the performance of YSZ based cells operating at reduced temperature, without the formation of insulating phases, several investigators have suggested the use of LSM-YSZ composite electrodes [17, 54, 68, 83]. In this type of electrode the LSM provides electrical conductivity, while the YSZ transports ions formed throughout the electrode to the electrolyte. Adding YSZ to undoped lanthanum manganite ($LaMnO_3$) led to a large improvement in electrode performance [58]. As the conductivity of the YSZ added was increased by controlling the dopant concentration, the performance also increased. By mixing LSM and YSZ in the electrode, it is also possible to prevent the formation of interfacial compounds at the electrode-electrolyte interface. Instead the reaction product $La_2Zr_2O_7$ formed within the electrode itself which, although not desirable, hurts the performance less than formation of that compound at the interface. Further it is possible, still, to prevent formation of zirconates by using A-site deficient lanthanum manganite. Because electrode performance tended to improve with increasing electrode thickness, it appears that more reaction sites are being formed within the electrode itself.

Work on LSM-YSZ composites indicate similar behaviour to that of the undoped manganite [59]. Again it was found that cathode performance increased with increasing YSZ content up to at least 40% YSZ, and it was also found that electrode/electrolyte adhesion also improved with the addition of YSZ. However, it is possible that, if the YSZ content of the electrode is too high, then La sub-stoichiometry may not be sufficient to prevent the formation of resistive zirconates. As the zirconia content of the electrode is increased, its electrical conductivity also drops [54], but this loss is overcome by an increase in 3PB sites. Thus there should be a compromise between optimum performance, which is favoured by high YSZ content, and cell lifetime, which is extended by the elimination of resistive second phases. Tests of LSM-YSZ cathodes [17] have shown that the effective thickness of these electrodes is less than 20 μm, which is in agreement with findings that performance of composite electrodes improved with thickness up to a value of about 10-15 μm [68]. The performance of cells using LSM-

YSZ composite electrodes, combined with appropriate anodes and electrolytes, is very promising for operation of SOFC's at temperatures at or even below 800 °C [51].

One of the major reasons for the success of YSZ electrolyte cells is the advanced state of electrode development. Despite higher ohmic losses than ceria or LSGM electrolytes, the high performance and stability of cathode materials like LSM-YSZ make YSZ cells the best performers even at temperatures below 800 °C. Further development of appropriate electrode materials for different electrolytes should one day allow high power densities to be achieved at even lower temperatures; however, there is still a significant amount of work to be done.

2.3 Anode Materials

Like the cathode, the primary function of the anode of a solid oxide fuel cell is to provide reaction sites for electrochemical processes. As such many of the design requirements are similar. In the case of the anode, the electrochemical reaction is the oxidation of the fuel; however, because of the fuel flexibility of the SOFC, it may be necessary for the anode to perform several other roles. In any case the anode should provide as many active reaction sites as possible for the oxidation reaction, which like the reduction reaction in the cathode, takes place at the 3PB. It should have high electronic conductivity, must not react with the electrolyte or interconnect/current collector, should have high catalytic activity for fuel oxidation, be stable for long times in a reducing atmosphere, and have a similar TEC to other cell components. The principles for maximizing 3PB sites are the same as for the cathode; therefore, they will not be discussed again here.

One major difference between anode and cathode is that the anode may also be called upon to play the role of reforming catalyst. The high operating temperature and oxide ion conductivity of the electrolyte lead to the possibility of directly using hydrocarbon fuels in SOFC's. This is seen as a major advantage since it eliminates the need for costly and complicated pre-reformers. It also means that an effective anode should have good catalytic activity for the appropriate fuel reforming reaction, whether that be steam reforming, partial oxidation, or direct electrochemical oxidation of hydrocarbons. This presents numerous technical problems, as we shall see, but once these are addressed it will make the SOFC highly applicable to remote power generation applications using existing infrastructure.

Another difference between anode and cathode is the operating environment. The fuel atmosphere is highly reducing, and there are comparatively few oxides that can withstand the rigors of long-term operation. Any metal that does not show excessive evaporation at the operating temperature, however, can be used. This opens the door to many transition metals that act as inexpensive catalysts for fuel oxidation and/or reforming. A problem can arise with TEC mismatch; therefore, it has become common practice to use ceramic-metal composites (cermets) as anodes. Typically, the metal is chosen for catalytic activity and the ceramic chosen for stability and compatibility with the electrolyte. Thus often the simplest choice for the ceramic is the electrolyte material itself. This has the added benefit of expanding the active electrode area into the bulk electrode volume, as we saw with the composite cathode.

The most common alternative to a composite anode is a mixed ionic-electronic conducting (MIEC)anode. These materials should have the same effect of expanding the active area as they do for the cathode, and minimize TEC mismatch with the electrolyte. Commercially, there is no focus on purely electronic conducting materials for the anode; however, in laboratory scale investigations focusing on either cathode or electrolyte properties, it is not uncommon to see platinum used as the anode material for added simplicity in cell fabrication. The remainder of this section will focus on the common materials used for SOFC anodes, and their properties in various operating conditions.

2.3.1 Ni-YSZ anodes

The standard anode material for YSZ based cells is a cermet consisting of nickel and YSZ (Ni-YSZ). The performance of these anodes is strongly affected by the relative amounts of nickel and YSZ [84]. As the Ni level is increased, the conductivity of the electrode increases, giving lower ohmic loss; however, polarization loss of the anode has been shown to increase at nickel concentrations greater than 40 vol%. There is also a sharp increase in electrode resistance below about 40 vol% Ni, due to poor contacting between nickel particles. Apart from increasing polarization losses, high nickel contents can also have a negative effect on cell lifetime due to sintering of the nickel. This agglomeration of Ni and its dewetting of the YSZ has been identified as a major cause of anode performance degradation [21, 85, 86]. The higher the nickel content of the anode, the greater the microstructural change even over relatively short periods of operation (e.g., 100 h). Some research has shown that performance degradation of the cermet anodes is worse at 850°C than at 1050°C [4]. This suggests that it is not only nickel sintering that contributes to performance loss, but also some other process. One possibility is aging of the YSZ component of the electrode, which we have already seen is a more significant problem at reduced temperatures [33, 37, 38].

The structure of the cermet anode is very important in determining the degradation characteristics of the electrode, with some structures showing noticeable degradation in as little as 100 h [85], while others [87] with higher nickel contents have been shown to be stable for at least 5500 h. The major determining factor then seems to be the ability of the zirconia phase to interfere with Ni agglomeration. In order to improve its ability to do this, the interfacial bond between the metallic and ceramic phases must be improved, or structural characteristics should be incorporated into the electrode which will prevent sintering. One example of such a structure is the preferential coating of the nickel grains with small grains of YSZ. Thus the ceramic phase, which does not sinter [86], can more easily impede nickel agglomeration. Typically, as the ceramic phase becomes more able to slow nickel sintering, the resistance through the metallic component increases due to interference in the electronic pathway from YSZ.

Another effect of nickel content on the anode is in terms of TEC. The TEC of metallic nickel is on the order of 13-14x10^{-6}/°C [44, 88], (as high as 16.5x10^{-6}/°C [89]), which is high enough to cause problems during thermal cycling of cells. It has been shown that the TEC of a porous Ni-YSZ cermet varies linearly with the nickel content

[90], and that for good mechanical compatibility it should be kept as low as is practical in terms of conductivity. The relatively poor interfacial bond between Ni and YSZ also affects the TEC mismatch problem [89]. Because the YSZ phase is not strongly attached to the metal it does not have as strong a mitigating effect on the TEC mismatch as would be expected for a perfectly bonded interface.

Apart from its role as an electronic conductor in the anode, nickel is also a catalyst for the fuel oxidation reaction. The most common fuel used in the literature to date has been hydrogen; however, due to its availability it is expected that the first commercially successful SOFC's will run on natural gas. For hydrogen oxidation, nickel has fairly good activity [91], and it has been shown that the anodic overpotential is independent of the hydrogen partial pressure [92, 93]. Somewhat surprising is the fact that the polarization resistance of the anode can be decreased significantly by adding water vapour to the fuel [92, 94, 95]. Jiang and Badawal [96] suggest that the increased oxygen partial pressure that results from the addition of water to the fuel can lead to the formation of adsorbed oxygen or sub-oxides on the Ni surface. This in turn enhances the dissociative adsorption/diffusion of hydrogen. Such a mechanism does require that the metal surface favour dissociative adsorption and/or sub oxide formation; therefore, the effect is expected to be lessened on noble electrodes. An alternative mechanism is that oxygen ions from the electrolyte initially oxidize the metallic electrode, which is subsequently reduced by the fuel [91]. The higher oxygen partial pressure in humidified hydrogen allows this to happen more easily, making the electrode reaction more rapid.

In the event that natural gas is to be used as the fuel, the catalytic requirements of the anode are quite different. The anode must be able to either reform the fuel into a useable mixture of CO and H_2, or directly electrochemically oxidize the methane. Additionally, the anode must be tolerant to sulfur in the fuel, since sulfur compounds are added to pipeline natural gas as odorants. Several methods for internally reforming natural gas have been proposed [97], including steam reforming, partial oxidation and autothermal reforming. The steam reforming reaction is the most widely accepted for SOFC's. In this reaction, methane is combined with water vapour in the anode chamber to produce a mixture of CO, CO_2, H_2 and H_2O. Metallic nickel is a good catalyst for this reaction [91], but it may be too good. Because the steam reforming reaction is endothermic, it can lead to significant cooling of the anode near the fuel inlet if the reaction occurs too quickly [98]. Additionally, it may become necessary to incorporate heat recovery systems to pre-heat the fuel [99].

Carbon deposition is a major problem for cells running on methane, since it blocks pores and deactivates the anode. The presence of even a small amount of steam in the fuel feed greatly reduces the amount of carbon deposited [100]; however, it also decreases efficiency and power density. A steam to methane ratio of less than 1 leads to C deposition on the anode [99], but it has been suggested that a ratio as high as 3:1 is required to completely eliminate carbon deposition [101]. It is also possible to remove the deposited carbon and recover the initial anodic performance by running oxygen through the anode chamber.

Partial oxidation of methane is an exothermic reaction which does not require a catalyst [97, 102]. The fuel is mixed with oxygen and partially combusted to form hydrogen and carbon monoxide; therefore, the anode need only have catalytic activity for the oxidation of these two fuels. Advantages to this technique derive from its oxidative nature, which lessens the likelihood of carbon deposition and improves tolerance to sulfur containing impurities. The high oxygen partial pressures involved in this type of reaction can, however, lead to oxidation of the nickel catalyst.

Autothermal reforming is a combination of partial oxidation and steam reforming in which the fuel is mixed with both steam and oxygen. The heat released by the partial oxidation reaction is used to drive the steam reforming reaction [97]. The major variables affecting carbon deposition here are temperature and amount of steam added to the fuel. The final option is to feed dry methane directly into the anode and electrochemically oxidize it. The major problem with this is that it leads to significant carbon deposition at temperatures above 800°C [103]. At temperatures below about 650°C, however, little or no carbon deposition was observed on Ni-YSZ based anodes over a period of 100 h. Some pre-reforming of the fuel may still be required in order to maintain anode conditions that will not result in the oxidation of nickel.

Variations of the Ni-YSZ anode have been suggested by several researchers for various reasons. The addition of a few mole percent TiO_2 to the YSZ network increases it electronic conductivity and improves its bonding with nickel [89]. Other authors have shown that, by replacing nickel with ruthenium, the sintering resistance of the electrode and the activity for hydrogen oxidation can be improved [104], although at significant financial penalty. Replacing Ni with copper [101], eliminated carbon deposition in dry methane, but gave poor performance. Other studies have tried to improve anode performance by replacing the YSZ with other electrolytes [91], or mixed ionic-electronic conductors [105]. There have also been investigations using mixed conducting interfacial layers to reduce interfacial resistance of Ni-YSZ anodes at reduced temperatures [106]. Such interfacial layers have also been used to enhance anode performance in dry methane in the temperature range of 500-700°C, where carbon deposition is less prevalent [103].

2.3.2 Perovskite Anodes

There have been several investigations into using perovskites as anodes for zirconia-based cells running on methane [107, 108]. The goal of this research is to develop an anode that is resistant to carbon deposition in dry methane, or with lower catalytic activity for steam reforming than Ni-YSZ, which will prevent unacceptable temperature gradients in the cell. Research has shown that materials with a small degree of both n- and p-type electronic conductivity, combined with large oxide ion conductivity show favourable catalytic activity for methane oxidation [109]. While investigations into actual electrode/electrolyte systems have shown they have a resistance to carbon deposition, the performance of these materials in hydrogen or methane is inferior to that of Ni-YSZ [110] which is at least partly due to their much lower total conductivity [111]. Additionally, the performance of these anodes degrades severely over time in reducing atmospheres, in some compositions due to the formation of interfacial reaction products [110], and in others in an unidentified manner which is reversible by oxidation of the anode [111]. Doped lanthanum chromites have a low activity towards methane steam reforming, thereby avoiding potential thermal gradients, and no carbon deposition was detected at temperatures up to 850°C [112]. Composite electrodes of this material mixed with YSZ have been examined, but the low catalytic activity makes them unacceptable for use in the virgin state. Addition of a dispersed ruthenium catalyst improved the electrode properties without leading to carbon deposition [112]. Similar improvements have been shown with the addition of Ni catalyst particles, but the performance is still inferior to that of traditional Ni-YSZ anodes [111].

2.3.3 Ni-Ceria Anodes

Cermet anodes of nickel and ceria or doped ceria have been investigated for use in cells with LSGM electrolytes [11, , 105,113, 114, 115]. The mixed conducting properties of doped ceria in reducing atmospheres are expected to greatly extend the reaction area, while the nickel phase should enhance the electrode activity. Also the addition of doped ceria to a metallic nickel electrode improves the contact between electrode and electrolyte, resulting in a lower electrode resistance [114]. Tests of the initial ageing behaviour of these anodes show little degradation, and in some cases even a slight improvement of performance [47]. However, at temperatures higher than the typical operating temperature, there is evidence of interdiffusion between electrode and electrolyte [115]. Lanthanum diffusion from the electrolyte into the anode can lead to the formation of highly resistive phases, and reactions between LSGM and Ni are known to lead to $LaNiO_3$ formation. One way to prevent this is to use lanthanum oxide-doped ceria (LDC) as the ceramic phase. At the proper doping level, this removes the driving force for La diffusion from the electrolyte into the electrode; however, LDC has lower conductivity than either samaria- or gadolinia-doped ceria. Even with LDC as the ceramic phase, it was still necessary to have a Ni free interlayer between the LSGM electrolyte and the composite anode to prevent $LaNiO_3$ formation.

These types of electrodes have also been used with ceria [81, 116] and zirconia [117] electrolyte cells with good results. Operation tests indicated that, when compared with other sources of voltage loss in such SOFC's, the anodic loss was negligible. In ceria electrolyte cells it is even more important to have high performance electrodes, since at open circuit conditions there is a leakage current that leads to polarization losses. Because of this requirement, nickel-ceria cermet anodes have become a leading choice for the anode of these cells.

2.3.4 LSGM-Ni Anodes

An alternative anode material for LSGM cells is a Ni-LSGM anode, since LSGM provides high ionic conductivity and cannot react with the electrolyte. Tests of cells with Ni-LSGM anodes show initial high performance [47, 113], with these anodes outperforming Ni-ceria ones in hydrogen. Unfortunately the anode potential drop doubled in only 20 h at 800°C. Although no definitive conclusions have been reached as to the cause of this degradation, it seems likely that either Ni sintering, or interaction between the LSGM and Ni to form $LaNiO_3$, are the culprits.

2.4 Interconnect Materials

Perhaps the most demanding conditions in the SOFC are those at the interconnect. The interconnect allows for the series electrical connection of the anode of one cell with the cathode of the next. In order to do this effectively, it must have high electronic conductivity in both anode and cathode environments, and no ionic conductivity. It must also be chemically and mechanically stable in these environments, and with respect to both the anode and cathode, with which it is in direct contact. In planar cell designs the interconnect also plays an important role in gas separation and distribution. To prevent mixing of fuel and oxidant gases it should be fully dense, while to allow for even distribution of the gases, it should be easily shaped to incorporate gas flow channels. At a traditional operating temperature of 1000°C there are very few materials that meet all of these requirements, and none that can meet them economically. This is a major reason why research into planar cells has focused on reducing the operating temperature. In tubular designs the interconnect is only a narrow strip and plays no role in gas distribution, so the problems associated with finding economical materials are not so daunting.

At high temperatures the choices are limited to electronically conducting ceramics, while at lower temperatures it becomes possible to use some heat resistant metallic alloys. This section will focus on the properties of more common materials used in each of these two classes, and on their interactions with cell components.

2.4.1 Perovskite Interconnects

As we have seen in the chapter on cathode materials, perovskite-type oxides can be doped to give high electronic conductivity. There are, however, very few of these types of oxides that are stable in the reducing conditions of the anode compartment. As a result the most common choice for the interconnect is lanthanum chromite ($LaCrO_3$) with strontium doping on the A site, so called LSC. LSC has good electrical conductivity, is resistant to both oxidizing and reducing atmospheres [22], and is reasonably compatible with the electrode materials [118]. Unfortunately, these seem to be its only advantages as an interconnect material. It has low thermal conductivity, which can lead to the formation of thermal gradients in the stack [21], and it is very brittle and expensive to manufacture due to its low workability. Additionally, it expands in reducing atmospheres [119], which can cause cracking or loss of electrical contact, both of which will hurt cell performance. Its conductivity is also much lower in reducing atmospheres than in oxidizing atmospheres. The problems with mechanical properties are aggravated by its poor sinterability [120]; however, the addition of small amounts of vanadium to the B site can aid in sintering [112]. From this brief analysis it is clear that finding a more suitable interconnect material is crucial to the development of the planar SOFC. That being said LSC has been quite successful as the interconnect in high temperature tubular cells designed by Westinghouse.

2.4.2 ODS Alloy Interconnects

At lower temperatures metals that form a protective oxide scale in the cathode atmosphere can be used as the interconnect. The most common scale forming elements are chromium and aluminum. In oxidizing atmospheres these elements form chromia (Cr_2O_3) and alumina (Al_2O_3), respectively. These surface scales inhibit further oxidation of the underlying metal. Pure chromium has a TEC similar to that of the YSZ electrolyte [121], and compared to ceramics is less expensive and much more workable. Uniformity of heat distribution in the stack is also improved, particularly when endothermic reformation reactions take place in the anode chamber [122]. Despite its mechanical advantages over ceramic materials, chromium has relatively poor mechanical properties, including a ductile to brittle transition temperature well above ambient [122]. In order to improve its mechanical properties, alloying additions of iron or cobalt can be used; however, to maintain high temperature corrosion resistance the amounts must be kept relatively low. The properties of the chromia scale are also less than ideal for fuel cell use. The conductivity of chromia is on the order of 10^{-1}-10^{-2} S/cm at 900°C, so it can make a significant contribution to the ohmic resistance of the stack [122]. Scale growth also becomes much more rapid at temperatures above 900°C, and during thermal cycling TEC mismatch between the scale and the underlying metal can lead to spalling, which then can cause pore blockage and electrode deactivation [121], as well as loss of chromium from the alloy which leads to rapid oxidation of the metal. Oxide dispersion strengthening (ODS), the addition of small amounts of oxide to the metal, can improve the adherence of the scale [122] and dramatically slow the growth rate of the oxide scale [121]. For these reasons the ODS alloy $Cr\text{-}5Fe\text{-}1Y_2O_3$ has been examined as a potential metallic interconnect material [119]. Although most of its properties are acceptable at temperatures as high as 900°C, tests in actual cell operating conditions have shown that deposition of Cr containing species at the cathode occurs [123]. This is due to the high vapour pressure of hexavalent chromium compounds in the cathode atmosphere [21, 123]. The vapourized species drift to the cathode, where they can react forming secondary phases that degrade electrode performance.

The alternative to chromia forming alloys are alumina forming alloys. These systems exhibits slower scale growth rates and better scale adherence [123, 124]; however, the conductivity of alumina is about six orders of magnitude lower than that of chromia, so the high resistive losses preclude their use as metallic interconnects[122].

Ideally, fuel cell developers would like to be able to use interconnects based on materials that are cheaper than chromium, such as ferritic stainless steels. At temperatures in the 600-800°C range this may be possible.

2.4.3 Nickel and Iron Based Chromia Formers

There also exist several commercial heat-resisting alloys which form a protective chromia layer. Most of these are based on nickel and are, therefore, still relatively expensive, but show good oxidation resistance [124]. Ferritic stainless steel interconnects are the most promising interconnect materials under development. They combine excellent thermal and electrical conductivity, with good machinability and gas tightness, all for a cost less than either chromium- or nickel-based systems [22]. These materials should contain more than 14 wt% Cr in order to stabilize the ferritic structure; however, this is a much lower content than Cr ODS alloys and, with addition of titanium and niobium to form stable carbides, the chromium content can be lowered even further [125]. This should lead to a lessening of chromium vapourization and deposition at the cathode. Although the conductivity of these alloys was shown to degrade steadily over 5000 h at 700°C, the overall performance of the interconnects remained better than that of ceramic materials, and at a fraction of the cost [125].

2.5 Sealing Materials

There has been very little published on the materials used to make seals for planar cell configurations. Most developers use proprietary sealing technologies, and many laboratories have specially developed glass seals. Sealing technology remains one of the major hurdles in SOFC development, with the requirement that seals not react with cell components and maintain good sealing over a wide range of temperatures through a number of thermal cycles. The majority of seals used are glasses or ceramic cements, with glasses giving the advantage of some stress relief once they reach their softening temperature [126]. Ceramic cements tend to be porous by nature, and are often incapable of providing sufficiently good seals [127]. The main alternative sealing technique is the use of compressive gaskets which for small-scale operations, such as laboratory testing, can be made of gold or for larger scale productions, mica. Investigations of the performance of mica seals [128] show that as the compressive stress increases, the sealing characteristics improve. The form of the mica gaskets is also important; when cleaved natural mica sheets are used the smooth surface gives very good sealing properties, even at relatively low compressive stress. Mica papers, on the other hand, which are made up of small mica platelets in an organic binder are much less smooth and, even at high compressive stresses, the seal is not appropriate for use in SOFC's. There is still much additional work to be done to test the compatibility of these types of seals with cell components in cell operating conditions over extended times.

Chapter 3 Manufacturing Techniques

This chapter will focus on the techniques used to manufacture cell electrodes with the ideal structures discussed above, as well as some of the methods that have been used for depositing thin, dense electrolyte layers onto porous ceramic substrates. Although techniques for producing the ceramic powders often used in manufacturing play a vital role in determining the properties of the final ceramic, they will not be discussed in detail, nor will fabrication of interconnects. The focus will be on the more novel techniques used, as opposed to traditional pressing and sintering of ceramic powders.

3.1 Electrolyte Manufacturing

In order to reduce cell operating temperature, it has become important to be able to deposit dense electrolyte layers with a thickness on the order of 10 μm over porous electrode substrates. Here techniques such as vapour deposition, sputtering, sol-gel and tape casting, which have all been used more or less successfully will be discussed.

3.1.1 Chemical Vapour Deposition

Several variations on chemical vapour deposition (CVD) have been used to fabricate thin electrolyte layers, most notably the electrochemical vapour deposition (EVD) technique used extensively by Westinghouse to fabricate their tubular cells. There are a number of textbooks and review articles on CVD [129, 130, 131, 132], but simply put chemical vapour deposition is a process whereby one or more gaseous species react to form a solid deposit on an active substrate. The substrate can be activated in a number of ways, with thermal activation being the simplest example. An example of a single reactant forming a deposit is the pyrolysis of silane (SiH_4) at 1000 °C to form a silicon deposit and release hydrogen. For ceramics the most common type of deposition reaction is an oxidative type reaction. Here a gaseous compound reacts with an oxidizing gas, usually oxygen, to form an oxide deposit. A common example from the microelectronics industry is the oxidation of silane to form silica (SiO_2).

The deposition reaction begins with the adsorption of the reacting species. Adsorbed species then diffuse to active sites, where they react. Any undesirable reaction product should be gaseous, so that it will not contaminate the film. Film formation occurs by a nucleation and growth process, where nuclei of a few atoms form, then grow into larger islands. These islands eventually coalesce to form a continuous film which can be polycrystalline, single crystal or amorphous, depending on the deposition conditions and nature of the substrate. At high pressures of reacting gases, homogenous nucleation can occur where the solid reaction product forms directly in the gas phase. This leads to formation of a fine powder which in most cases is undesirable; however, the resulting powder tends to be highly sinterable and, in some cases, is the desired product.

For the fabrication of oxide ceramics CVD has the ability to form thin dense layers without resorting to very high sintering temperatures [133], as may be necessary with conventional techniques. However, it requires a clean deposition system and operating at reduced pressure; therefore, production costs tend to be higher than for more traditional slurry techniques or pressing and sintering. Oxide electrolytes provide an additional challenge because they are multicomponent systems. For deposition of YSZ, two separate reactants are required, one for yttria and the other for zirconia. The reactants must be mixed in appropriate amounts to give the desired film composition. Equations 11 and 12 are the most common ones used for CVD of YSZ films, although it is not uncommon for oxygen to be replaced by water, which leads to the formation of HCl instead of Cl_2 [134].

$$2YCl_3 + \frac{3}{2}O_2 \rightarrow Y_2O_3 + 3Cl_2$$

Equation 11: CVD of yttria

$$ZrCl_4 + O_2 \rightarrow ZrO_2 + 2Cl_2$$

Equation 12: CVD of zirconia

The final film composition is controlled by the relative vapour pressures of the chloride vapours; however, kinetic factors have to be taken into account as a mixture with 16 vol%YCl_3 will give less than 8 mol%YSZ. There are various forms of vapour sources for thin film deposition by CVD including metallorganics [133]; however, for the deposition of YSZ, powders of yttrium and zirconium chlorides are most often used. These powders are heated under reduced pressure to give appropriate evaporation rates for the desired deposit composition. The rate of evaporation is given by the Hertz-Knudsen equation (equation 13) which relates the molar rate of evaporation to the absolute temperature, T, and the equilibrium vapour pressure at that temperature, p^*. [135]. In the equation A represents the surface area of the evaporation source, p the background pressure in the system, m is the mass of the evaporant, and α is the evaporation coefficient.

$$\frac{dN}{Adt} = \alpha(2\pi mkT)^{-1/2}(p^* - p)$$

Equation 13: Hertz-Knudsen molar evaporation rate

Although zirconia films have been grown by CVD [133, 136], there is a more useful process for growth of thin YSZ films on porous substrates. Electrochemical vapour deposition (EVD) in a modified version of CVD which takes advantage of the electrolytic properties of the YSZ deposit. This process was developed at Westinghouse in the 1970's and is still used today. Their approach is to start with a porous cathode support tube, fabricated by traditional ceramic processing techniques. A thin layer of YSZ electrolyte is then deposited onto the outer surface of the tube by EVD. The process is actually a combination of both CVD and EVD. The porous support initially separates the metal chloride vapours on the outside of the tube from the oxidizing gas on the inside of the tube. Inside the porous structure the gases mix, leading to the formation of YSZ deposits on the pore walls by CVD. Eventually, the deposits close off the pores, giving complete separation of the two gases.

After this the reaction proceeds electrochemically, with oxygen being reduced at the cathode (inside the tube). The oxide ions then migrate through the YSZ deposit to the halide environment where they react with these gases according to the electrochemical reactions 14 and 15. Electrons released in this reaction migrate back through the electrolyte to the cathode where they reduce more oxygen, and the reaction continues. The low electronic conductivity of YSZ leads to relatively slow growth rates; however, the nature of the process itself ensures uniform film thickness. This is because when the film grows its resistance increases, which slows the growth rate in thicker areas. Thus the thinner areas will grow more quickly and the film thickness will be self-levelling. The process is illustrated schematically in figure 11. Increasing the electronic conductivity of the deposit by either doping or control of yttria content increases film growth rate.

$$3O^{2-} + 2YCl_3 \rightarrow Y_2O_3 + 3Cl_2 + 6e^-$$

Equation 14: EVD of yttria

$$2O^{2-} + ZrCl_4 \rightarrow ZrO_2 + 2Cl_2 + 4e^-$$

Equation 15: EVD of zirconia

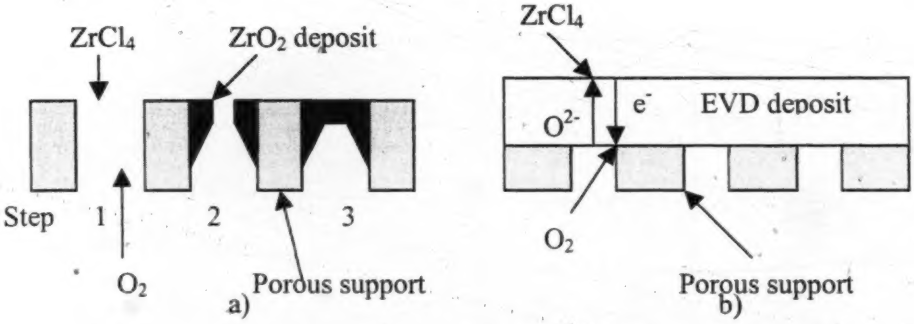

Figure 11: (A) Pore closure by CVD (B) Film growth by EVD

Using this process it is possible to grow dense YSZ films over substrates with over 30% porosity, assuming the deposit has some degree of both ionic and electronic conductivity. In order to attain sufficient defect mobility in 8YSZ, a deposition temperature of around 1150°C is required [137], which is significantly lower than typical sintering temperatures for electrolytes made from mixed oxide powders (typically 1500°C). Growth rates at this temperature are acceptable with a 10 μm thickness, the typical minimum for fuel cell applications, taking about 3 h [137]. Typically, the cost of fabrication is higher than with other techniques, but EVD allows the formation of uniform, thin, dense films well suited for use as SOFC electrolytes.

3.1.2 Physical Vapour Deposition

The success of CVD and its derivatives has led to the application of various other thin film deposition techniques to SOFC component fabrication, including the family of processes known as physical vapour deposition (PVD). These techniques include vacuum evapouration, laser ablation and rf sputtering. Reactive magnetron sputtering, which is a hybrid of CVD and PVD, can also be included under this heading. PVD includes processes whereby a species in the vapour phase is condensed to form a solid deposit on the substrate. In vacuum evaporation a source material is heated either resistively or by an electron beam to give a significant vapour pressure. The material in the gas phase then condenses on the substrate, and every other surface in the deposition chamber, giving a thin film. This is not the most useful technique for depositing refractory materials such as zirconia, since the high temperatures required to evaporate them may only be attained by electron beam evaporation and at, these temperatures, dissociation tends to be combined with the evaporation reaction giving oxygen deficient films [135]. An alternative to electron beam evaporation is pulsed laser deposition (PLD). In this process a high-energy laser beam is pulsed across the target. This causes species from the target (ions, electrons, neutral species, particulate) to be ablated, forming a plume, which is intercepted by the substrate. The plume condenses on the substrate forming a film. Attempts to grow thin YSZ films on porous anode substrates (NiO-YSZ) result in oxygen deficient films at the low oxygen pressures in the gas [138]. This problem can be solved by post annealing the film in air. PLD gives very slow film growth rates, and the films examined were only 2 μm thick. Although this thickness would give exceptionally low ohmic losses, it has proven insufficient to prevent gas leakage across the electrolyte.

The final form of PVD which has found some degree of application to the fabrication of thin electrolyte layers is sputtering. Sputtering is a process whereby particles from a target are ejected due to momentum transfer upon impact from an energetic species. A glow discharge is used to ionize argon to Ar^+. In the glow discharge, electrons from the cathode (usually the target material) strike argon atoms, creating Ar^+ by electron impact ionization and releasing more electrons. The argon ions are then accelerated towards the target by a negative bias. When the ions hit the target they cause the ejection of atoms and electrons from the target; the atoms then travel to the substrate where they hopefully stick and form a film while the electrons are accelerated away from the negatively biased target and return to the glow discharge. Two specialized forms of sputtering have found the greatest application to fuel cell electrolyte fabrication. These are radio frequency (rf) sputtering and reactive magnetron sputtering.

If the target to be sputtered is a non-conducting ceramic, a dc glow discharge cannot be maintained due to charge accumulation at the target. For the purposes of sputtering YSZ can be considered to be an insulating material; therefore, it is immediately apparent that a problem exists. One way to circumvent this difficulty is to use an rf voltage. When this happens the electrode (target) spends some time at a positive voltage and some time at a negative voltage. Because electrons have much higher mobility than ions they give a much higher current in the positive cycle than the ions do in the negative cycle. Thus, in order to conserve charge, the electrode self biases to a negative voltage so that the net current over a full cycle is zero. During the now much longer negative cycle ions are attracted to the target causing sputtering to occur. During the positive cycle, on the other hand, fast moving electrons respond quickly and bombard the target; the slower ions do not have time to reverse direction and their momentum from the negative cycle carries them on to the target. Although this process works, it has a couple of drawbacks in that it is difficult to scale up and it generates rf noise which can interfere with other nearby electrical systems. An attempt to deposit a thin YSZ film onto a porous Ni substrate was reported by Fragnaud et al [26]. It was possible to use a sintered YSZ disk of the same composition as the desired product. The resulting film was dense and, when the substrate was heated during deposition, crack free. The major drawback to this process is its very low deposition rate, which for this experiment was only 0.5 μm/h. Deposition rate can be increased by increasing the rf power; however, the nature of the bonds in refractory ceramics intrinsically leads to low sputter yields.

In order to increase the deposition rate an alternative form of sputtering, magnetron sputtering, may be used. Here a magnetic field is used to trap electrons near the surface of a metallic target, resulting in increased electron impact ionization in this region. The result is that more ions bombard the target and more atoms are sputtered away. Because the target must be conducting, the sputtered species are metallic. In order to deposit a YSZ layer, the metal atoms must be oxidized. This can be done either after deposition by oxidation at increased temperature in air, or in situ by reactive magnetron sputtering. Reactive magnetron sputtering can be considered a form of CVD, rather than PVD, since the vapourized species reacts with another species in the vapour and forms a deposit; however, unlike other CVD processes there is no exhaust gas produced. To form a YSZ layer by reactive magnetron sputtering, a target of either a yttrium-zirconium alloy or a bimetallic target is used. In either case the film composition is determined by the target composition and the sputter yields of the two materials in the target.

Oxygen gas is added to the sputtering gas (argon), where it reacts with the sputtered metal atoms to produce an oxide deposit. The partial pressure of oxygen in the system must be carefully controlled; if it is too high the target will oxidize and the deposition rate will drop off. On the other hand if the oxygen partial pressure is too low an oxygen deficient deposit will result [26]. If this is the case the deposit may be oxidized after deposition, although this could lead to cracking of the film due to volume changes. Results of deposition runs on porous NiO-YSZ substrates show that, even at oxygen partial pressures as high as 6×10^{-4} torr, tetragonal zirconia was formed in addition to the cubic YSZ [139]. A post anneal in an oxidizing atmosphere was required to transform the film into a single cubic phase. Helium leakage tests on the as-deposited electrolyte layer show that gas tightness increases with electrolyte thickness in the range of 1-9 μm; however, in order to achieve sufficient gas tightness for use in SOFC's, the layer has to be sintered in air at temperatures up to 1300°C. Deposition rates for reactive sputtering are about half of what they are for metallic sputtering, and both require post annealing in air for the layer to be made functional. The major advantage, therefore, to reactive sputtering would be the smaller volume change on oxidation which should reduce the stress levels in the film [26, 139].

Compared with CVD techniques, the PVD techniques discussed here give longer processing times, including post annealing. However, they do allow for lower processing temperatures. For fabrication of planar cells they also have the advantage over EVD of not requiring sealing. Sealless tubular cells, on the other hand, are much better suited to electrolyte deposition by EVD due to their more complicated geometry and the fact that they do not require high temperature seals.

The two vapour deposition techniques discussed so far require controlled atmospheres and very clean deposition systems to avoid film contamination. This makes them more expensive and more difficult to scale up than traditional ceramic processing techniques. We will now look at three techniques that can be done at atmospheric pressure in air, and have been proven capable of depositing YSZ layers with thicknesses in the range of 10 μm: tape casting, sol-gel coating and electrophoretic deposition.

3.1.3 Tape Casting

Tape casting is a scalable, continuous process ideal for manufacturing flat ceramic plates and films. A suspension of ceramic particles in a liquid is spread over a flat, moving substrate, such as a polymer sheet, and the solvent is evaporated, leaving a flexible tape of ceramic powder in a binder [140]. The green tape can be mechanically processed to give more complex geometries or multiple layers, which are then subjected to heat treatment to give the final cured ceramic body. The suspension or slip consists of the ceramic powder, binders, plasticisers and dispersants in a solvent system. The binder forms a film around the ceramic particles, giving the green tape sufficient mechanical strength to be handled. Plasticisers are added to reduce binder viscosity and improve tape flexibility. Dispersants are used to avoid flocculation in the slip and give a homogenous tape. The solvent is chosen to dissolve all of these additives and evaporate slowly after the tape is cast.

In a typical tape casting operation, as shown in figure 12, a reservoir of the slip is carried under a flat doctor blade which distributes it evenly over the surface of a moving carrier film. The tape is then dried in air to remove the solvent, leaving a flexible green tape. Thickness of the final film is controlled by the size of the gap between the doctor blade and the substrate. In this way a large variety of thicknesses can be realized. By shaping the green YSZ tape, researchers have fabricated ribbed electrolytes suitable for use in monolithic cells [140]. This technique has also been used to fabricate electrolyte films on the order of tens of microns thick [8]. These films can then be laminated with thicker anode tapes in a two roll mill. Careful control of firing conditions and tape shrinkage characteristics are required to obtain flaw free, flat laminates. The resulting anode-electrolyte sheets consisted of 20-40 μm dense YSZ layers on porous, 500-750 μm NiO-YSZ. These cells, with screen printed cathodes, show excellent performance over extended operating times in the operating temperature range of 750°C. The major advantages of tape casting as a production technique for electrode supported planar type fuel cells are its low cost and mass production capability. This technique however is not suitable for fabrication of tubular SOFC's.

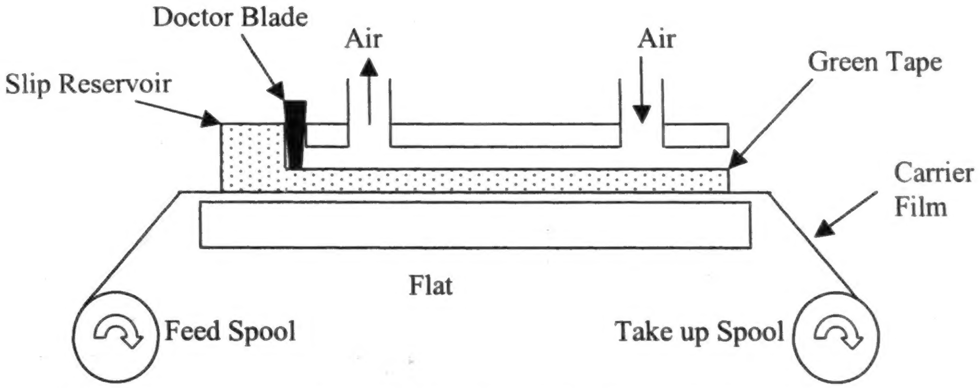

Figure 12: Tape casting apparatus

Tape casting has also been used successfully to deposit 30 μm thick ceria layers onto tape cast nickel-ceria cermet anode supports [81]. There was no decrease in OCV observed at 500°C when compared to thicker ceria electrolytes at this temperature as the electrode is fairly thick and the temperature is quite low. This reasserts the potential of ceria to be used as an electrolyte for cells operating in this low temperature range.

3.1.4 Sol-Gel Electrolytes

An alternative route to fabricating thin oxide films is sol-gel processing. This non-vacuum technique is described in several textbooks and review articles [141, 142, 143]. Strictly speaking a sol is a suspension of colloidal particles in a solution. That means the particles are so small (less than 1 μm) that they are unaffected by gravity, responding only to surface charges and van der Waals forces. Sol-gel processing has expanded this definition of a sol to include solutions containing hydrolyzable alkoxides.

?

This second type of sol, the so-called polymeric sol, is the type of interest for the fabrication of ceramic thin films. These consist of metal alkoxides, in which a metal ion is attached to several alcohol molecules in place of the hydrogen on the hydroxyl group, and a suitable solvent. Such an alcohol, called an alkoxy, can be very long and may or may not have branch molecules sticking out from the main chain. The number of alkoxy groups in a metal alkoxide is determined by the charge on the metal ion; for zirconium, with a charge of 4+, there are four, while yttrium would have only three. Partial hydrolysis of alkoxides leads to the formation of active precursors, which can then link by condensation polymerization to form long chain molecules (see equations 16 and 17).

$$Zr(OR)_4 + H_2O \rightarrow (OR)_3Zr - OH$$

Equation 16: Sol-gel active precursor formation

$$(OR)_3Zr - OH + HO - Zr(OR)_3 \rightarrow (OR)_3Zr - O - Zr(OR)_3 + H_2O$$

Equation 17: Condensation polymerization reaction

In the case where each metal alkoxide is capable of forming three bonds, cross-linking can occur and a large 3D molecule can form. Gelation, which is induced by an increase in alkoxide concentration due to solvent evaporation, occurs at the point where the cross-linked polymer molecule extends throughout the solution. Once formed the gel is then fired, burning off the organic component and oxidizing the metal. The dimensions of the gel are also less than 1 μm, giving a very active surface and allowing the gel to be heat treated at lower temperatures than possible in traditional ceramic processing.

The porosity of the final film is determined by the degree of branching of the alkoxide molecules and the rate of cross-linking (condensation rate) of the sol. More highly branched alkoxides do not interpenetrate as well as linear ones, so the gel is less dense, and so is the fired film. Additionally, if the condensation rate is slow, then upon drying, very few cross links are able to form and the gel formed is very compliant and compresses well, leading to a denser film. By manipulating these parameters it is possible to obtain films with a wide range of porosities [141].

There are two common techniques for sol-gel coating that will be discussed briefly here. In dip coating the substrate to be coated is immersed in the sol and withdrawn at a constant rate. In spin coating the substrate is spun and the sol poured onto its centre. Obviously dip coating results in both sides of the substrate being coated, while spin coating covers only one side. As a result of this dip coating may be useful for application of electrolytes to tubular cells, while spin coating is more useful for planar cells.

When a sample to be dip coated is withdrawn from the bath, some of the sol will be trapped in the boundary layer near the substrate surface, while the rest runs back into the bath. Evaporation of solvent from this trapped layer increases the concentration of the precursor and leads to polymerization reactions. Eventually a gel will form, coating the entire surface of the substrate that was in contact with the sol. Manipulation of the film thickness is best accomplished by altering the withdrawal speed. As this speed increases, the viscous drag increases, trapping more sol in the boundary layer and giving a thicker film.

For coating one side of a flat substrate spin coating is ideal. An excess amount of sol is poured onto the centre of a spinning substrate. The centrifugal force spreads the liquid evenly across the surface of the substrate, with any excess sol spinning off the edges as droplets. As the film thins due to the centrifugal force, evaporation becomes important in increasing the precursor concentration which once again leads to gelation. By increasing the spinning speed the centrifugal force can be increased leading to a thinner film. Conversely, increasing the viscosity of the sol will reduce its sensitivity to spinning, giving a thicker film. While these two processes seem well suited to the fabrication of thin electrolytes on either tubular or planar substrates, there is a problem with film thickness. A significant amount of shrinkage occurs when the film is fired, leading to large amounts of stress which can lead to cracking of the electrolyte layer. To avoid this very thin films of less than about half a micron should be deposited. Therefore, multiple coatings are required to obtain an electrolyte thick enough for SOFC application.

Attempts to fabricate a thin YSZ layer on a porous LSM substrate by dip coating required 10 applications of the sol in order to achieve a 5 μm film [144]. After each coating was applied the sample was dried and sintered at 600°C. After the final coating was applied the samples were again sintered, this time at higher temperatures, and the resulting film was examined by microscopy and hydrogen permeation measurements. Microscopic examinations indicated that sintering at a temperature of around 1100°C gave a dense film, while cracking and porosity of the film were observed at higher sintering temperatures. However, even the sample sintered at 1100 °C showed hydrogen permittivity. Other attempts to grow thin YSZ films, this time on fused quartz substrates, produced similar results with lower sintering temperatures, leading to seemingly more dense, crack free films [145]. The explanation put forth for this is that the resulting film is not dense at all and, at the higher sintering temperatures, there is enough energy available to induce densification. Because the film is constrained by its intimate bond with the substrate it cannot shrink in the direction parallel to the substrate surface, which leads to what is known as constrained sintering cracking if the driving force for sintering is large enough. This includes the formation of cracks and discrete dense particles. The effect of cracking can be reduced by applying more layers and obtaining a thicker film, since shrinkage can then occur in the direction perpendicular to the substrate surface; however, the resulting film still exhibits high porosity. A possible solution to this problem is to increase the green density of the gel, which can be as low as 25%, thereby decreasing the amount of shrinkage necessary for densification. At present no reports of highly successful sol-gel electrolytes have been published, but another colloidal technique, electrophoretic deposition, has shown promise.

3.1.5 Electrophoretic Deposition

Like the sol-gel process, electrophoretic deposition (EPD) is a colloidal deposition technique; however, in this process particulate sols are used. The process takes advantage of the fact that colloidal particles are primarily affected by surface charge rather than gravity. A suspension of the particles to be deposited in an appropriate solvent is prepared, and an electric field is used to propel the particles towards the substrate where they stick. In order for this to work there are certain requirements of the system. First the substrate, which acts as one electrode, must be conductive, and second, the particles must have an appropriate surface charge in the given solution to allow them to be affected by the applied field. For deposition of YSZ as the electrolyte for SOFC's, the anode in its reduced state is a suitable substrate since the nickel provides reasonable conductivity at room temperature [146]. The apparent surface charge, or zeta potential, of the YSZ particles in a given solvent is strongly affected by the pH of the solution [147]. At low pH a sufficient positive zeta potential is reached to deposit thin YSZ films from ketone sols.

The amount of deposited powder can be monitored through the current, and controlled by the deposition time and voltage [147]. There are, however, various factors which can affect the relation between current passed and ceramic deposited, and these may need to be determined experimentally. Firstly, particularly when the pH is very low, some of the current may be carried by free protons in the solution, rather than YSZ particles. Also, as the deposit builds up, it can have a shielding effect which decreases the deposition current. In general, increasing deposition time, deposition voltage or particle concentration in the sol are the best ways to increase film thickness. If the concentration of the particles is made too high, however, agglomeration can occur which leads to a non-uniform deposit. Also it is important that the electric field be uniform as this can also lead to inhomogeneous deposits [147].

The application of this approach to supported electrolyte SOFC's [146,147] shows that the process is capable of depositing thin, crack free layers on porous substrates. In order to achieve this it is important to match the sintering characteristics of the deposit and the substrate fairly well. Additionally, microporosity can also be a problem as results for single layer EPD films on porous anode substrates show that the maximum OCV is less than 85% of its theoretical value. Through the use of multiple coating-sintering steps, the maximum OCV can be increased to very near the theoretical value [147], but the added cost of multiple heat treatments is a definite disadvantage. Plus, to maintain conductivity in the substrate for subsequent depositions, the furnace atmosphere must be controlled to prevent oxidation of nickel. Multiple deposition runs have a minimal effect on the thickness of the deposit, due to the shielding effect of the sintered YSZ layer, but do have a significant effect on its density as pin holes in the deposit become preferred deposition sites [147]. As a result 5 μm layers have been deposited which give OCV's very near the theoretical value. In order for EPD to be competitive with techniques such as tape casting and EVD, it is important to be able to deposit thin, sufficiently dense layers of YSZ in a single deposition/sintering step, and on cathode as well as anode substrates.

3.1.6 Other Electrolyte Systems

Fabrication of thin electrolyte layers of ceria and LSGM has not been as hotly pursued as it has for YSZ. In part this is because the higher conductivity of these electrolytes allows them to be used a thick layers at lower temperatures. Additionally, for the case of LSGM, the increased complexity of the electrolyte makes it much more difficult to fabricate thin layers with the desired properties. Clearly, if the thickness of these electrolytes can also be reduced to the order of tens of microns, then operating temperature could be reduced even further to around the 500-700°C mark. In this temperature range it is expected that carbon deposition from methane on nickel anodes will not be problem [103]. This section will focus on efforts to produce thin layer LSGM electrolytes.

Because of the multi-component nature of LSGM, EVD is poorly suited to the fabrication of thin layers of LSGM, and the reactivity of LSGM with nickel makes it impractical to deposit a thin layer on an anode substrate by tape casting followed by sintering [148]. In order to prevent such a reaction a pure, highly porous (>60%), YSZ substrate can used [148]. A slurry of fine LSGM particles is then applied and this assembly is fired in order to densify the LSGM film. Final film thickness on the order of 15 μm can be achieved. After the electrolyte is sintered at high temperature (1400°C), the anode substrate can be impregnated with a nickel nitrate solution and dried. After drying the assembly is heated to 700°C to decompose the nitrate and leave NiO in the pores. Several repetitions of this process are required to obtain sufficient nickel concentration in the anode, before a final sintering step is conducted at 1000°C.

While this process results in thin, dense LSGM layers and a significant reduction in reactivity between the anode and electrolyte, there is still significant interdiffusion of species from the electrodes and the electrolyte. This leads to higher than anticipated electrolyte resistance [148]. Therefore, it is clear that the possibility of manufacturing supported LSGM electrolytes exists; however, it is vitally important to find supporting electrode materials that are compatible with LSGM during fabrication as well as at operating temperature.

Another attempt to manufacture thin LSGM electrolytes used the EPD process with acetone as the solvent [149]. Addition of iodine to the solvent results in sufficient surface charging of the LSGM powder to allow deposition at voltages around 30 V. After deposition the sample is allowed to dry in air before sintering. In order to obtain sufficient density, several deposition runs are required and after each deposition the sample must be dried in air and sintered at 1400°C. After five repetitions of these deposition and sintering steps a dense LSGM layer of about 4 μm thick can be obtained. Although the films resulting from this procedure have high conductivity and reasonable density, the requirement for multiple sintering steps is a serious drawback, and it is still important to find a substrate material that will not react with LSGM during sintering.

3.2 Electrode Manufacturing

As has already been discussed the microstructure of fuel cell electrodes plays a major role in determining how well they perform. Therefore, it is important for a successful manufacturing process to give highly reproducible results at a reasonable cost. In this section several potentially commercially viable procedures will be described and their advantages and limitations discussed. Because in many cases one of the electrodes is a supporting structural member, they can be fabricated by conventional bulk ceramic processing techniques. An example is the extrusion technique used by Westinghouse to fabricate cathode support tubes for their sealless tubular cells. However, in all cases at least one electrode, be it anode or cathode, is deposited onto the existing cell as a film. Many different techniques have been applied to this problem with varying degrees of success.

An important factor in determining the structure of any ceramic or cermet structure is the characteristics of the starting powder, which are highly influenced by the techniques used to manufacture the powder. These techniques are beyond the scope of this work; however, in general a fine homogeneous powder is desired. Finer powders are more active for sintering; therefore, shorter sintering times and lower sintering temperatures can be used to get the desired structure, whether it be dense or porous. This means that there will be less interaction between the various components of the fuel cell during fabrication.

3.2.1 Pressing and Sintering

The simplest technique for fabricating electrode substrates for SOFC's is to press oxide powders into pellets and sinter them to the appropriate density. This technique is widely used in experimental studies [20, 54, 90, 95, 106, 150], where the size of the cell is relatively small. Commercial cell development, on the other hand, tends to require much larger cell areas. This requires roll pressing in order to manufacture these cells efficiently.

A variation of pressing and sintering is the coat-mix process [151]. In this process powders of NiO and YSZ are mixed with a hot binder solution. Cooling this mixture with acidified water causes the binder to envelop the powder. The resulting powder can be easily pressed into substrates that are suitable for handling. Substrates made by this technique have been shown to have good gas permeability and a fine pore structure; however, in order to improve anode performance and lower pore size for thin film electrolyte application, a finer active anode layer is often applied by a slip casting process [152].

3.2.2 Tape Casting

This technique, which is so applicable to electrolyte fabrication, brings the same advantages to electrode manufacturing. Tape casting has been used to make porous anode substrates ranging in thickness from 500-1500 μm [8, 151]. Although designed for the manufacture of thin dense layers, it can be readily adapted to form porous layers. Green tapes can then be laminated to electrolyte tapes and cut to the desired geometry quite easily [151]. In order to avoid warpage or cracking when sintering these anode-electrolyte laminates, it is important that the differential sintering shrinkage of the two layers be kept below about 5% [153]. This can be difficult since one of the layers is, by design, fully dense while the other is highly porous. One technique proposed to minimize this difference is the addition of pore forming agents (PFA's) to the anode slip [153, 154, 155]. PFA's are organic additives that are burned off during binder removal and sintering steps, leaving voids behind. Examples include starch, polyethylene beads or graphite flakes. The amount of PFA required to form a continuous open path through the electrode substrate is dependent on the morphology of the PFA. The flat graphite is capable of forming such a network at lower additions than are spherical particles. Addition of PFA to the slip does alter its properties; therefore, it is important to make appropriate additions of other organic additives so that the green tape is still handleable.

Using this technique it has been shown that layers of 80% porosity and fully dense layers can be successfully laminated together. A similar technique, also using pore formers, has been used by Ceramic Fuel Cells Limited [8]. With appropriate firing conditions and kiln furniture, flat, crack free anode-electrolyte laminates suitable for use in SOFC stacks can be produced. Because tape casting is a well developed technique capable of mass production and bearing the above reported results in mind, it seems likely that it will play a major role in the commercialization of SOFC technology.

3.2.3 Extrusion

The previous two techniques discussed, although useful for manufacturing planar substrates, are not applicable to tubular designs. The approach taken by Westinghouse to fabricate their tubular cathode supports is extrusion. In this technique a plastic feed material is forced through a die into the desired shape, in this case a tube [156]. The plastic feed is generally prepared by mixing the required organic additives with ceramic powder. Once the feed is shredded and de-aired it is forced through the extrusion die using an auger. The formed tube is then fired to give a porous ceramic body. Like tape casting, extrusion is a well established industrial process that is capable of mass production [126]. The difficulty, therefore, with fabricating tubular cells is not substrate fabrication but deposition of the electrolyte and interconnect, which are typically done by EVD.

To this point the focus has been on techniques for the mass production of thick electrode substrates, rather than on techniques that are used to control electrode microstructure or deposit the second electrode. These will be discussed next.

3.2.4 Screen Printing

Screen printing is a simple procedure capable of depositing electrode layers on flat self supported or electrode supported electrolytes. For cathode deposition, a slurry of LSM or LSM and YSZ powders is prepared. This slurry is then forced through a stenciled screen, giving a patterned layer. The slurry can then be dried and fired to give a solid, porous electrode. The openings in the screen should be several times larger than the size of the particles in the slurry, and the slurry should flow well. Screen printing has been used to print anodes [87,157] and cathodes [76]. For anode deposition a mixture of NiO and YSZ is used as the typical starting powder. Aqueous or organic solvents can be used, and the resulting electrode layer is typically a random dispersion of the starting powders with a thickness from a few to several tens of microns. Multiple coatings can be applied to increase the thickness and changing the slurry characteristics between applications can lead to graded electrode structures. The simplicity and low cost of this technique make it very useful for applying the cathode to tape cast anode supported anode/electrolyte plates for commercial applications [8].

3.2.5 Powder Spray Techniques

An alternative method for the deposition of non-load bearing electrodes are spray painting techniques. Here powders of the electrode material are dispersed in a solvent and sprayed onto the electrolyte [4, 158]. Usually a dispersant is added to the spray mixture to prevent agglomeration of the particles, allowing for a finer, more active microstructure. During the spraying process some of the solvent evaporates; however enough, is left behind that the deposited layer can flow and level itself. After the deposit is completely dried, the binder is removed and the ceramic is sintered in a single step [158, 159]. The spraying mechanism is nothing more than a modified paint gun, and the electrode can be patterned easily by the use of a mask. The thickness of each layer is dependent on the spray parameters and particle size, and the total thickness can be increased by using multiple coatings. This technique has been used to make composite anodes [4] and cathodes [152, 158, 159, 160], as well as graded structures in which an LSM-YSZ cathode is deposited on the electrolyte layer, and this layer is then covered with a pure LSM current collecting layer [158, 160]. Scaling to larger substrates is easily achieved by spraying a series of overlapping stripes, and it is also possible to coat curved substrates, increasing the applicability of the process.

3.2.6 EVD

For sealless tubular cells the anode is applied to the outside of the tube over the thin YSZ electrolyte using the EVD technique [126]. Once the tubular cathode-electrolyte structure has been fabricated by methods already discussed, metallic particles are slurry coated onto the electrolyte [104]. Once this layer has been deposited, the EVD technique is used to apply a layer of YSZ over the metal making a cermet electrode. Unlike EVD of the electrolyte, which gives self-leveling growth, this process leads to preferential growth of the oxide layer along the metallic surface. Again the source materials for the YSZ layer are yttrium and zirconium chloride vapours, and oxygen is delivered through the ceramic electrolyte. A reaction between the chloride vapours and the oxygen ions at the three-phase boundary (3PB) leads to the deposition of YSZ and the release of electrons. Electrons are then returned through the electrolyte to the cathode due to the small degree of electronic conductivity present in YSZ. From this initial deposit growth is possible in two directions, along the electrolyte surface or along the metal surface; this is shown in figure 13. For growth along the electrolyte surface, ions can come from the electrolyte film, or the YSZ deposit, and electrons are returned directly to the electrolyte film. When the oxide grows along the metal surface, ions have to pass through the deposit; however, at the deposition temperature the ionic conductivity of the deposit is quite high; therefore, this process is rapid. The electrons released by the reaction can be returned to the electrolyte film through the high conductivity metallic particles. Initially, this provides little advantage over growth along the electrolyte film surface, so growth should occur equally by both mechanisms. The result is a thickening of the electrolyte film which leads to an increase in electronic resistance of the film. Once this has occurred growth becomes faster when electrons can take a short cut through the metallic particles. Then growth becomes faster along the metal surface. The result is a coating of YSZ over the metal particles which leads to a large increase in available 3PB sites (figure 13).

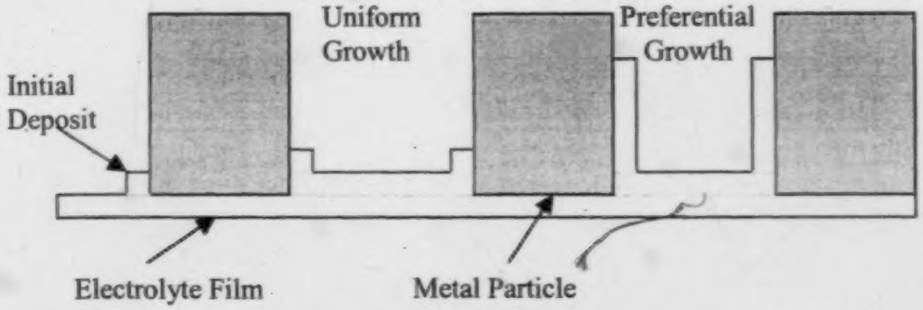

Figure 13: Cermet growth by EVD

Unlike the electrode fabrication techniques discussed before, EVD gives a predictable arrangement of the ceramic and metal phases. The ceramic coating helps to support the metallic phase, limiting ageing due to nickel agglomeration and providing very good contact between the metal and electrolyte. Experiments using ruthenium as the metallic phase show that very fine structures can be fabricated in this way and result in excellent performance [104]. The technique is best suited to tubular designs since the requirement of high temperature sealing is avoided; however, it could still be used on planar cells. Drawbacks are that it leads to an increase in electrolyte thickness, and it requires electronic conductivity in the electrolyte phase in order for growth to occur. Therefore, a conflict between cell performance and maximum growth rates exists.

3.2.7 PEVD

Polarized electrochemical vapour deposition (PEVD) is a modified form of CVD which seeks to eliminate the drawbacks of EVD. Like EVD the growth of an electrolytic film is caused by the electrochemical reaction of vapour species with oxygen ions. The difference is that, rather than a chemical potential difference being the driving force for ion migration, it is an externally applied electrical potential difference [161]. This allows for much better monitoring and control of the deposition process, and should improve the deposition rate. The current can be used to monitor the deposition kinetics, since the electronic conductivity of the electrolyte is very low [161]. This means that it can reasonably be assumed that the current being passed through the external circuit is equal to the ionic current through the electrolyte. By monitoring the current in the external circuit then, it is possible to monitor the extent of deposition.

Another similarity to EVD is the growth pattern of the deposit; however, because there exists a short circuit electronic path from the anode to the cathode, thickening of the electrolyte layer should be less prevalent. Therefore, the deposit occurs only at the 3PB and growth is highly favoured along the metal surface. As a result the layer grows over the metal enveloping it completely. This moment of complete coverage of the metal is accompanied by a sharp drop in current [161]. Once the entire metallic surface has been covered the film begins to thicken [162]. Because the electronic conductivity of the YSZ is very low, the deposited film is very thin [163]. Unlike slurry methods which used mixed particles of Ni and YSZ, the ceramic phase in PEVD does not interfere with the electronic path that exists through the metal. The result is a cermet with nearly the electronic conductivity of the porous metal. Additionally, the coating prevents sintering and vapour loss of the metallic phase as well as preventing poisoning of the anode by impurities in the fuel.

The deposition temperature for PEVD is on the order of 1000°C, which is lower than typical firing temperatures for cell components produced by more traditional means. Because of this, interdiffusion and reaction problems between cell components should be reduced. The very nature of the deposition process ensures intimate contact between the metal and ceramic phases in the electrode, which helps inhibit sintering, and also ensures good contact between the anode and electrolyte, thereby reducing interfacial resistance. The coating layer will affect the porosity of the electrode; however, since studies have shown that the deposit is usually very thin this should not be too much of a problem [162, 164]. Potential major drawbacks of PEVD electrodes are a loss of catalytic activity, due to complete coverage of the metal surface, and poor electronic conductivity of the coating. The latter prevents electrons from moving from the free surface where the reaction with the fuel occurs to the metallic phase, and could lead to increased contact resistance between the electrode and the interconnect or current collector.

Chapter 4 Experimental

4.1 PEVD Processing

The PEVD process was used to apply a thin YSZ coating over a platinum electrode on a self-supporting 8YSZ electrolyte disk. The purpose being to determine how the electrochemical performance of cells treated by PEVD depended on the deposition conditions, particularly deposition time, temperature, and the bias voltage in order to determine an optimum processing route for PEVD. YSZ disks (Ceraflex 8Y, Nikki Shoji Co. Ltd.) were 25 mm in diameter with a nominal thickness of 0.5 mm. Typical analysis of these electrolytes is given in table 1 (section 4.4). Prior to deposition of platinum electrodes on the electrolyte, the disks were washed with ethanol and calcined at 700°C for one hour to ensure a clean surface. Circular electrodes were applied by screen printing Electro-Science Laboratories platinum paste (5542-J-1) onto the electrolyte. Electrode diameter was 13 mm and four layers were applied to each side to build up electrode thickness. A single layer of Pt paste was applied to the anode side as a reference electrode at a distance of about 1 mm from the anode. After each layer of platinum was deposited, it was dried at 90°C for 20-30 minutes and fired at 950°C for 10 minutes in an electric furnace. Platinum mesh was pressed into the final layer on both the anode and cathode side, before firing, as a current collector. Platinum lead wires were then attached to the current collectors by spot welding and a lead wire was attached to the reference electrode using additional platinum paste.

The cell, thus prepared, was then attached to an alumina support tube using high temperature cement (Aremco 503). This setup is shown schematically in figure 14. Other sealing materials were also tried including Heraeus IP9105HT, most of the glasses tried had too low a softening temperature, while the IP9105HT did not have the an appropriate TEC The cement was cured according to the manufacturer's specifications with slight modification. First the cement was dried for two to four hours at 90°C in a drying oven. After initial drying the cement was cooled and examined for cracks, which were repaired as necessary. Then the cement was again dried at 90°C for 2 h, this time in the PEVD reactor furnace. After this second drying period the cement was cured for 2 h at 260°C, and 2 h at 370°C. Once curing was complete the tube and cell were heated directly to the deposition temperature, which ranged from 900 to 1050°C.

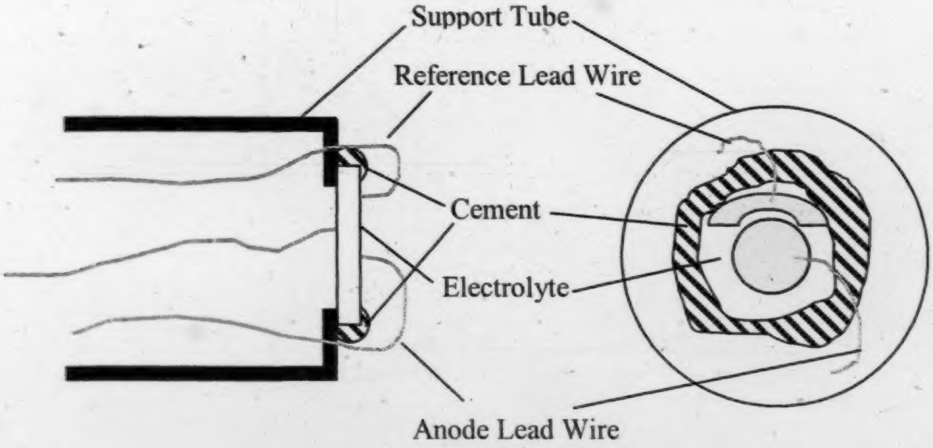

Figure 14: Support tube/electrolyte setup

The PEVD reactor consists of a tube furnace and an alumina reactor tube. The ends of the reactor tube are sealed to an aluminum frame which allows for easy insertion and removal of the support tube, as well as the PEVD source material. A schematic of the PEVD setup is shown in figure 15. Powders of yttrium and zirconium chlorides (Aldrich 99.99% YCl_3 and 99.9+% $ZrCl_4$) were used as the source material. The powders were stored in a glove box connected to the reactor under a dry air atmosphere, to prevent reaction with atmospheric water prior to deposition. For deposition the chlorides were placed in glass sublimation tubes and inserted into the reactor until they reached the desired temperature. The temperature of each chloride was monitored by a K-type thermocouple mounted in the sublimation tube and an Omega model HH22 microprocessor thermometer. The reaction chamber was evacuated to a total pressure of less than 1 torr, as measured by a Pirani gauge, using a Welch Duo-Seal vacuum pump. A second pump was used to evacuate the inside of the support tube. Argon (Praxair, pre-purified) was passed through a drying column containing magnesium perchlorate (Fischer M54-500) and Drierite ("the versatile desiccant") as an indicator and then through the sublimation tubes as a carrier gas. An additional flow of dry argon was used to maintain gas flow throughout the chamber. Argon flow was monitored via rotameters (Cole-Parmer), and the flow rate was controlled manually. Air (Praxair, T.O.C. grade) was bled into the inside of the support tube to act as an oxygen source for the deposition reaction. A mass flowmeter (Omega FMA-5605) was used to monitor the air flow rate, while a needle valve was used to make necessary adjustments.

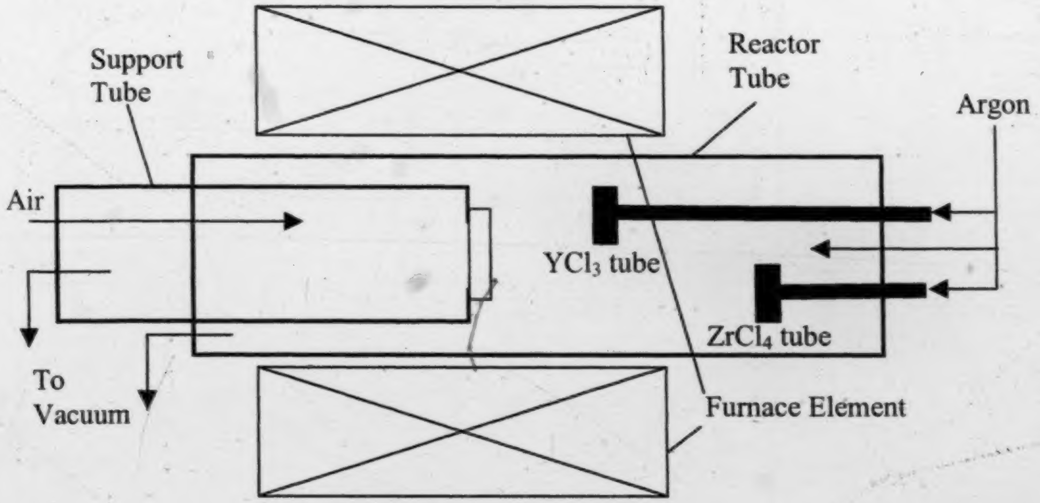

Figure 15: PEVD reactor schematic

The open end of the support tube was sealed with a rubber stopper, which had holes through it to accommodate the air inlet and vacuum tubes. Lead wires for the anode, cathode and reference electrodes also exited at this end. For most of the deposition runs the three leads were connected to a Princeton Applied Research model 371 potentiostat-galvanostat (PAR 371). The anode was connected to the working electrode and the cathode was the counter electrode. In some cases a constant voltage was maintained between anode and cathode, and in others between the anode and reference electrode. The voltage range used for all runs with the potentiostat was from -500 to +300 mV, and the corresponding current was recorded with a dual channel analog chart recorder (Brinkmann Instruments).

For a few of the deposition runs, the anode and cathode lead wires were connected through a decade resistance box. The resistance was varied to control the deposition current, which was again recorded by the chart recorder. Cell voltage during the deposition run, as well as the voltage drop between the anode and the reference electrode, were intermittently recorded during deposition.

4.2 Electrochemical Investigation

In order to determine the effect of the deposition voltages investigated electrochemical performance of the cells was measured after deposition under different conditions. Electrochemical characterization of the cells was done at three or four different temperatures before and after deposition. Polarization curves were generated using the decade resistance box, a Keithley 612 electrometer to record cell voltage and a digital multimeter to record current. The setup is shown schematically in figure 16. Initially the circuit was opened and the voltage recorded. Then the circuit was closed, and the voltage and current through the circuit were measured and recorded. The resistance of the resistance box was lowered in steps and the current and voltage were recorded at regular intervals. The voltage was then plotted as a function of current to generate the polarization curve. For cells where deposition was conducted at 950°C or less, these I-V curves were generated at 750, 850 and 950°C both before and after deposition. Hydrogen (Praxair, pre-purified), humidified by bubbling through water at room temperature, was used as the fuel while compressed air (Praxair, T.O.C. grade) was used as the oxidant. Argon was mixed with the hydrogen fuel at a volume ratio of about 1:1 as this was observed to give higher, more stable open circuit voltages. The hydrogen flow rate was measured using a rotameter, while the same mass flowmeter was used for air flow measurement as in deposition. These electrochemical tests were conducted upon heating of the sample before deposition and during cooling of the sample after deposition in order to clearly illustrate the effect of PEVD on cell performance. From these polarization curves power density curves were also generated by multiplying the current density by the voltage. This product was then plotted as a function of current density. The voltage drop due to electrolyte resistance was removed from these curves using published data for the conductivity of YSZ [31].

For some cells complex impedance plots were also made using a Princeton Applied Research 273 potentiostat (PAR 273) and a Solartron 1255 frequency response analyzer controlled by a computer running Corrware and Z-plot electrochemical and impedance software. These tests were not done on all the cells because some drift was detected in the potetntiostat output. This made it impossible to compare the results of one test run to another, but did not affect the ability to track changes during a single deposition run. All of the data used in the following section, with the exception of impedance data was generated using the PAR 371, which functioned well throughout testing.

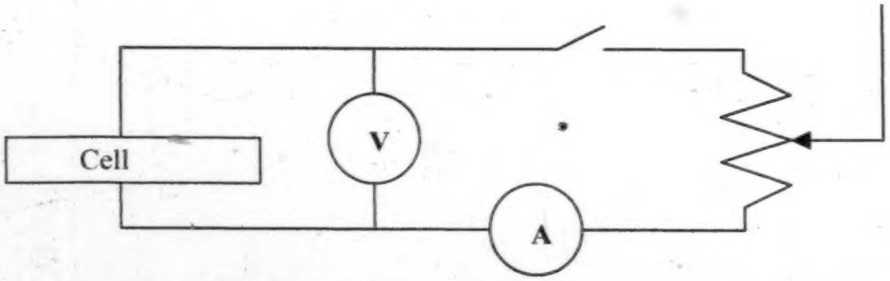

Figure 16: Schematic of setup for polarization measurements

4.3 Microstructural Examination

After deposition and electrochemical testing, the samples were prepared for microstructural examination. Plan views of the sample were examined by SEM (Hitachi H-2700) and EDX (Princeton Gamma Tech, Prism IG, Intrinsic Germanium Detector with thin film window and PGT Imix analysis) after carbon coating. Cross sections were prepared either by mounting the specimens in Lucite followed by sectioning with a diamond wafering blade (Beta diamond products 515-H) and a precision saw (Buhler Isomet 4000) or by fracturing the samples. After sectioning the mounted samples, one cross section was ground down to a 600 grit finish using silicon carbide paper then polished using 6 μm diamond paste. Both the polished and as sectioned cross sections were carbon coated and again examined by SEM and EDX. Fractured samples had a less disturbed microstructure; however, the surface was much rougher, leading to increased difficulty in characterizing the electrode by EDX.

Some samples were also examined using an electron microprobe equipped with wavelength dispersive x-ray spectrometers (WDX), and a cathodo-luminescence (CL) detector. The higher resolution of WDX compared to EDX was required to resolve the low energy zirconia peaks, which overlap with those of platinum. Because zirconia is somewhat cathodoluminescent the CL detector could be used to identify areas with sufficient YSZ content for analysis by WDX. X-ray diffraction (XRD) was also used on some of the samples to identify the phases present in the electrodes. In order to do this a thin film setup was required.

4.4 Materials

The tables in this section show the compositions of the materials used in these experiments.

Table 1: Analysis of YSZ electrolytes

Component	Weight %
Y_2O_3	13.79
HfO_2	1.6
Al_2O_3	0.074
Na_2O	0.035
SiO_2	0.032
Fe_2O_3	0.003
MgO	0.001
ZrO_2	remainder

Table 2: Analysis of YCl_3 powder

Component	Concentration (ppm)
Si	67
B	2
Co	0.8
Mg	0.7
Fe	0.5
Yb	0.5
Lu	0.1
YCl_3	Remainder

Table 3: Analysis of $ZrCl_4$ powder

Component	Concentration (ppm)
Sn	25
Mn	6.7
Fe	3.3
Na	1.8
$ZrCl_4$	Remainder

4.5 Engineered Porosity Samples

In addition to the tests above on home made samples, tests were also done on samples made at the University of Waterloo using the coated pore forming agent technique discussed in section 3.2.2. This technique allows direct control of the porosity and pore size of the electrode without leading to excessive shrinkage during firing. The samples used were NiO-YSZ composite anodes with varying nickel compositions, and a thin, pre attached YSZ electrolyte. The amount of nickel in the electrode ranged from approximately 10.8 to 14.0 vol% and were made using graphite as the PFA. The samples were reduced in a hydrogen atmosphere at 800°C for two hours, following which the resistances of the samples were measured at room temperature with a two-point setup, and in cases where the conductivity was high, a four-point probe as well. For electrochemical testing a platinum cathode was screen printed onto the electrolyte and a lead wire was attached to the cathode. Then the anode was again reduced in a hydrogen atmosphere to convert the NiO to Ni, and a lead wire was attached using platinum paste. The cell was then mounted on the ceramic support tube as shown in section 4.1. Polarization measurements were made in a moist hydrogen atmosphere with air in the cathode chamber.

Chapter 5 Results and Discussion

5.1 Deposition

The major manipulated variables in the deposition process were the temperature of the cell, the deposition time and the driving force for deposition. Other variables such as chloride temperature, gas flow rates and system pressure were generally kept as constant as possible using the given equipment. That being said the nature of the experiment, a high temperature, vacuum process, makes it difficult to control these variables. The chloride temperatures were measured with K-type thermocouples that were placed very near the chloride powders. These allow for temperature monitoring accurate to about 0.4%. Temperature control was achieved by manually adjusting the position of the sublimation tubes in the furnace. By this technique it was usually possible to reproduce chloride temperatures to within ± 5°C from run to run. This small deviation should not have too much effect on the composition of the final deposit, but from the beginning of the deposition run to the end, the temperature of each chloride tended to increase by as much as 5-10°C without adjusting the tube position. In most runs, no compensation was made for this fluctuation; however, in cases where the temperature increase was substantial the tube was withdrawn slightly. A 10°C increase in yttrium chloride temperature from 835 to 845°C, with a corresponding increase in zirconium chloride temperature from 165 to 175°C, would alter the composition from 8.4 mol% yttria initially, to 6.0 mol% yttria at the final chloride temperatures. This may not seem like a large difference in composition of the deposit; however, this composition is right at the edge of the stable range for the cubic phase and could have a significant effect on deposit conductivity.

An additional source of error in the final yttria content could come from the Hertz-Knudsen relation (equation 13) used for calculating evaporation rates of the chlorides as a function of temperature. Two assumptions, which may not be entirely valid, were made in the application of this equation. First it is assumed that the area for evaporation (surface area) of the two chlorides is equal. This is likely untrue, since the sublimation temperature for the yttrium chloride is above its melting point while the zirconium chloride is still solid at its sublimation temperature. Thus the yttrium surface area will be the surface of the liquid pool in the sublimation tube. The zirconium chloride, being a powder still, can have a much larger surface area. Only the zirconium chloride surfaces that are directly exposed to the atmosphere will likely make a significant contribution to the evaporation rate though, as the other surfaces are likely to encounter a significant background pressure of the chloride.

The second assumption is that the evaporation coefficient, α, is unity for both chloride powders. Initially, this is probably true, since for clean surfaces this factor is very close to one. However, as the test runs and indeed as the storage time of the chlorides increases, oxidation or contamination of the powder may occur, reducing the evaporation coefficient. To limit the effect of long storage times on the chloride powders the zirconium chloride was stored in a sealed bottle while not in use; however, due to its small particle size, it is still possible that some oxidation of the chloride did occur over time. The yttrium chloride was stored in the dry box in an open container. Because it comes in bead form, however, it must be ground immediately before use. This exposes a clean surface which should allow for a high evaporation coefficient. It was hoped that these measures would, at least initially, give a predictable and repeatable evaporation rate. At high temperatures the chlorides are more susceptible to reactions with contaminants; therefore, in order to prevent contamination, it is vital to have a good vacuum system and clean gas supplies.

The evaporation rates of the two chlorides, calculated from the Hertz-Knudsen relation and two different sets of vapour pressure data, are shown in figure 17 as a function of temperature for an evaporation coefficient of one.

The melting temperature of yttrium chloride is around 710°C and, as can be seen from the graph, its evaporation rate can be quite low compared to that of zirconium chloride in the temperature ranges shown in figure 17, depending on the source data used. To determine the yttrium chloride temperature needed to get an 8mol% YSZ deposit, the temperature of the zirconium chloride was first set. For example, using one set of data, when the zirconium chloride temperature is set to 200°C, an evaporation rate of about 2.8×10^{-3} mol/s/cm^2 is calculated from equation 12 using $\alpha=1$. Thus, assuming the deposition rates of the two chlorides are the same, an evaporation rate of 4.8×10^{-4} mol/s/cm^2 is required for the yttrium chloride. From figure 17 b), this occurs at a temperature near 875°C. This temperature is fairly high, especially when the deposition temperature was only 900°C, so normally the zirconium chloride temperature was set to a temperature in the range of 160-170°C and the yttrium chloride temperature used was 720-730°C.

Calculations of the yttria contents of the films based solely on the evaporation rates of the chlorides have shown significant discrepancies in published data. Using one set of data [165] for the evaporation of yttrium chloride at 880°C and zirconium chloride at 200°C, the yttria content of the film should be just over 8 mol%. Using another set of data [165], with the same conditions, gives a yttria content of only 3.4 mol%. This shortfall in yttria content according to the second set of data became more pronounced at the temperatures commonly used in these experiments. For example, when the yttrium chloride temperature is 735°C and the zirconium chloride is at 163°C, the maximum yttria content arrived at from the gas composition is only 0.8 mol%, while the other set of data yields a yttria content of 15 mol%.

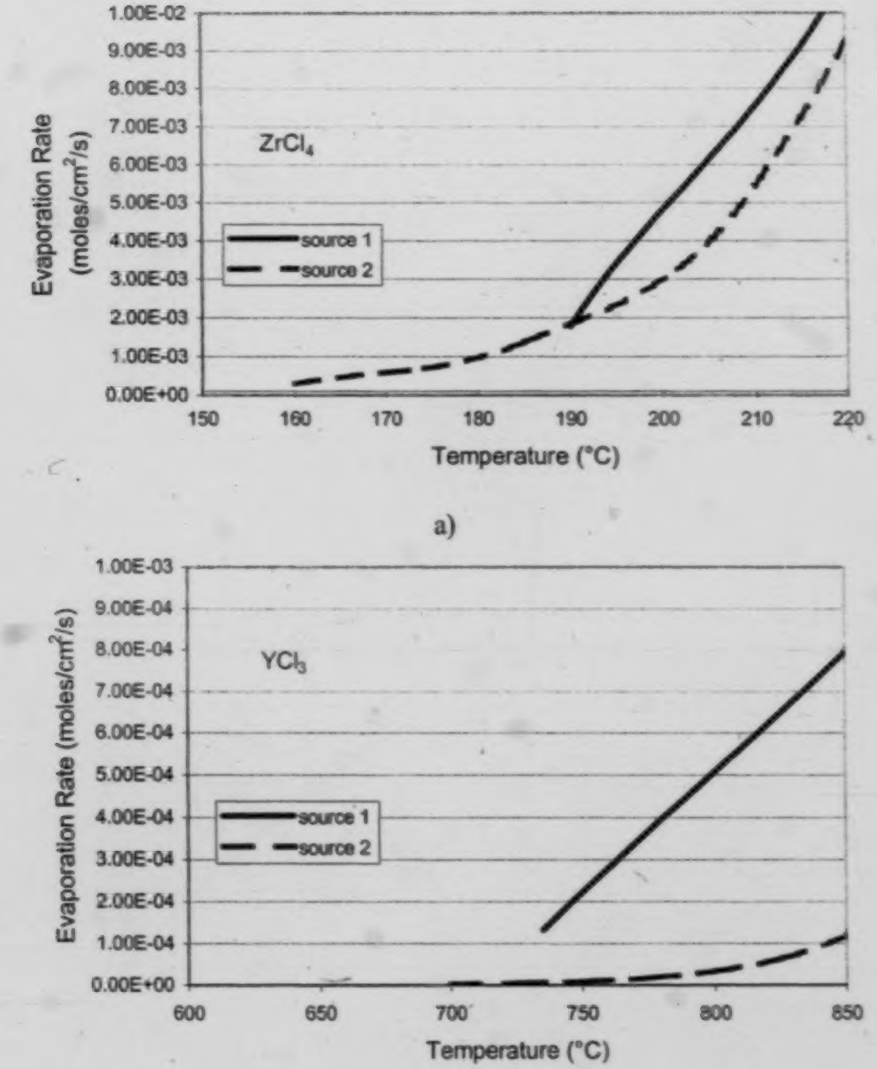

a)

b)

Figure 17: Molar evaporation rates for zirconium (a) and yttrium (b) chlorides from two different data sources

The final film composition may well be different than that expected from the ratio of the two reacting constituents in the gas phase, due to different reaction rates. In order to determine the relationship between film composition and gas phase composition it would be necessary to directly measure the composition of the gas phase, since we have seen that there are significant variations in gas compositions calculated using different sets of published data. In order to do this some changes would need to be made to the current experimental setup, but this could lead to a better understanding of the PEVD reaction.

Two other factors that may be important for the deposition reaction are the system pressure and the gas flow rates. The gas flow rates determine the delivery rate of the chlorides to the cell and play a role in determining the evaporation rates of the chlorides. When the gas flow rate is high enough the background chloride pressure that the powders are exposed to is essentially zero, so the evaporation rate is maximized. If the flow rate is too low an appreciable background pressure of chloride may exist, which would lower the evaporation rate from that calculated. Keeping the argon backflow as the dominant gas flow ensures that the relative amount of each chloride reaching the reaction zone per second is determined by its evaporation rate, rather than its carrier gas flow rate. A higher gas flow rate should reduce the thickness of the diffusion boundary layer at the cell surface and thereby reduce the effect of diffusion on the reaction rate.

It is also important to have a good vacuum to prevent reaction of chloride vapours away from the electrode. This requires a leak free system and removal of contaminants from the reactor surfaces before deposition. To remove contaminants, the surfaces were heated to the deposition temperature under argon, and then the reactor was pumped down to the deposition pressure. After this, a dry mixture of argon and hydrogen (5% H_2 in Ar) was passed through the system. This eliminated any free oxygen from the system. To purge the system of water vapour, dry argon was again run through the reactor. A shielding flow of dry argon was maintained through the sublimation tubes throughout this process to protect the chlorides from accidental oxidation.

By controlling the system pressure it is possible to control the mean free path of the components in the gas phase. In this case, it was desirable to have enough gas phase collisions to attain an even distribution of the reacting gases. With the current setup the only way to control the system pressure was by altering the gas flow rates. This proved difficult to do at reduced pressure, with the valves available. As a result, for the deposition runs, the system pressure was in the range of 0.5 to 0.7 torr, giving a mean free path of about 0.5 μm in the deposition region if a molecular diameter of 0.3 nm is assumed for all constituents. This distance is short enough that a large number of collisions will occur before the vapour species arrive at the cell.

Another variable that should affect deposition rate, along with arrival rate of reactants, is the deposition voltage. The deposition voltage was controlled using a potentiostat and either a two or three electrode setup. In most cases the anode was held at a negative voltage with respect to either the cathode or the reference electrode in the anode environment. It was found that there was very little correlation between the deposition voltage and the reaction rate, as measured by the current. In two different runs, both at the same voltage and with other conditions very similar, the current differed by close to two orders of magnitude. This suggests that there is some other factor that plays a role in determining reaction rate. Of the monitored deposition variables, the only one that differed was the gas flow rate where, in the case with the lower current, no back flow of argon was maintained. The flow rates of argon through the sublimation tubes were higher for that run though, so the total argon flow rate through the system was similar for the two runs.

One factor which has an effect on the current is the cathode reaction rate. In both of the deposition runs mentioned above, the air flow rate to the cathode was identical; however, the active cathode area may have been different. In the process of attaching the cell to the support tube a layer of cement is placed around the hole in the tube and the cell is pressed into this layer. This causes cement to squeeze towards the centre of the cell, which can partially cover the cathode. The degree of cathode coverage was not carefully monitored from run to run and it is reasonable to assume that when more cathode area is covered, the cathode reaction rate will decrease, which may play some role in determining deposition current. Another possible contributing factor is contact resistance in the cell.

5.2 Deposition at 1050 °C and -300mV

For the early tests electrochemical analysis consisted of electrochemical impedance spectroscopy as well as current-voltage measurements. Impedance measurements were done before, during and after deposition in the chloride environment and after deposition in a fuel cell operational environment. The purpose of these measurements was to determine the extent of deposition required for optimum cell characteristics. However, due to a malfunction in the potentiostat (PAR 273), the data generated may be erroneous in some cases. The same can be said for the polarization curves generated with this instrument. Later tests (cell 500-15 onwards) were done using an older potentiostat, with no interface for the frequency response analyzer. Therefore, no impedance data were collected and polarization curves alone made up the electrochemical analysis. These were done in a cathode atmosphere of air and an anode environment of moist hydrogen mixed with argon. The reason the fuel was mixed with argon was that it was observed that this tended to lead to higher, more stable, open circuit voltages.

The key deposition statistics for the cells deposited under these conditions are shown in table 4, while Figures 18 and 19 show the I-V and power density vs. current density curves, respectively for these cells at all four testing temperatures. By carefully examining these curves it is hoped that more knowledge of what goes on during deposition can be obtained.

Table 4: Deposition statistics for cells deposited at 1050°C and -300mV

Cell	Deposition Time (min)
500-19	1346
500-20	1396
500-21	2654
500-26	8470
500-27	4014
500-39	3210

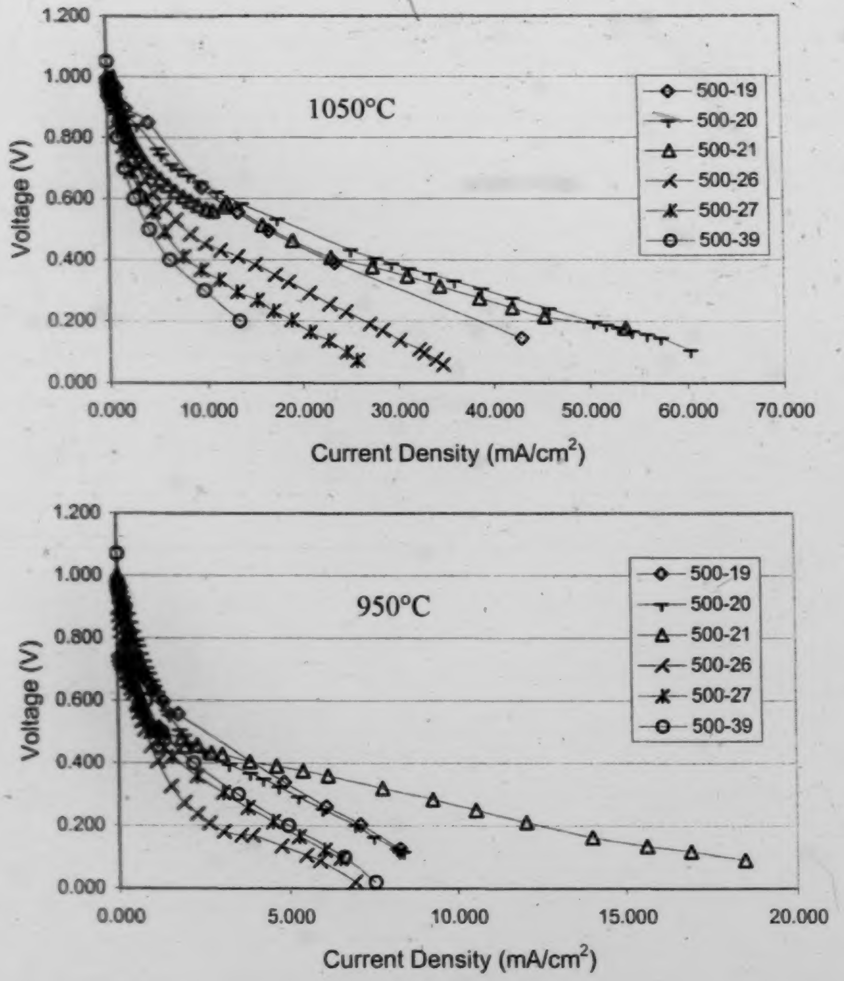

Figure 18: I-V characteristics of cells deposited at 1050 °C and -300mV

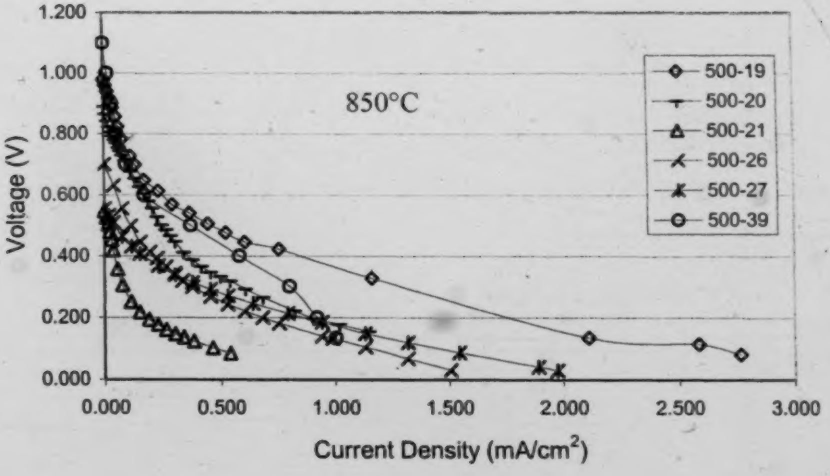

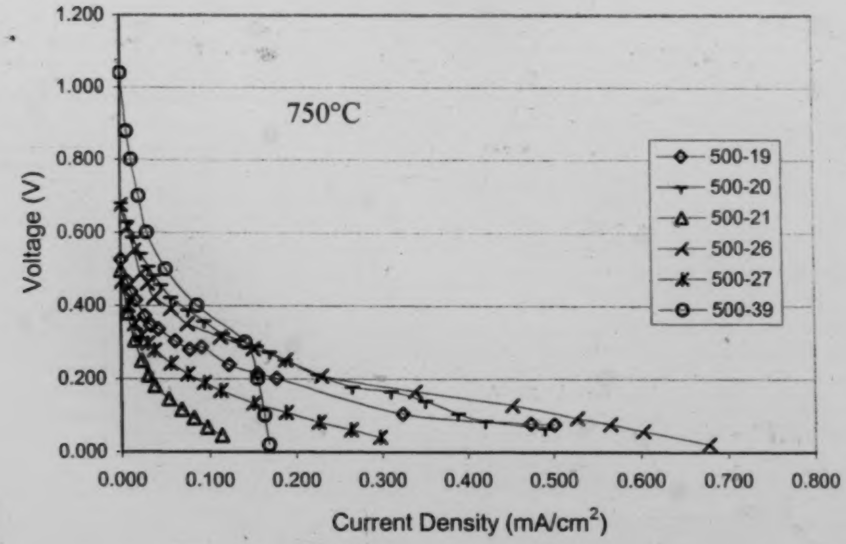

Figure 18(cont'd)*:* I-V characteristics of cells deposited at 1050 °C and -300mV

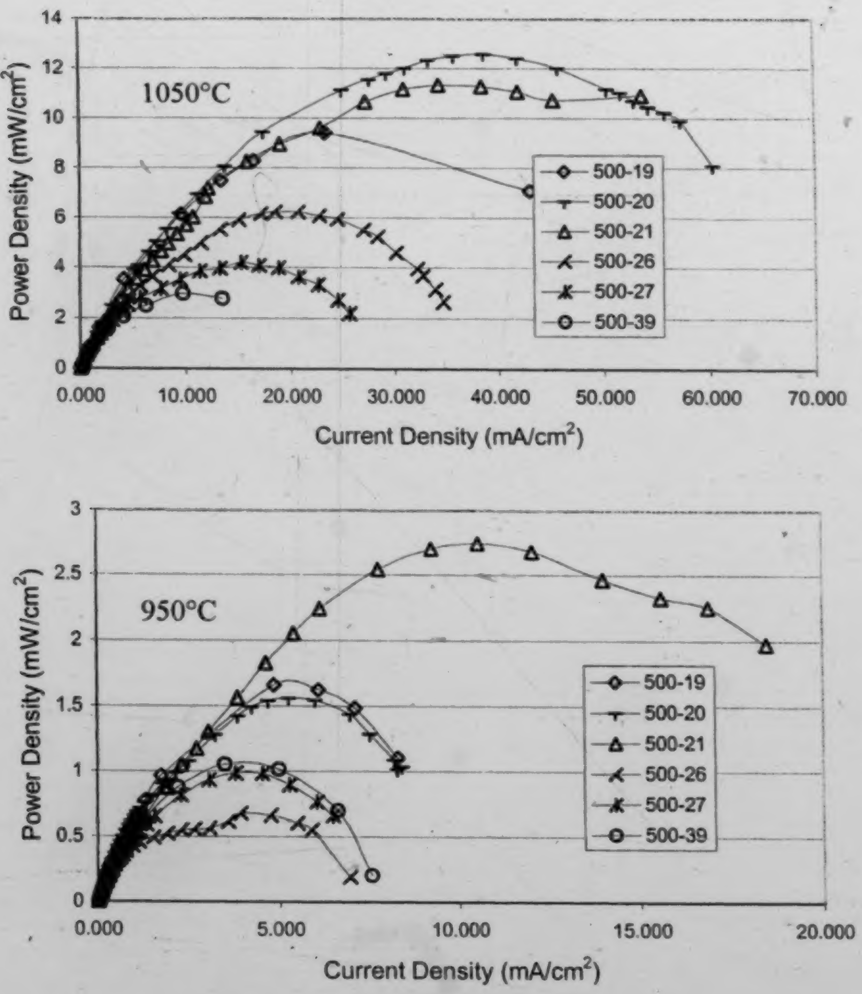

Figure 19: Power density for cells deposited at 1050°C and -300mV

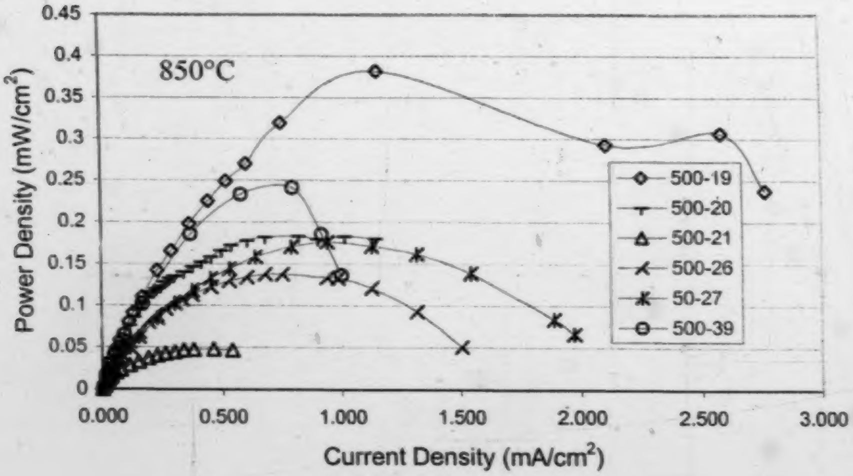

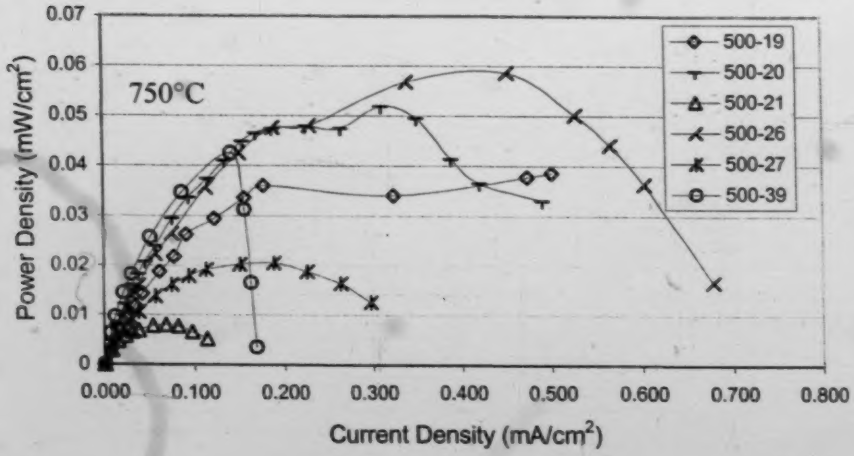

Figure 19(cont'd)*:* **Power density for cells deposited at 1050°C and -300mV**

When the performance of each individual cell is examined temperature by temperature, some features stand out. For example, with cell 500-19 it is seen that the power output is among the best for all temperatures, but at 850°C is significantly better than all of the other cells. The open circuit voltage for this cell at this temperature is higher than for all the other cells except cell 39, which is part of the reason for the better performance. In fact, when the higher OCV is ignored, the shape of the I-V curve is quite similar to that of both 500-20 and 500-26. At other temperatures there is nothing about the performance of this cell that stands out. Because this variation in OCV between the different cells, and even between different temperatures for the same cell, is observed it is perhaps best to analyze the cell performance based on the relative slopes of the I-V curves. The power output is dependent on both the polarization of the cell and the initial voltage, while the slope of the I-V curve is determined solely by the polarization of the electrodes and the cell resistance. The major contributor to cell resistance should be the electrolyte, and this will have a similar resistance for all of the cells. The resistance of the electrodes themselves and the contact resistance between the electrode and lead wires should be low, so the major unknown is the contact resistance between the electrodes and the electrolyte. In cells where this interface does not adhere well, there will be very high contact resistance, which should become much lower in better adhering cells.

Cell 500-20 shows the most consistent performance of all the cells examined in this set. The I-V curve shows a dramatic change in slope at around 1.5 mA/cm^2 at 950°C and a similar but less pronounced shift at 0.5 mA/cm^2 and 850°C. This is shown in figure 20 for the case at 950°C, where linear least squares best-fit lines are shown for the two portions of the graph. The equations accompanying the trend lines show that the portion at high current density has a slope that is about 1/5th that of the initial curve. The slopes of these two regions represent the area specific resistances (ASR in Ωcm^2) of the processes that cause them. Typically, the initial slope is associated with activation polarization, while the second portion is associated with ohmic losses in the cell. A third portion, not seen here, is caused by concentration polarization. In this region, which occurs at high current densities, the slope becomes vertical. An example of this may be seen in the I-V curve for cell 39 at 750°C (figure 18). The variation in these slopes from cell to cell should give some insight into the effect of deposition on both cell activity and cell resistance.

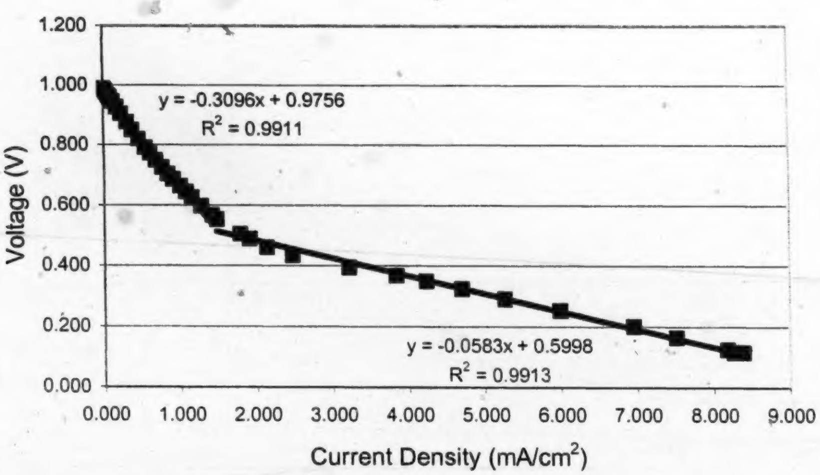

Figure 20: I-V curve for cell 500-20 at 950°C showing two distinct slope regimes

Perhaps the most interesting behaviour is shown by cell 500-21. At the higher temperatures (1050 and 950°C) it has very good performance; however, when the temperature drops to 850°C and below it gives the worst performance of all the cells. In part, at least, this is due to the lower OCV exhibited at these temperatures. One potential reason for the poor performance of the cell at 750 and 850°C may be anode-electrolyte interface degradation. When the cell was dismantled after testing, the anode layer was no longer well attached to the electrolyte, sticking better to the lead wire. This kind of detachment was seen earlier in many of the cells but no cause was ever identified.

Cell 500-26 performed poorly relative to the other cells in this group at all temperatures except for 750°C. Although it did have one of the highest OCV's of the five cells at this temperature, this alone does not account for its good performance. At 1050°C it also had one of the highest OCV's and did not perform well. For a better understanding of the causes of the performance variation it is necessary to examine the microstructures of the cells. It is unlikely that any microstructural changes occur at 750°C; however, the same may not be true for testing at higher temperatures. For example, at 1050°C the diffusion rate of the platinum electrode is high enough to allow a diffusion distance of about 4.5 μm using a diffusion coefficient of 2.7×10^{-16} m^2/s [166] and a time of 1300 minutes. The surface diffusion rate will be even higher [167], and can be further enhanced by the presence of hydrogen in the atmosphere and an electric field. Because the average pore size of the platinum electrode is initially less than 10 μm, this amount of diffusion is sufficient to close off many of the pores. If the anode is completely coated by the PEVD process, then this should not be a problem; however, a complete coating was not observed in any of the cells tested.

Like all of the cells examined, the cells deposited at 1050°C and -300 mV were examined by SEM and EDX. The secondary electron (SE) images collected for these samples at intermediate magnification are shown in figure 21. All of these images were taken at the same magnification, with the scale bar seen on the top corner of each image reading 60 μm. The cross sections of these cells were also examined (figure 22). The magnification in figure 22 is the same as that in figure 21.

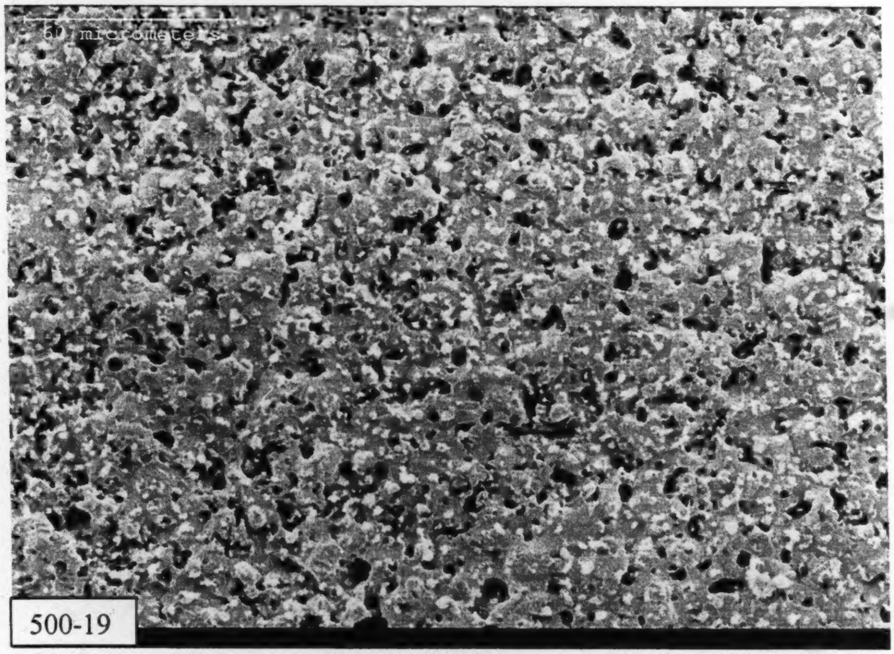

Figure 21: Intermediate magnification SE images of cells deposited at 1050°C and -300 mV

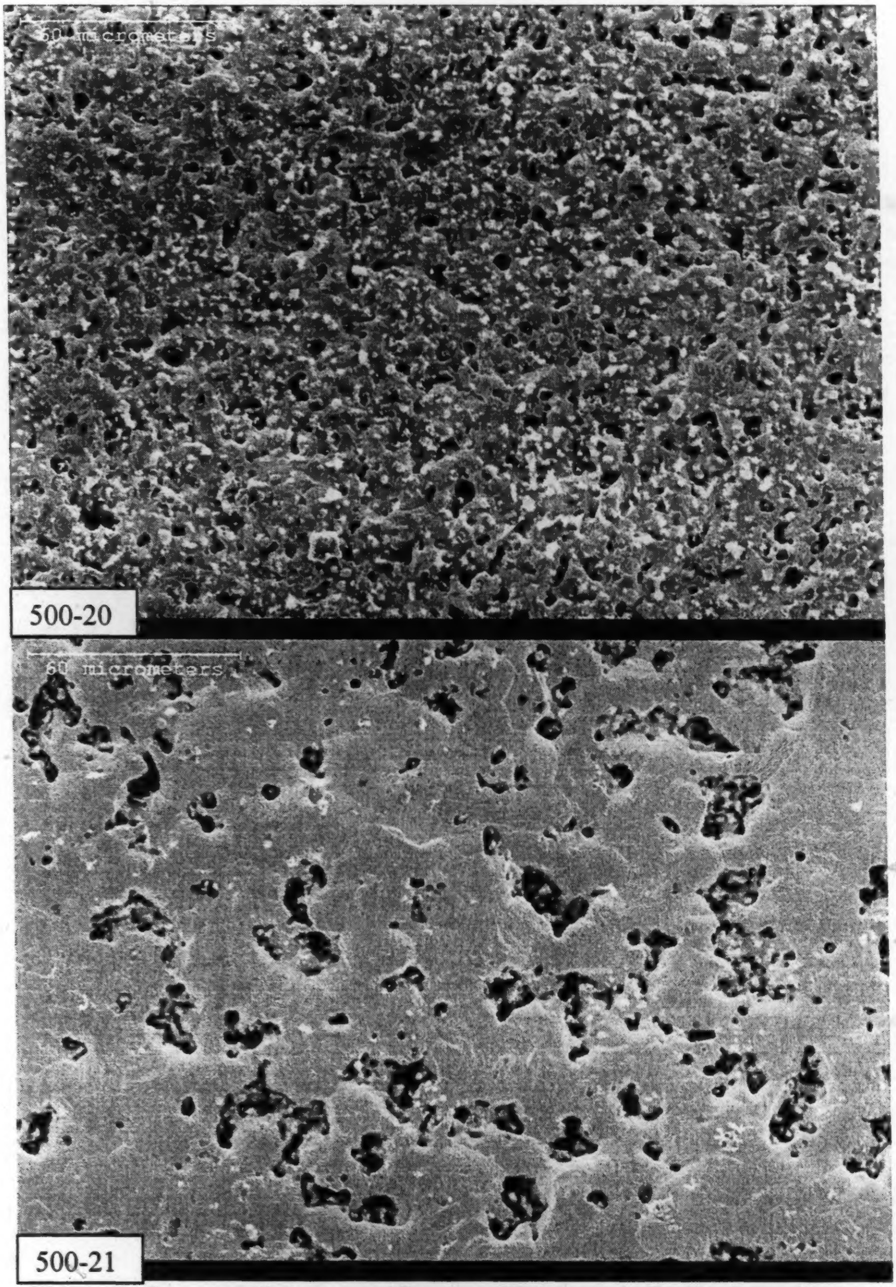
60 micrometers
500-20
60 micrometers
500-21

Figure 21(cont): Intermediate magnification SE images of cells deposited at 1050°C and -300 mV

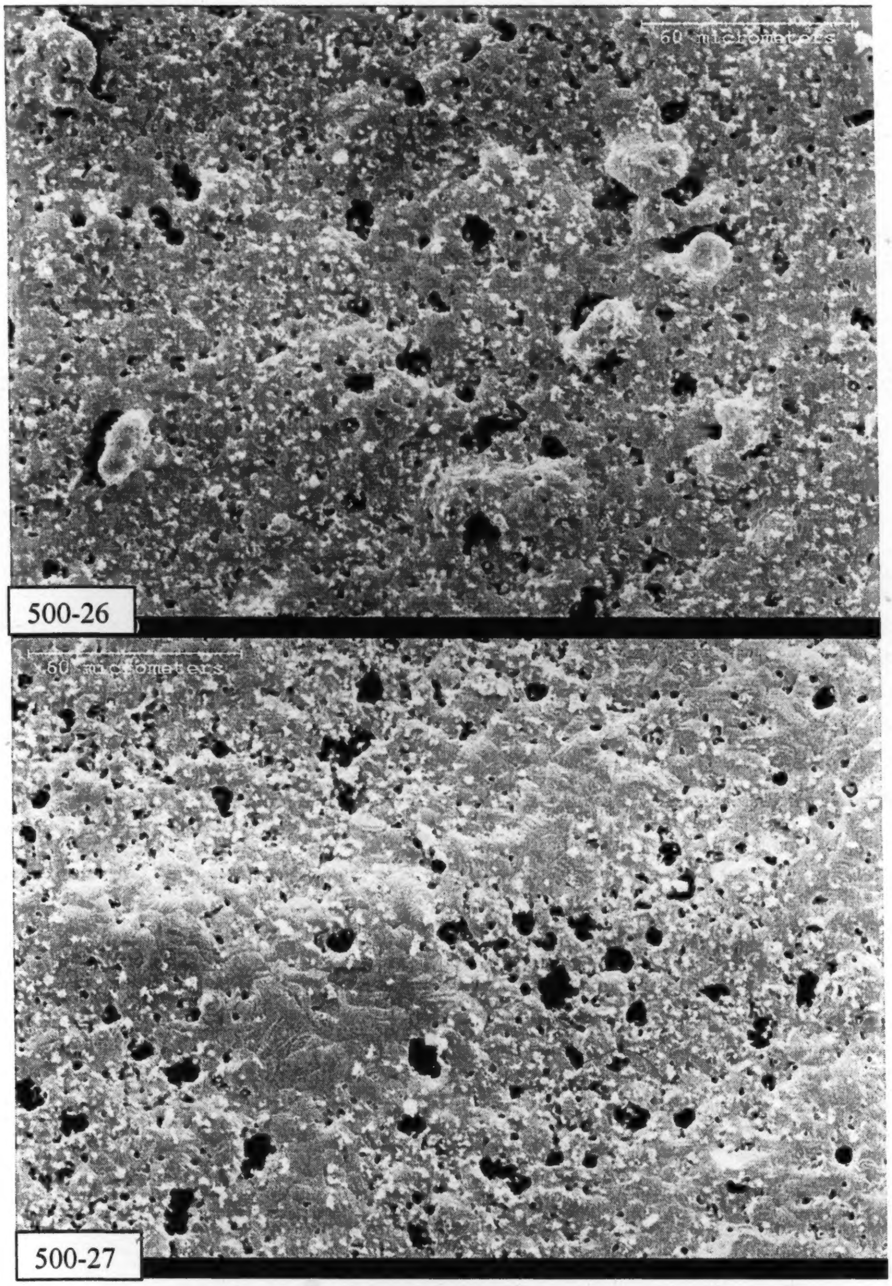
60 micrometers
500-26
60 micrometers
500-27

Figure 21 (cont): Intermediate magnification SE images of cells deposited at 1050°C and -300 mV

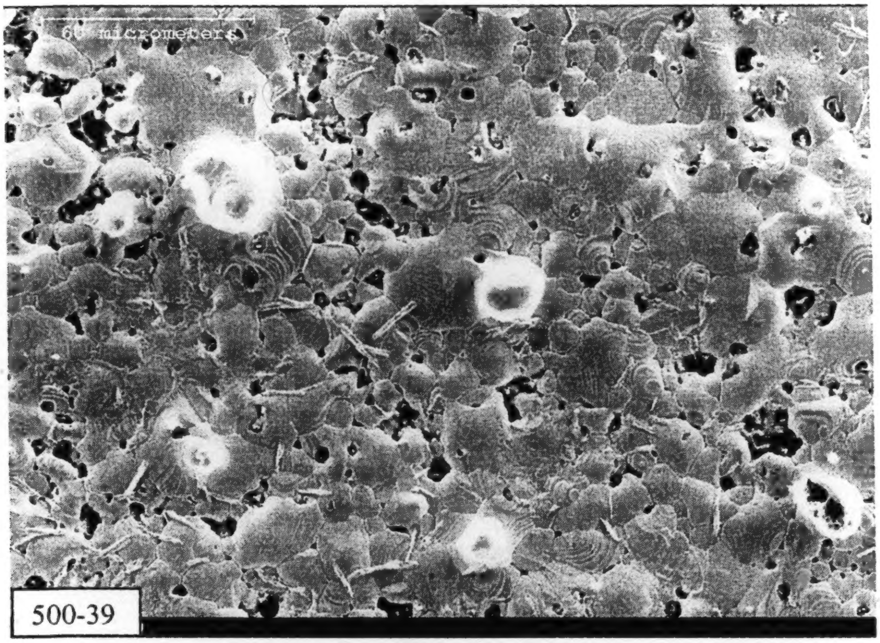
60 micrometers
500-39

Figure 21 (cont): Intermediate magnification SE images of cells deposited at 1050°C and -300 mV

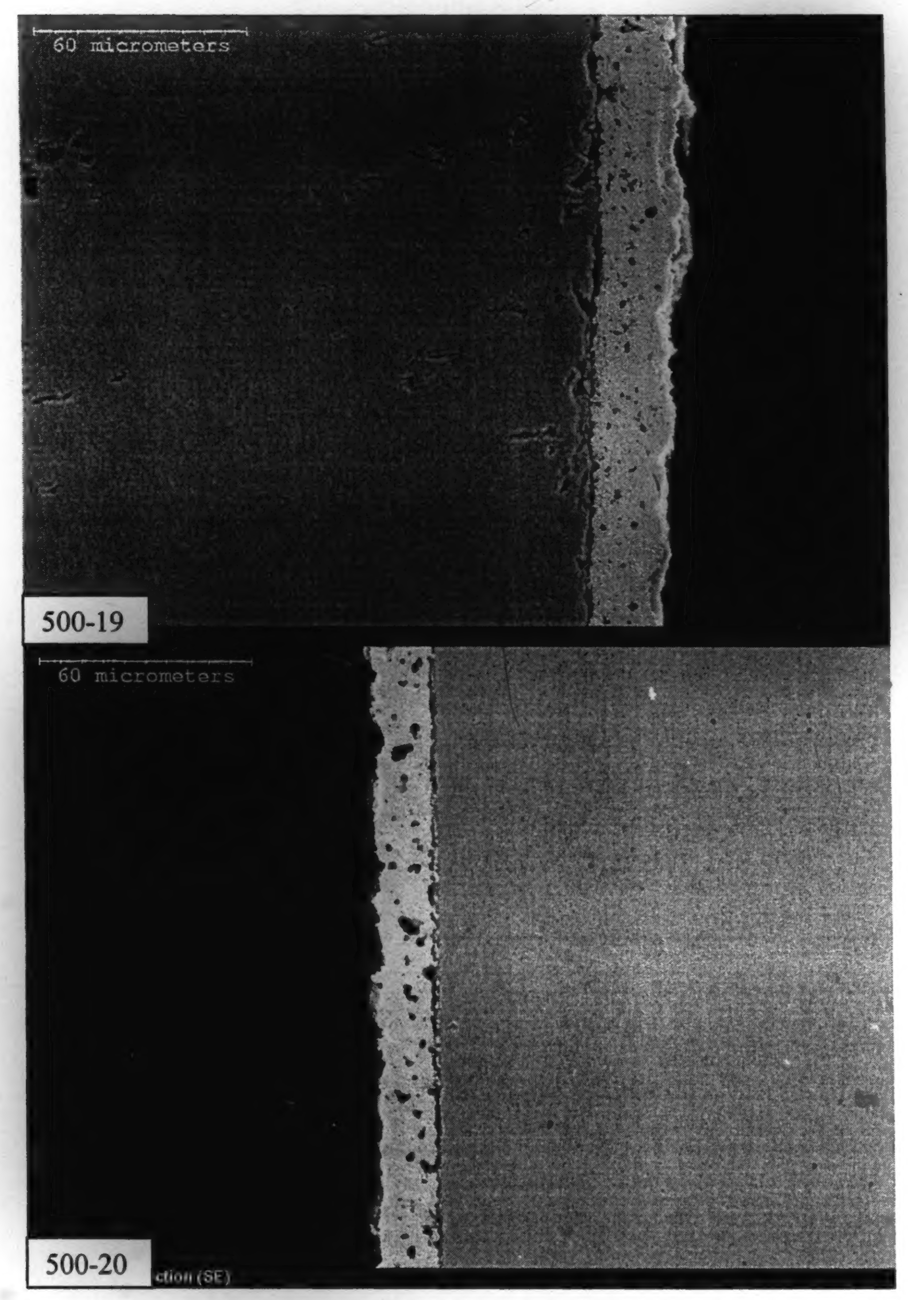
60 micrometers
500-19
60 micrometers
500-20
ction (SE)

Figure 22: Cross sectional SE images of cells deposited at 1050°C and -300 mV

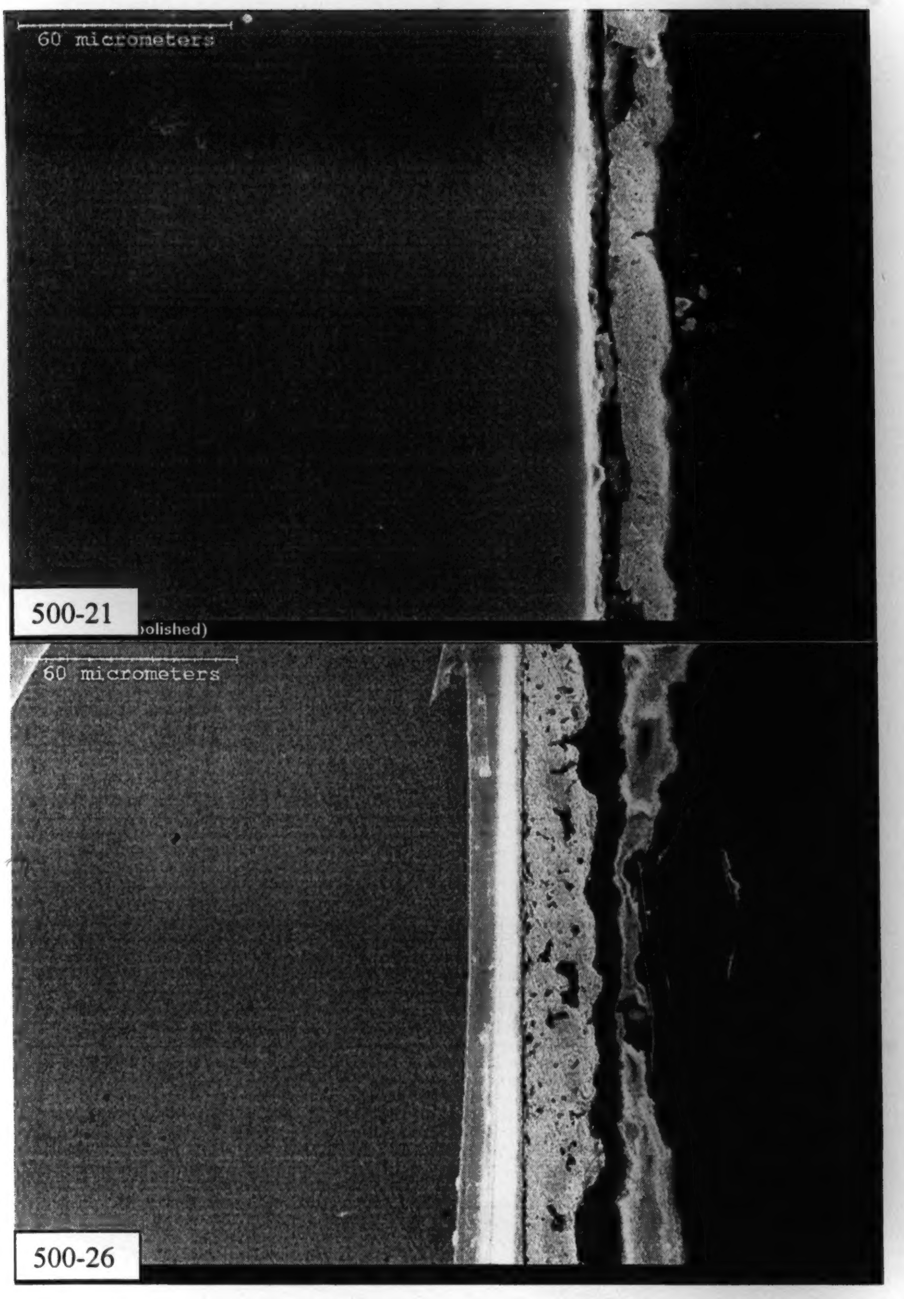
60 micrometers
500-21
olished)
60 micrometers
500-26

Figure 22(cont): Cross sectional SE images of cells deposited at 1050°C and -300 mV

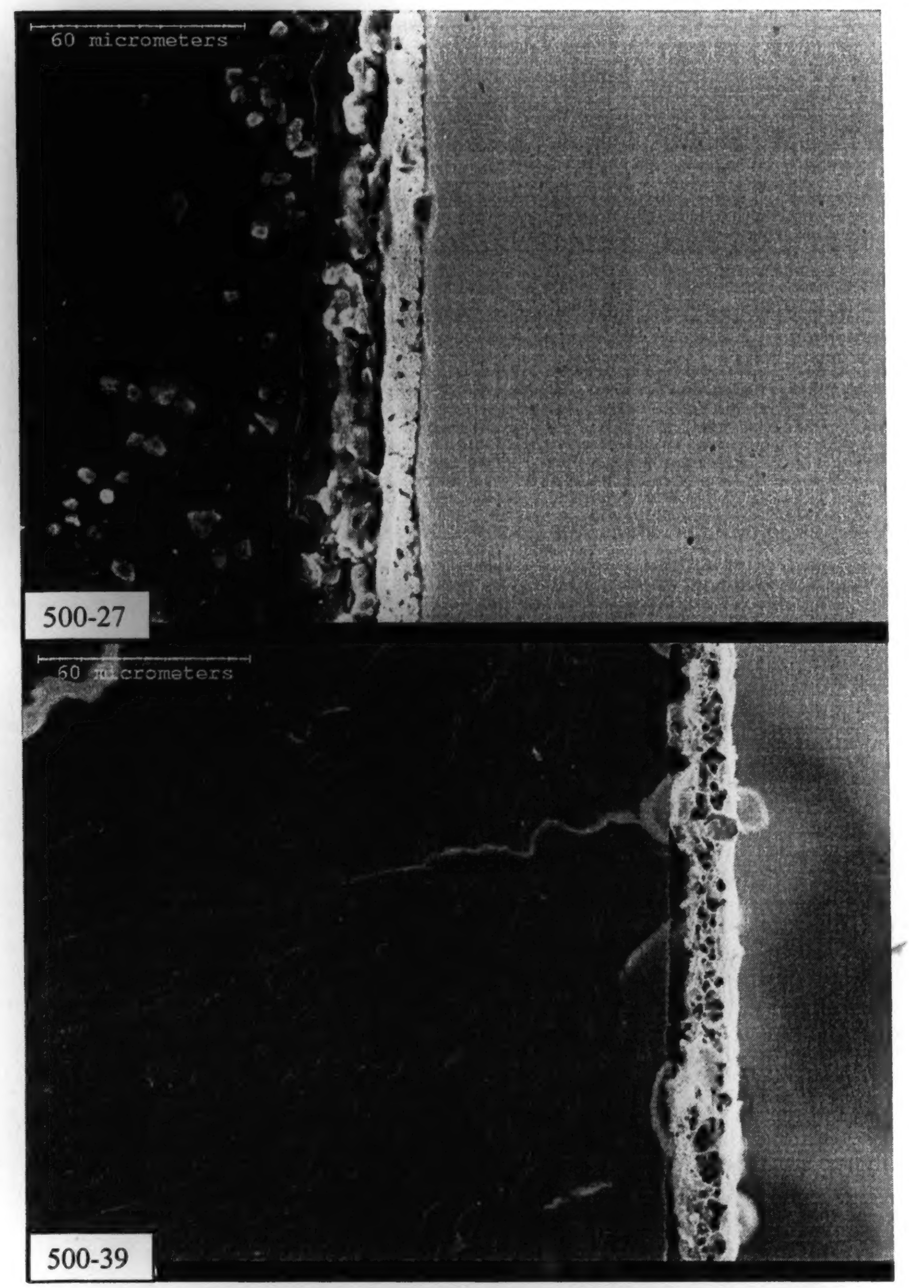

Figure 22(cont): Cross sectional SE images of cells deposited at 1050°C and -300 mV

In order to draw any conclusions from the microstructures of these cells it is beneficial to first review the features seen in each of the cells. Starting with the plan view of cell 500-19 it is clear that this cell has a large amount of open porosity and a fairly rough surface. There are also a large number of light colored protrusions from the electrode surface. Figure 23 (scale bar = 12 μm), which includes a BSE image, shows that these features at higher magnification. EDX analysis of the surface was performed (figure 24) and showed that the deposit contained higher amounts of silicon and magnesium; likely in oxide form as indicated by the large oxygen peak. Several other minor peaks are also seen.

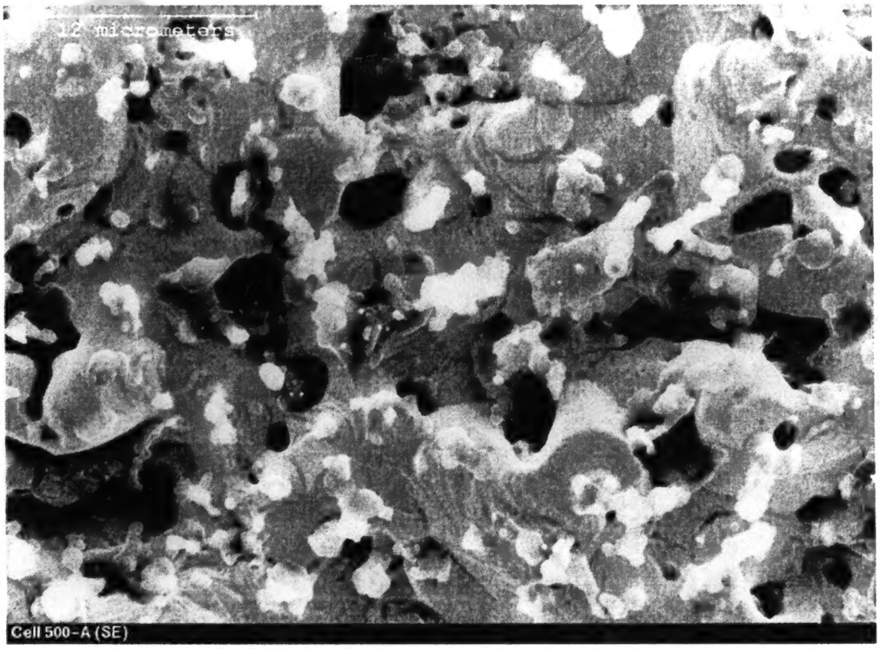

a)

Figure 23: High magnification SE (a) and BSE (b) images of cell 500-19

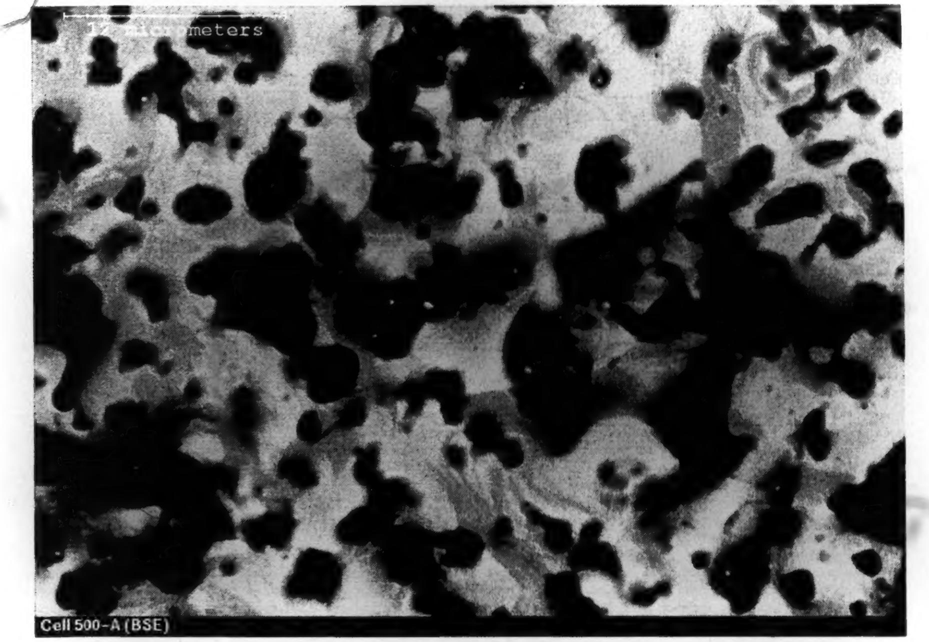

b)

Figure 23 (cont): High magnification SE (a) and BSE (b) images of cell 500-19

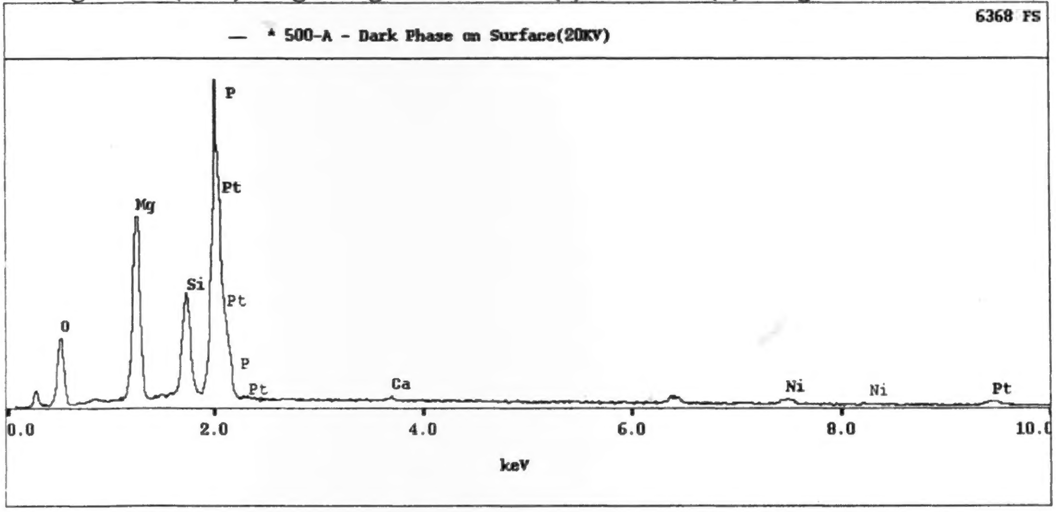

Figure 24: EDX spectrum for dark surface phase seen in figure 23 (b)

Due to the nature of the materials used in the electrode and the characteristics of the EDX system, further examination of this spectrum is required. First of all there is the presence of a small peak for calcium, as well as one for nickel. No source for either nickel or calcium contamination can be readily identified. There is also a peak at around

6.4 keV which is unlabeled. This peak is characteristic of iron and is likely caused by secondary fluorescence from microscope components, which contain iron, near the detector. Other impurities seen in the spectrum are magnesium, silicon and phosphorous. The magnesium and silicon could both come from the glass sublimation tubes; however, the magnesium shows a much larger peak than would be expected from its concentration in the glass. The most likely source of phosphorous is the cement used to attach the cell to the tube. A phosphoric acid based thinner is used in the alumina cement and, as shown in figure 25, residual phosphorous is present in the cured cement.

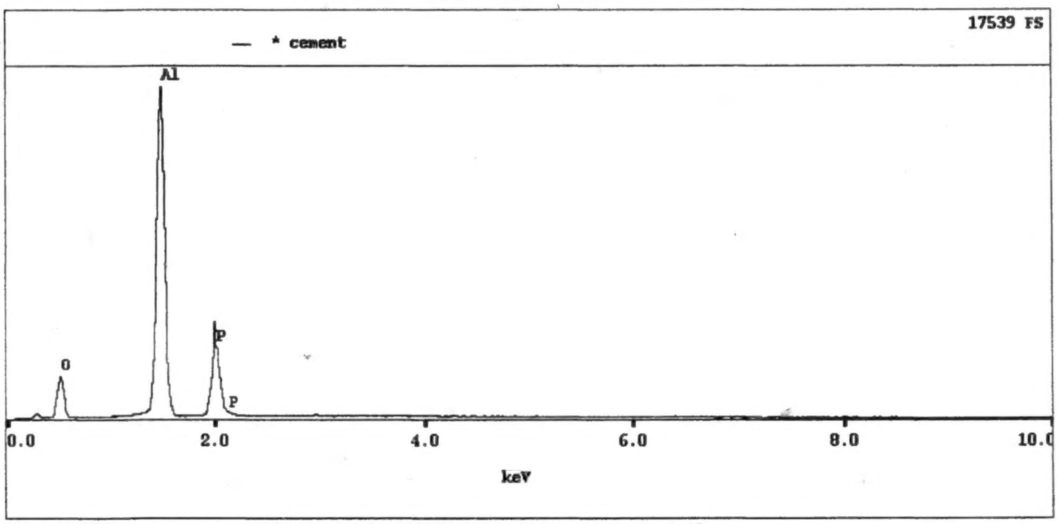

Figure 25: EDX spectrum for cured cement

Figure 26 shows the EDX spectrum for a platinum electrode that was not coated by PEVD. This electrode was mounted in cement and heated to 900°C in the deposition furnace. Conversely, figure 27 shows the spectrum for a single platinum layer on a YSZ disc, which was not treated in the deposition furnace.

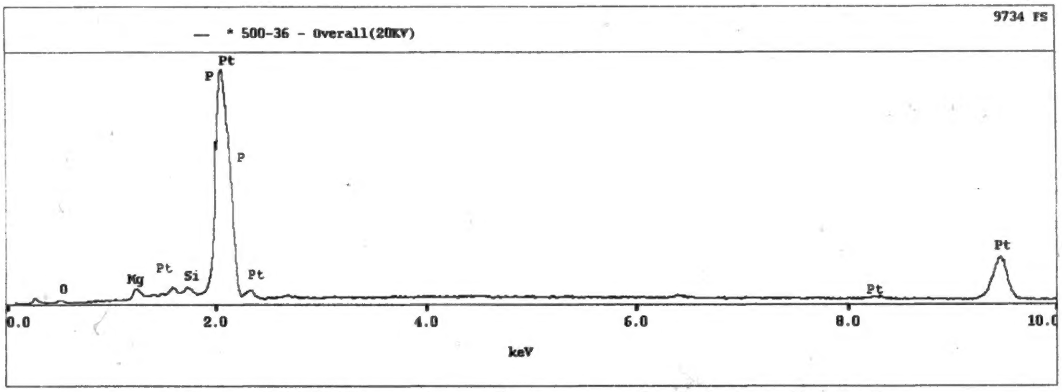

Figure 26:EDX spectrum for uncoated platinum electrode

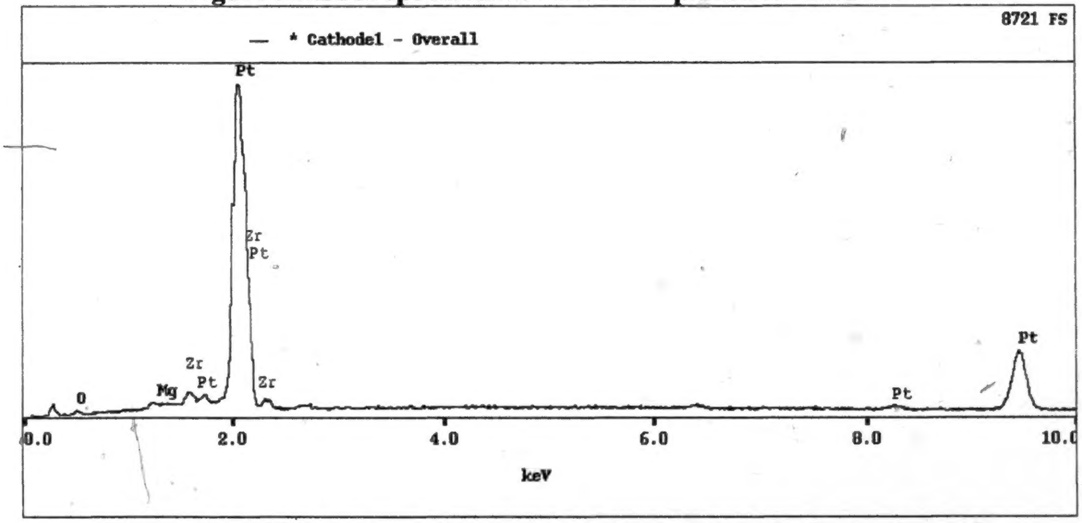

Figure 27: EDX spectrum for uncoated, unmounted platinum electrode

In both of these spectra platinum is the dominant constituent. There is a shoulder on the low energy side of the major platinum peak in both of the spectra. In figure 26 this is still attributable to phosphorous from the cement; however, in figure 27, a different explanation must be sought. One possibility is the presence of yttrium, which has a peak at about 1.9 keV. It is possible that yttrium in the substrate is causing this, as the platinum layer in this sample is relatively thin and highly porous. Even if this is the case, it should not have a large effect on the spectrum as the concentration of yttria in the substrate is only 8 mol%. Both samples also show a small magnesium peak; however, it is less distinct in the sample that was not put in the reactor. This suggests that the magnesium in the electrode is not only due to contamination in the reactor. Small peaks are also observed near the main peak. These are labeled as platinum, silicon and zirconium; however, they are so close together that it is impossible to say what element these minor peaks actually come from based on these spectra.

From this brief discussion it is apparent that with the current materials of construction it is very difficult to get a clear analysis of the deposit by EDX. One possible solution is to increase the accelerating voltage to 30 kV. This allows for the emission of higher energy characteristic x-rays, including the yttrium and zirconium K lines at 14.9 and 15.6 keV, respectively. These peaks are far enough apart that they are resolvable, and are not overlapped by peaks from any of the other elements observed at lower energy. The major drawback to this is that the coating being examined is quite thin and increasing the accelerating voltage also increases the size of the sampled volume. Thus more platinum is included in the analysis, and the results are skewed. Other options for analysis include wavelength dispersive x-ray spectrometry (WDX), which has a much higher peak resolution than EDX, as well as X-ray diffraction (XRD). In the case of WDX it is difficult to focus on the surface because of the rough nature of the porous electrode, which prevents accurate quantitative analysis. Also there is still some overlap of the low energy platinum and zirconium peaks. The biggest problems with XRD are isolation of the electrode from the electrolyte and its insensitivity to minor elements. This is required because the ceramic phase being identified in the electrode is the same as the electrolyte material.

It is possible that magnesium does not have a high concentration in the deposited phase. Magnesium has quite a high mass absorption coefficient for platinum M_α radiation (1877 cm^2/g). This means that a lot of the characteristic platinum x-rays from the electrode will be absorbed by magnesium atoms in the deposit, leaving the magnesium in an excited state. De-excitation of these atoms can result in a larger than expected magnesium peak, even though only about 2.6% of de-excitation reactions in magnesium will result in characteristic x-ray emission. It is certain, however, that there is some magnesium in this deposit and, therefore, there must be some contamination of the reactor.

Comparing the structures of this set of cells (figure 21) it is apparent that cell 500-19 and 500-20 have higher porosity than any of the other cells. The other cells show a generally dense structure with isolated pores or pore clusters. From this it is expected that cells 19 and 20 should have the highest active area and, therefore, give the best performance. Figures 18 and 19 do show that at all temperatures these cells are among the best performers; however, there seems also to be an exception at each temperature. At 1050°C cell 500-21 outperforms 19, despite its denser structure, while at 950°C it significantly outperforms both cells 19 and 20. At 850°C cell 19 gives the highest power output, but cell 39 gives better power density than cell 20. Additionally, closer examination of figure 18 reveals that the slope of the I-V curve for cell 27 is shallower than it is for either cell 19 or 20. The reason that it does not outperform them is its lower OCV. Finally at 750°C cell 500-26 gives the highest power density.

In order to attempt an explanation of this behaviour it is necessary to examine the cross sectional structure of the electrodes. Figure 22 indicates that all cells, except 500-21, have a similar degree of porosity. It should be noted that cell 500-39 was prepared by fracturing the sample rather than sectioning and polishing. This is the reason for its apparent high porosity. When these images are matched with the plan views in figure 21 it suggests that only the surface of the other cells has densified appreciably. The cross section of cell 39 supports this, as it shows a much higher porosity in cross section than in plan view. This is not as apparent in the other cross sections since they were polished, which smeared the microstructure.

While densification of the surface would certainly increase concentration polarization effects, it may not have as pronounced an effect on activation polarization. This might allow all of the cells to perform similarly despite their apparent differences in structure. Explanation of the structure of cell 21 is more difficult. From the micrograph it is clear that the electrode is not well attached to the electrolyte. As was hypothesized earlier this is the likely cause of the poor performance at 850 and 750°C. In fact, it seems unlikely that the high performance observed at 1050 and 950°C would have been possible if the electrode were detached.

The combination of high performance and low porosity seen in cell 500-21 at the higher temperatures could be due to an extensive fine pore structure. Sectioning the cell and polishing the cross section would have obscured a fine pore structure by smearing the platinum. Although this would explain the high performance seen at high temperatures, it gives no insight as to why so few large pores are visible in the final microstructure. No aspect of deposition or sample preparation gives any clues as to why this might be the case. One other change that was made after cell 500-20 was the yttrium chloride source material. This should not make too much difference though, as it was from the same supplier as the original and they were ordered at the same time.

To clarify the effects of deposition time under these conditions, it is best to eliminate the cell-by-cell variability in the electrode microstructure. Therefore the same cell should be tested after various times of deposition. This was done with cell 500-39. Its I-V characteristics were measured at 1050°C, in a moist hydrogen atmosphere for deposition times of 0 minutes, 180 minutes, 855 minutes, 1050 minutes, 1905 minutes and 3210 minutes. The I-V curves resulting from this test are shown in figure 28.

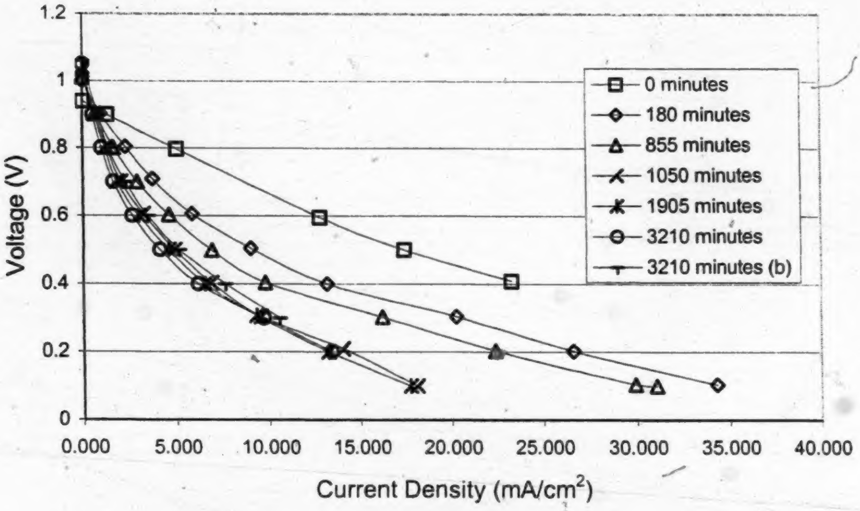

Figure 28: I-V curves for cell 500-39 at 1050°C

From this graph it is clear that the performance of the cell deteriorates with deposition time, eventually reaching a steady value. Deposition times of 1050 minutes and beyond show little effect on the power output of the cell; therefore, any structural changes in the anode must have already taken place by this time. By analyzing the slopes of the two main regions of these curves it is seen that the activation polarization increases with deposition time up to about 1500 minutes, where it reaches a plateau. The cell resistance, represented by the second portion of the curve, also increases with deposition time, but at a much lower rate and it does not seem to plateau in the time frame covered by this test. These features are illustrated in figure 29. ASR 1 is the activation portion of the curve, while ASR 2 is the cell resistance. As shown in figure 21, electrode densification may be the overpowering structural change. Cell 500-40, which will be discussed later, was deposited in a similar manner and gave very different results.

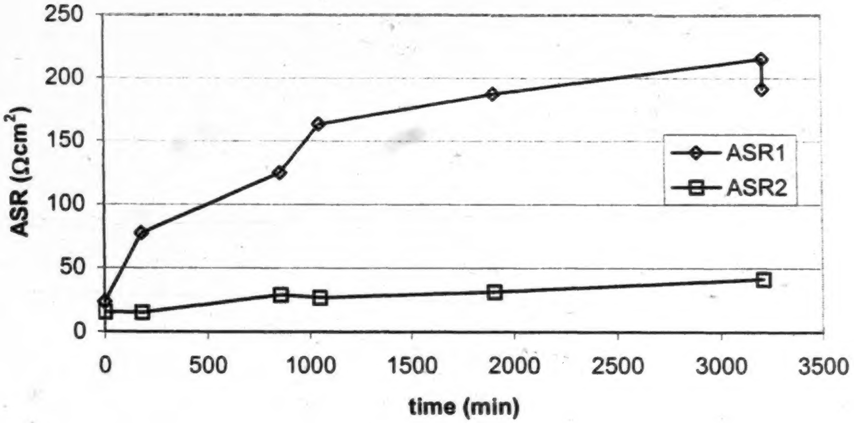

Figure 29: Area Specific Resistance (ASR) of cell processes as a function of deposition time

5.3 Effect of Deposition Voltage

The deposition conditions of 1050°C and -300 mV can be considered as a starting point for this investigation, and the first variable changed was the deposition voltage. Other cells deposited at 1050°C used applied biases of -250 mV, -200 mV, -100 mV, 0 mV and +300 mV. The cells deposited at 0 mV used the oxygen potential gradient as the sole driving force for oxygen diffusion and the current was controlled by a decade resistance box. Figures 30 and 31 show the polarization and power density curves for this set of cells. Because of the number of cells in this group it is the power density charts were split into high and low performance groups at each temperature so that they are easier to interpret. The deposition conditions for each cell are shown in table 5.

Table 5: Deposition conditions for cells deposited at 1050°C

Cell	V(mV)	t(min)
500-16	-200	1472
500-18	-200	1354
500-22	300	1434
500-23	300	1436
500-24	-250	1770
500-25	-250	1620
500-30	-100	2866
500-31	0	2556
500-32	0	4390

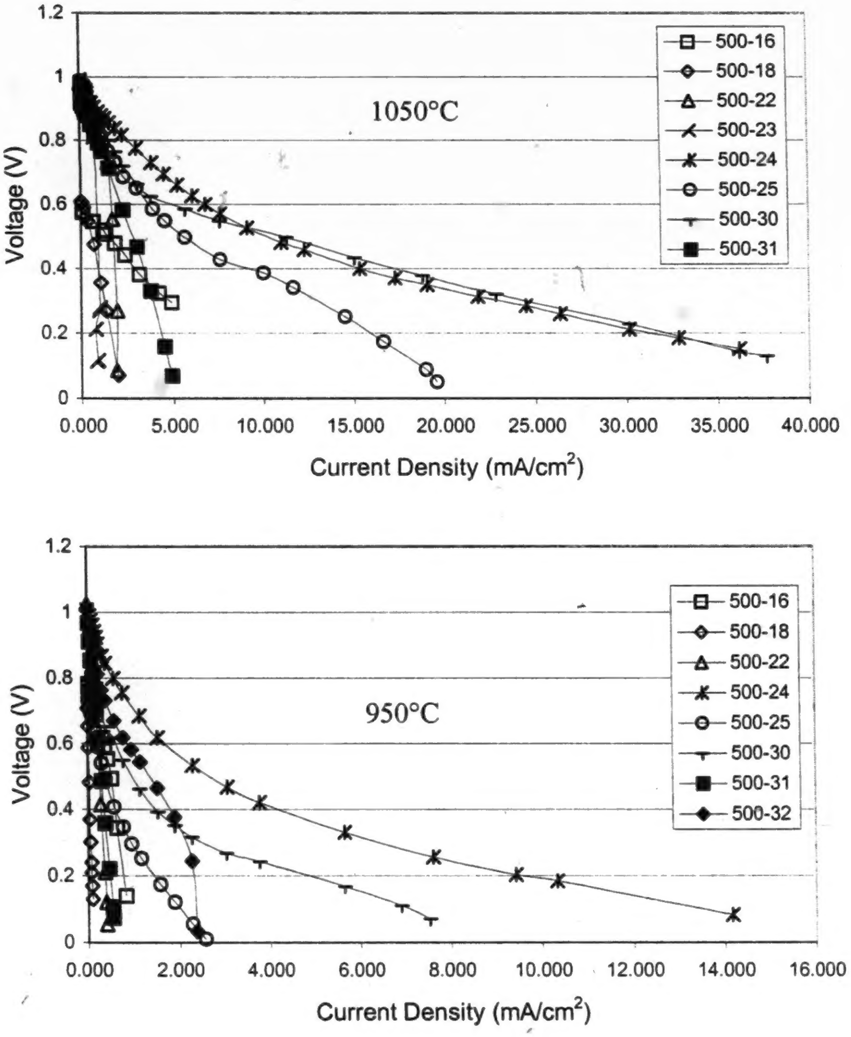

Figure 30: I-V curves for cells deposited at 1050°C and deposition voltages other than -300mV

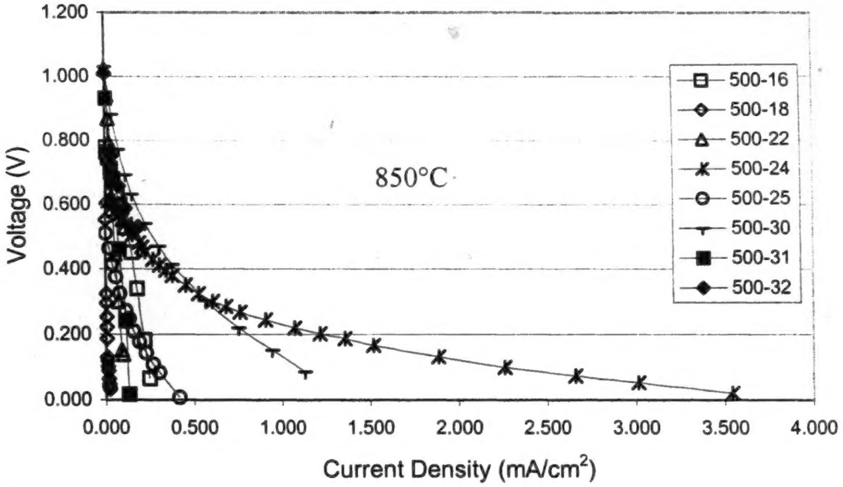

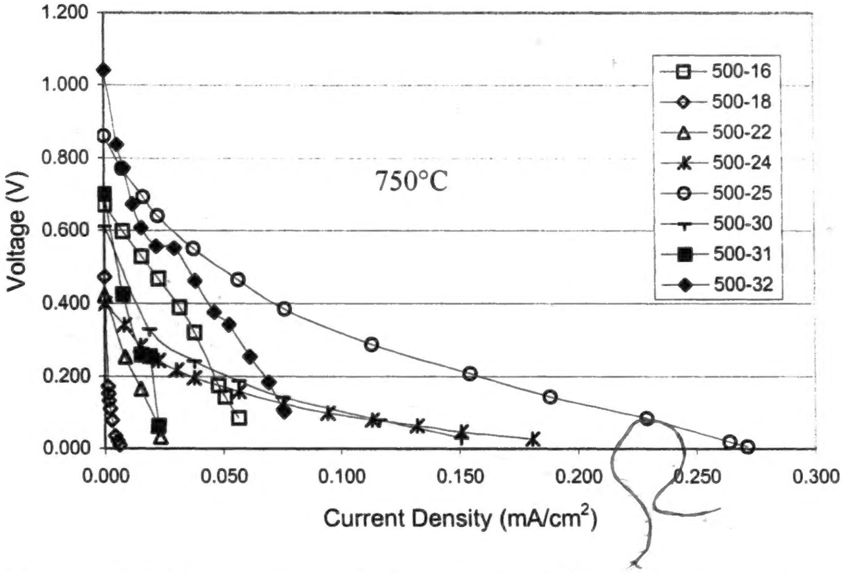

Figure 30(cont'd): I-V curves for cells deposited at 1050°C and deposition voltages other than -300mV

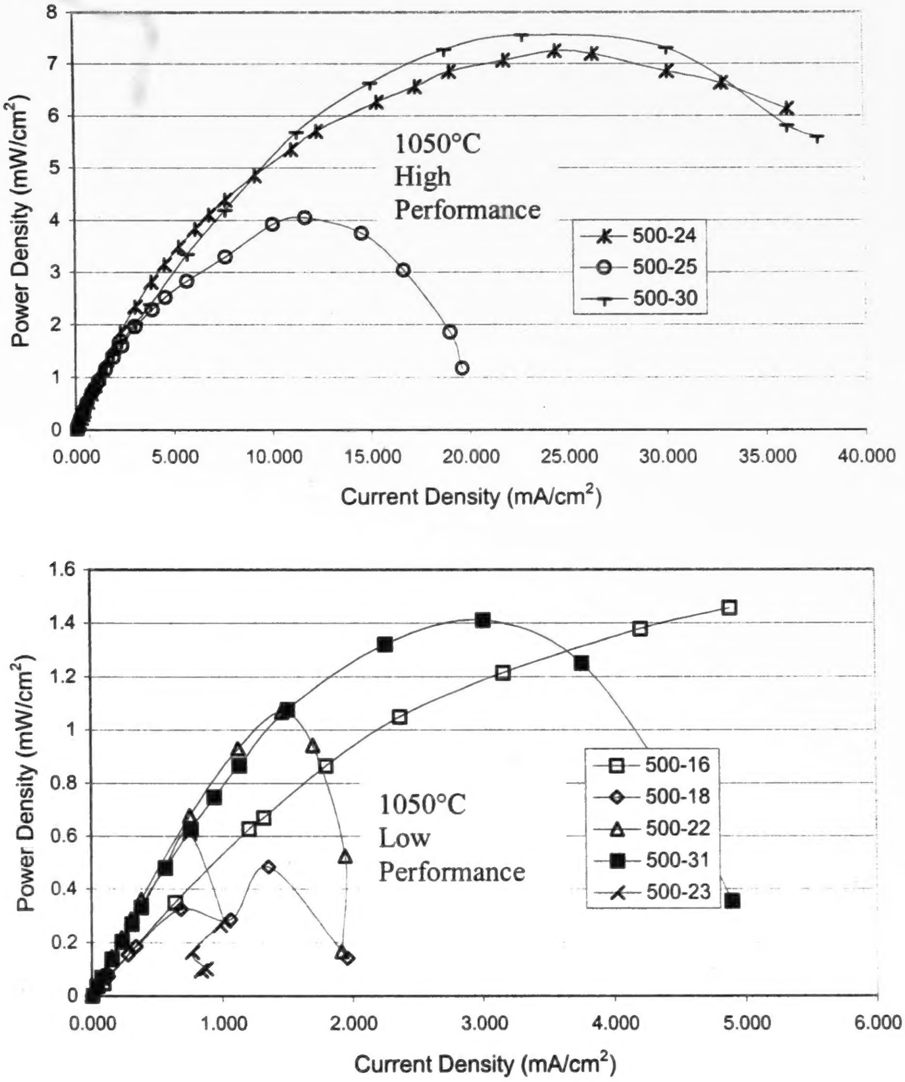

Figure 31: Power density curves for cells deposited at 1050°C and voltages other than -300mV

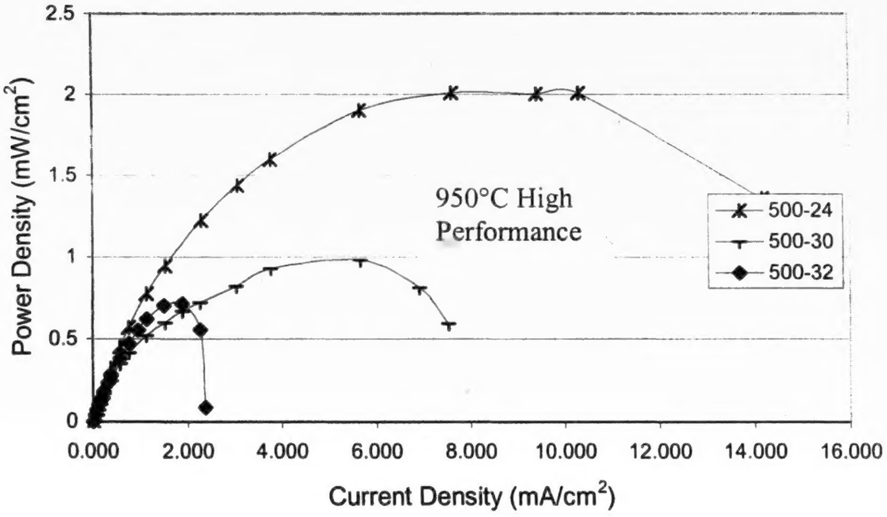

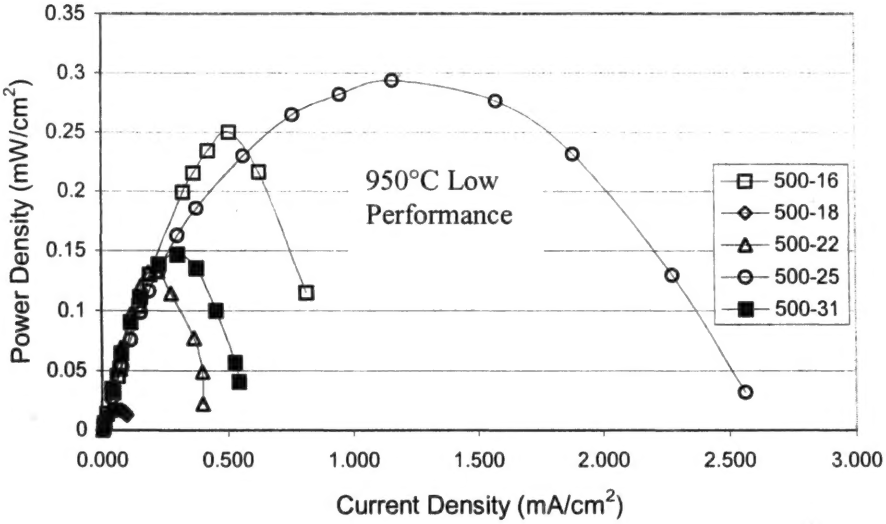

Figure 31(cont'd): Power density curves for cells deposited at 1050°C and voltages other than -300mV

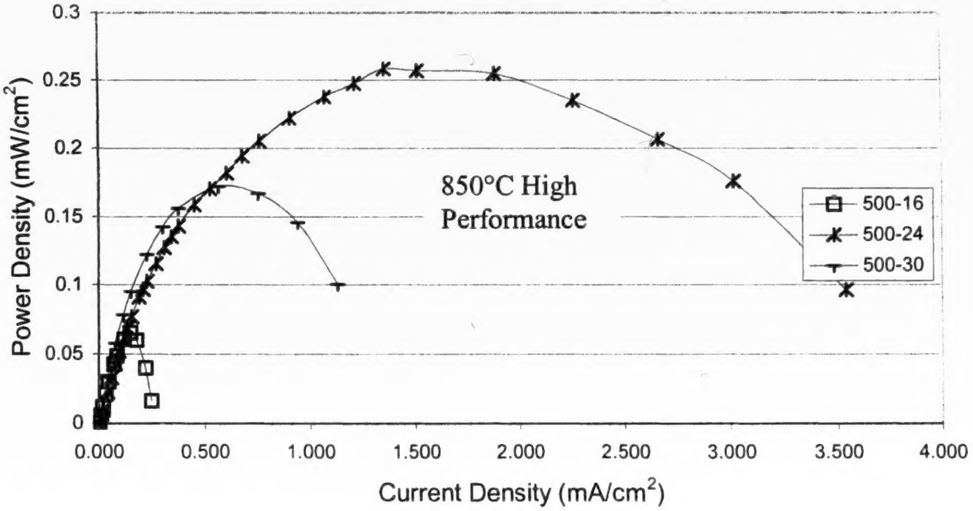

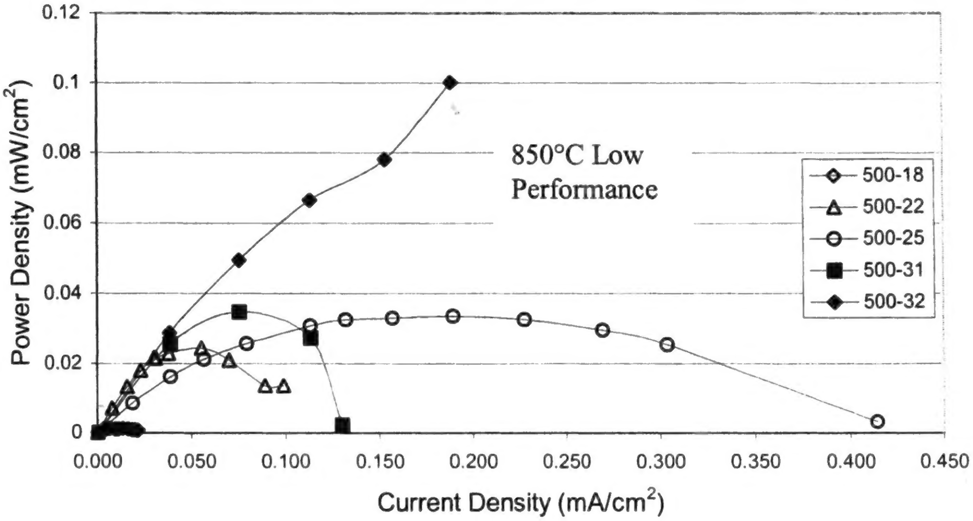

Figure 31(cont'd): Power density curves for cells deposited at 1050°C and voltages other than -300mV

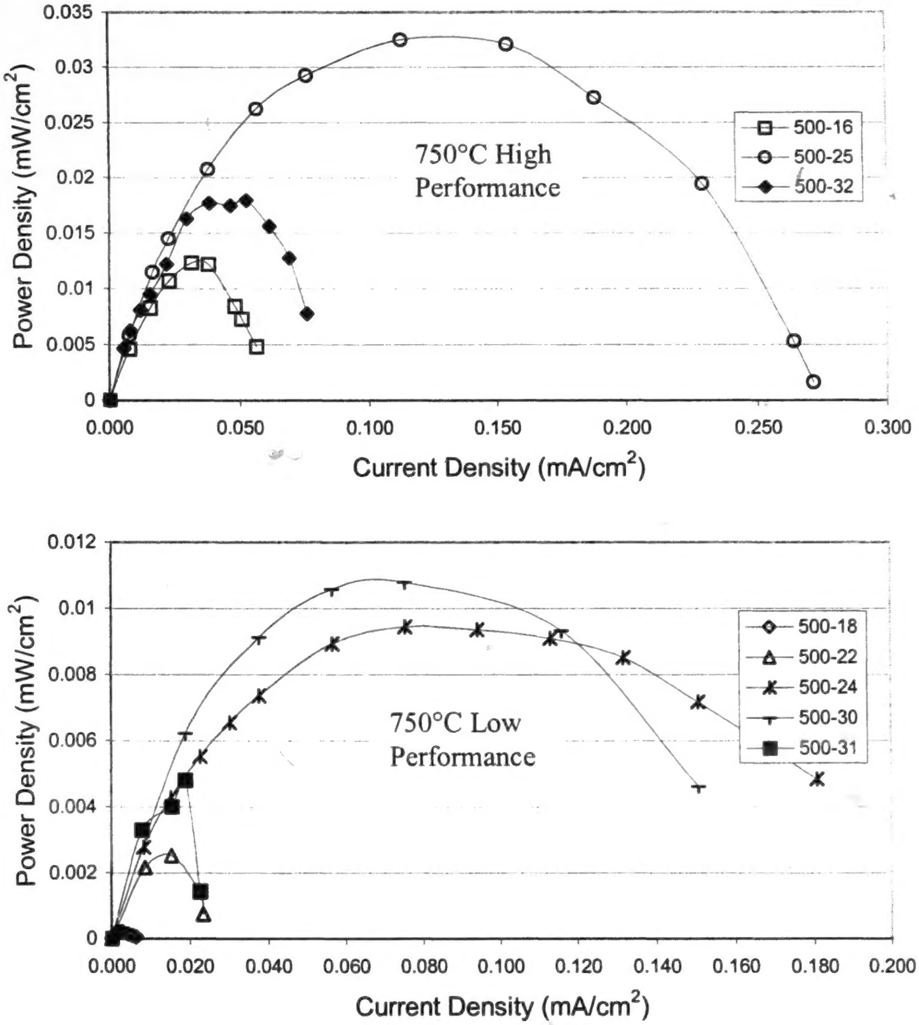

Figure 31(cont'd): Power density curves for cells deposited at 1050°C and voltages other than -300mV

Examination of these data shows that the best performance was generally obtained from cells 500-24, deposited at -250 mV, 500-30, deposited at -100 mV and cell 500-25, deposited at -250 mV. Again the power output, particularly at lower temperatures, is affected by the OCV of the cell. Cells 500-24 and 30, which show excellent performance at higher temperatures, give poor performance at 750°C. This is at least partially due to OCV's of 0.4 V for 500-24 and 0.6 V for 500-30, compared with 0.85 V for 500-25.

The worst power density in all cases is that of cell 500-18. Although it does not have a very high OCV this plays quite a small role in the power output as figure 30 shows that activation polarization causes a near vertical drop in voltage. 500-16, deposited in similar conditions, shows better performance. In general, it appears that power density tends to increase as the deposition voltage becomes more negative, with none of the cells in this set giving a higher power density than the best cells deposited at -300 mV. Variations within this trend are seen, like the high power densities produced by cell 500-30 (-100 mV), which may be due to variability in the starting structure. There may be other variables at work also; however, it seems that cells deposited with no bias voltage (500-31, 500-32), or a positive bias (500-22, 500-23) give less desirable properties.

In order to help clarify the root causes of the variation in power density and polarization behaviour, the microstructures of the more interesting cells are shown in figure 32. The magnification of these pictures is shown by the scale bar in the top of the image, which is 60 μm.

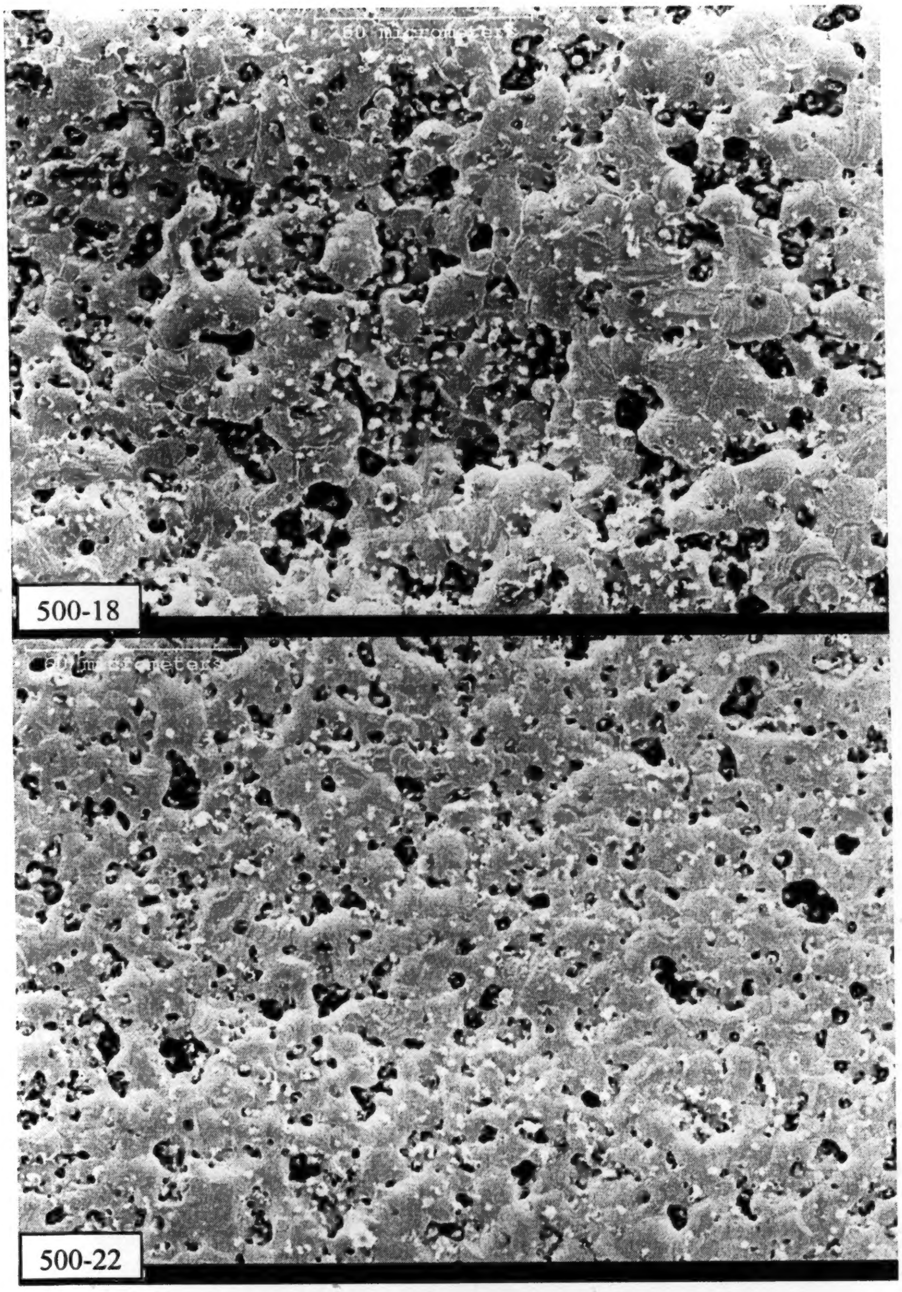
60 micrometers
500-18
60 micrometers
500-22

Figure 32: Selected SE images of cells deposited at 1050°C, and voltages other than -300mV

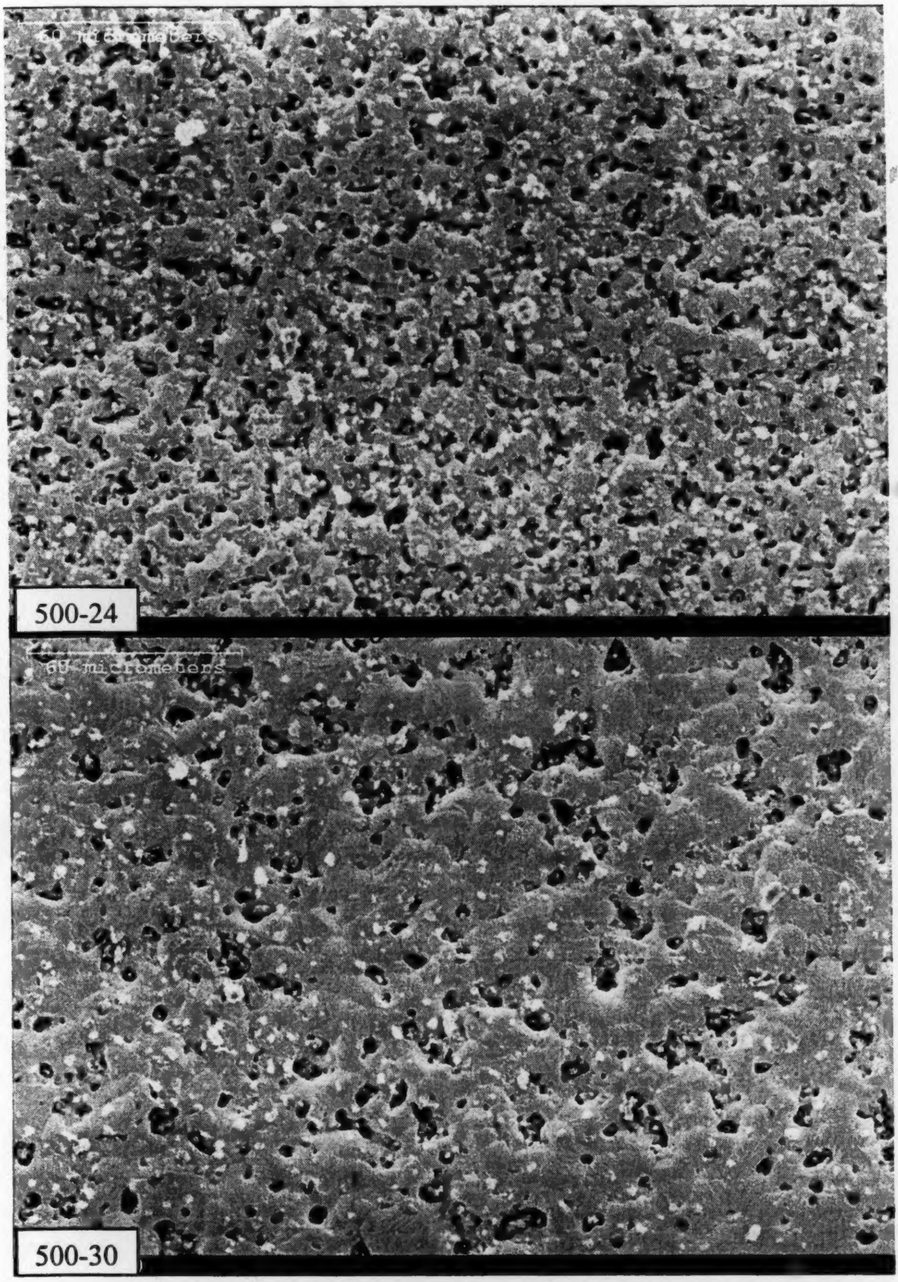
60 micrometers
500-24
60 micrometers
500-30

Figure 32(cont): Selected SE images of cells deposited at 1050°C, and voltages other than -300mV

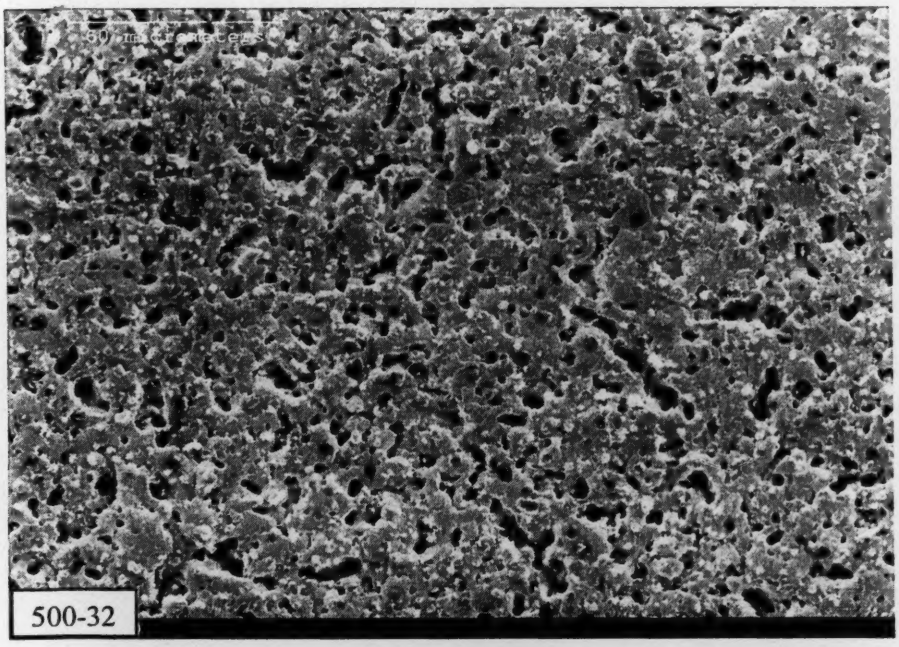

Figure 32(cont): Selected SE images of cells deposited at 1050°C, and voltages other than -300mV

These images show that the most porous microstructures belong to cells 24 and 32. Cell 24 shows the best performance of this group, while 32 shows competitive initial polarization behaviour but the sharp lessening of the slope of the I-V curve at higher current densities, seen in other cells, is not present. This leads to very low short circuit currents. Part of the reason for the high porosity seen in cell 500-32 may be that it was not tested in hydrogen at 1050°C. Cell 500-18, which in all cases shows the worst performance, has a more porous structure than do either 500-22 or 500-30. Surprisingly, cell 500-30, which shows the second best polarization behaviour, has the least porous structure. Cross sections of these electrodes at the same magnification are shown in figure 33.

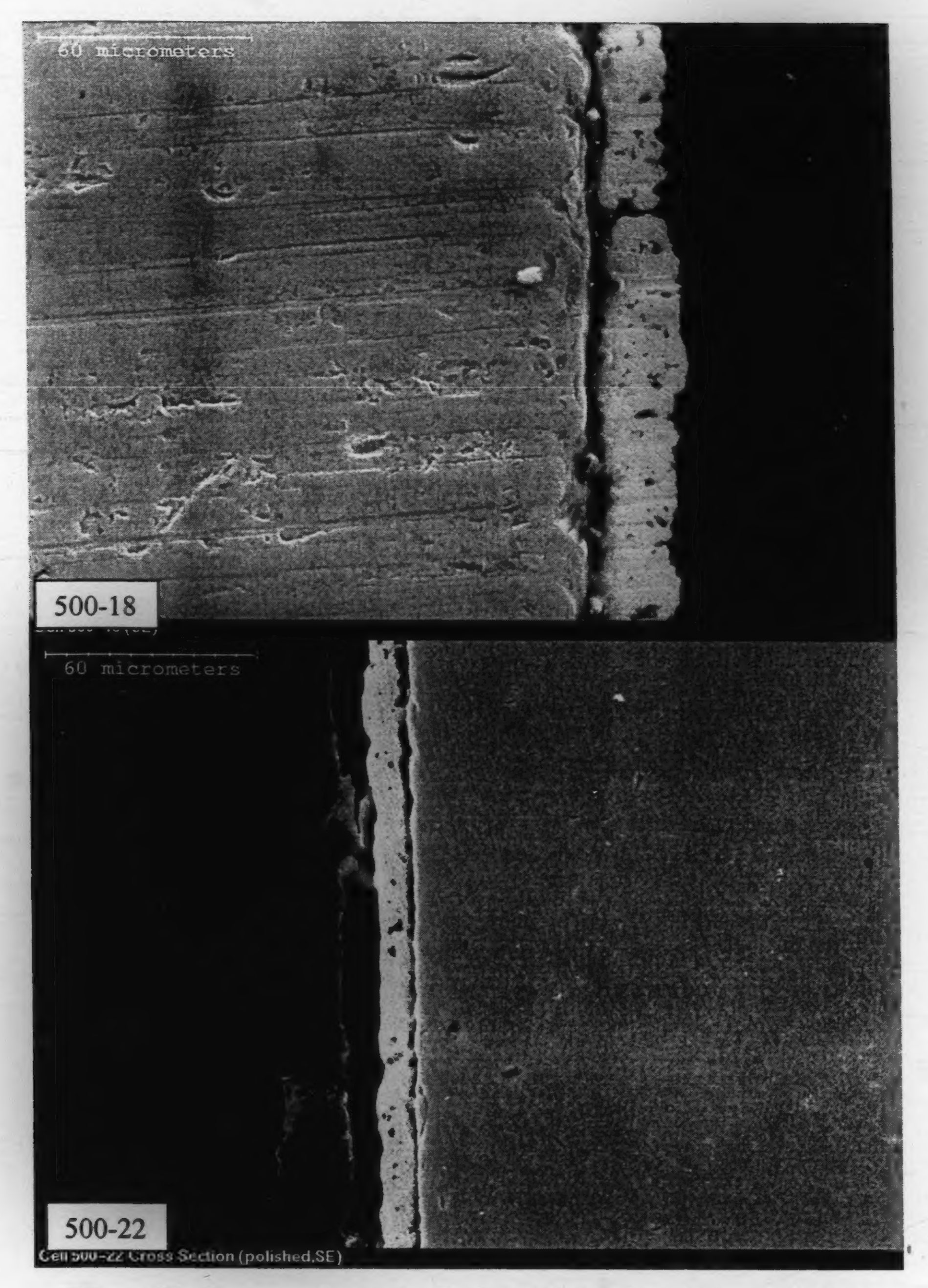
60 micrometers
500-18
60 micrometers
500-22
Cell 500-22 Cross Section (polished,SE)

Figure 33: Cross sections of cells deposited at 1050°C and -300mV

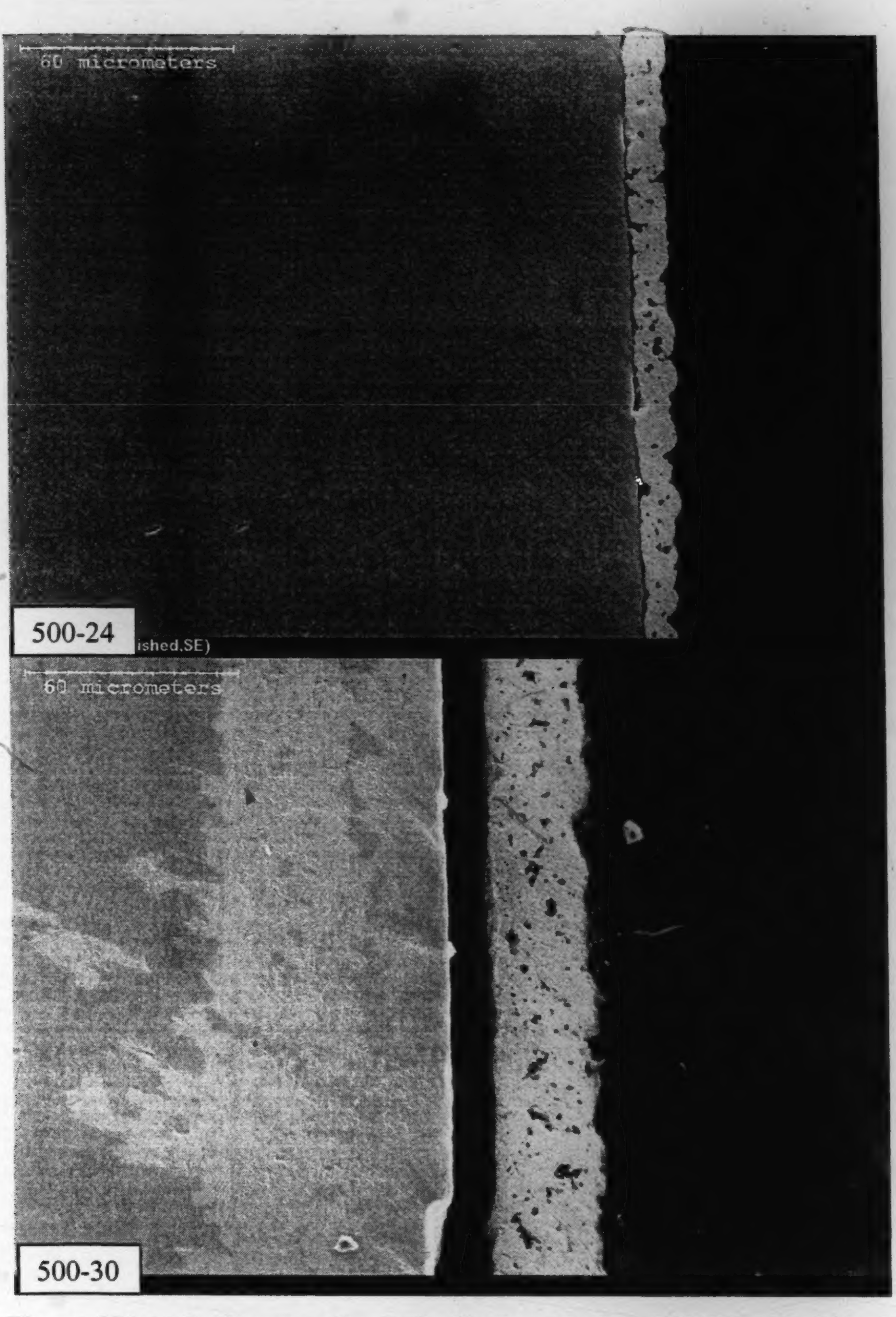
60 micrometers
500-24
ished,SE)
60 micrometers
500-30

Figure 33(cont): Cross sections of cells deposited at 1050°C and -300mV

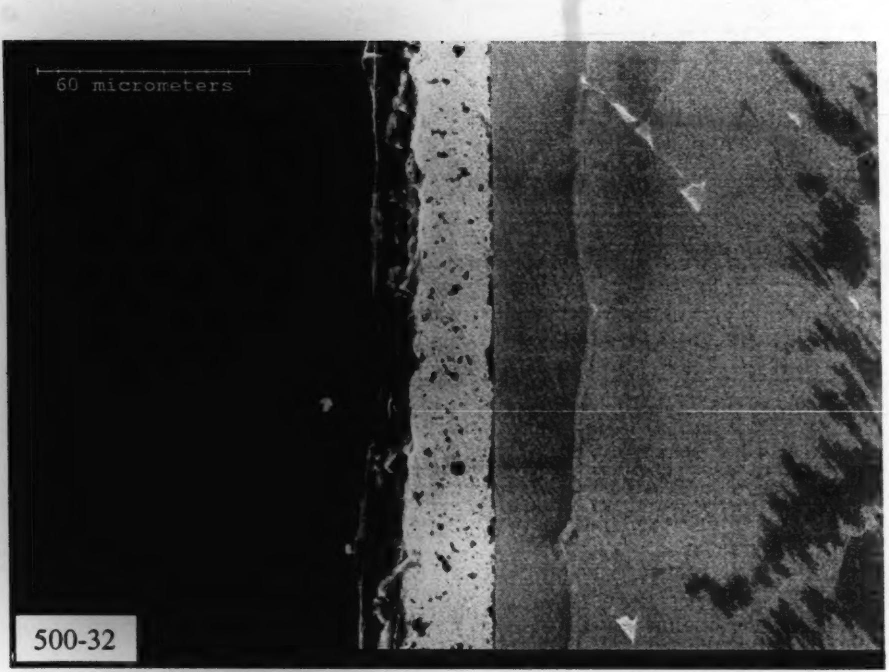

Figure 33(cont): Cross sections of cells deposited at 1050°C and -300mV

In this view the cells all seem to have comparable porosity. One notable difference between the cells is the quality of the electrode-electrolyte interface. In cell 500-24, where the performance was good, the interface is also good. Conversely, cell 500-18, which gave the worst performance, has a poor interface. The interfaces of cells 22 and 30 are not particularly good either, but it is likely that the detachment occurred during polishing of the sample and, therefore, would not affect the cell's performance.

Figure 34 shows the surface of cell 500-24 at higher magnification in both SE and BSE modes. Like the cells shown in the previous section there are small surface deposits of a dark appearing phase in the BSE image. These same deposits are light coloured in the SE image. Two of these deposits are labeled as points 1 and 2 in the BSE image (figure 34 b). EDX analysis of both of these points revealed them to have a similar composition. The spectrum collected for point 1 is shown in figure 35.

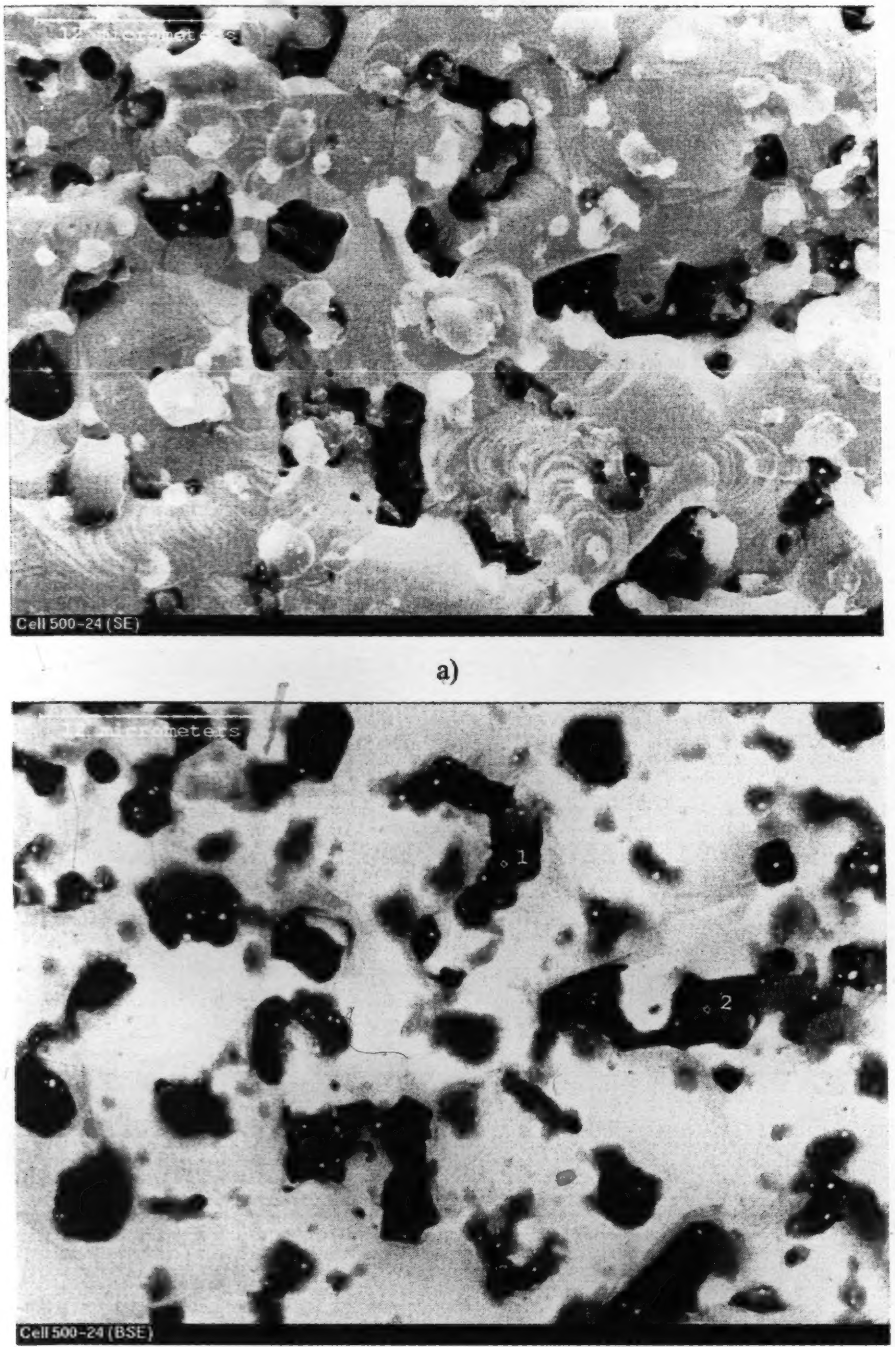
12 micrometers
Cell 500-24 (SE)
12 micrometers
1
2
Cell 500-24 (BSE)

a)

b)

Figure 34: SE(a) and BSE (b) images of the electrode surface of cell 500-24

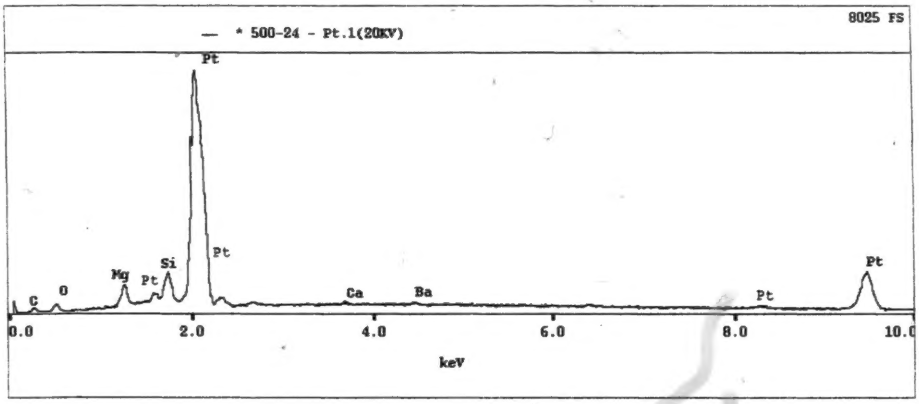

Figure 35: EDX spectrum for point 1 in figure 34 (b)

The peaks seen in this spectrum are similar to those seen in the surface deposit in cells deposited at -300 mV (figure 24). In figure 36 the spectrum for the electrode as a whole is shown. There is no significant difference between the spectrum for point 1 compared to that for the whole electrode. Because the deposit has a smaller atomic number than the base electrode, it is expected that the peaks for the low atomic number elements would decrease, relative to the platinum peak when the entire electrode area is scanned. That this is not observed suggests that a significant amount of platinum electrode is being sampled in the analysis of the dark phase. One possible cause of this is the geometry of the area being tested. Because the deposit is inside a pore, both backscattered electrons and x-rays from the deposit are likely to strike the pore walls, which are platinum. This can cause secondary fluorescence in the pore walls, giving an artificially inflated amount of platinum in the deposit.

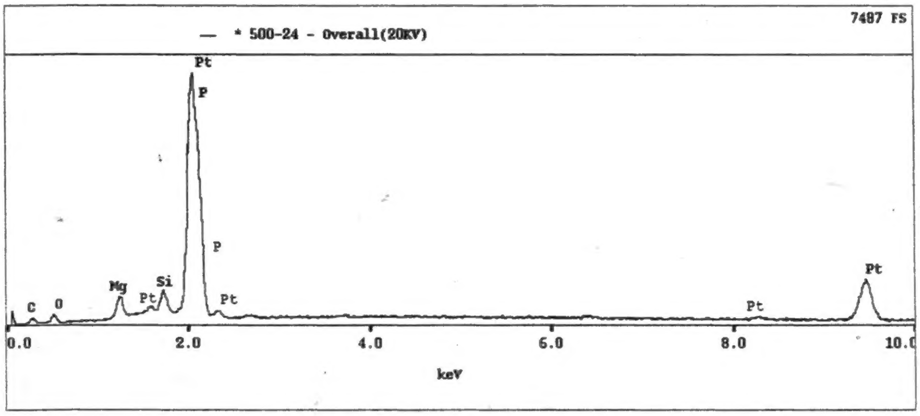

Figure 36: EDX spectrum for the entire electrode of cell 500-24

Points on the cross section of the sample were also analyzed with EDX. The focus was again on the dark phase in the pores of the sample. A spectrum collected at 30 kV from cell 500-24 is shown in figure 37. Because of the higher accelerating voltage it is possible to see the zirconium and yttrium K_α peaks, which occur at and above 15 keV. Although the zirconium peak is small, it is definitely present which clearly shows that there was some deposition in the pores by PEVD. The yttrium peak is so small that it could easily be overlooked on this scale. In part this is due to the large platinum peaks, which relegate small peaks to the background. The size of the peak indicates a low yttrium concentration, even relative to the zirconium peak. If this is the case, and a detailed quantitative analysis with another technique would be required to determine this, it could be part of the reason for incomplete coverage. Low yttrium content would result in low ionic conductivity in the deposit and slow growth. This in turn could lead to only partial coverage of the sample in the time allotted for deposition. Deposits did not grow very thick either, with typical deposit thickness through the cross section less than half a micron. The surface deposits seen in several of the images are thicker than those through the cross section.

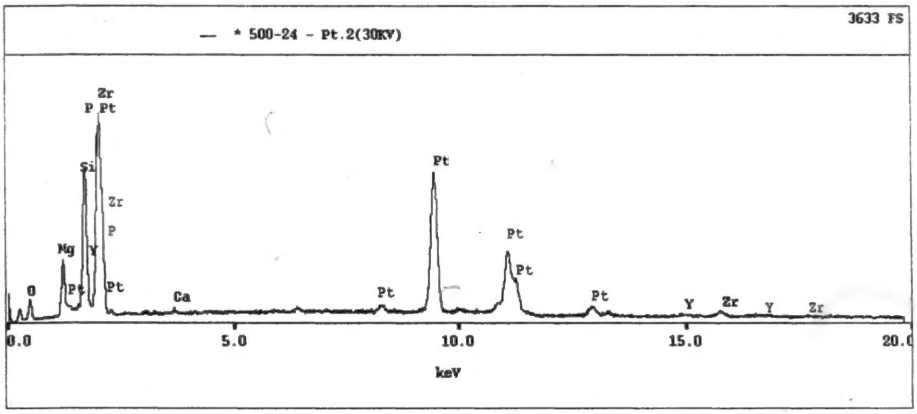

Figure 37: EDX spectrum for dark phase in pores of the cross section

The EDX results for the cross sections of other cells in this series were similar, with small zirconium K_α peaks visible, but little or no yttrium peak. The exception to this was cell 500-18, which did not show a distinct zirconium peak. If no deposition occurred, it could help explain the poor electrode adhesion, since the deposit must be in intimate contact with both electrode and electrolyte, so any deposit would improve contact. On the other hand, if the electrode detached before deposition, then there would be no deposit on the electrode.

When PEVD is carried out at 1050°C the performance of the cells tends to improve as the deposition voltage is made more negative. Other factors can affect this trend, such as electrode-electrolyte adhesion, and any leakage of the seal. In the next section the effect of deposition temperature will be examined.

5.4 Deposition Temperature

The next variable to be adjusted was the deposition temperature. A series of cells were deposited at 900°C as well as one at 950°C. The cells were deposited using a variety of deposition voltages, with the specific conditions for each cell shown in table 6. The electrochemical test results are shown in figures 38 and 39.

Table 6: Deposition conditions for cells deposited at less than 1050°C

Cell	T(°C)	t(min)	V(mV)
500-15	950	1440	-200
500-33	900	4240	0
500-34	900	1800	0
500-35	900	2580	-300
500-37	900	2940	-400
500-38	900	5600	-400
500-40	900	3507	-500

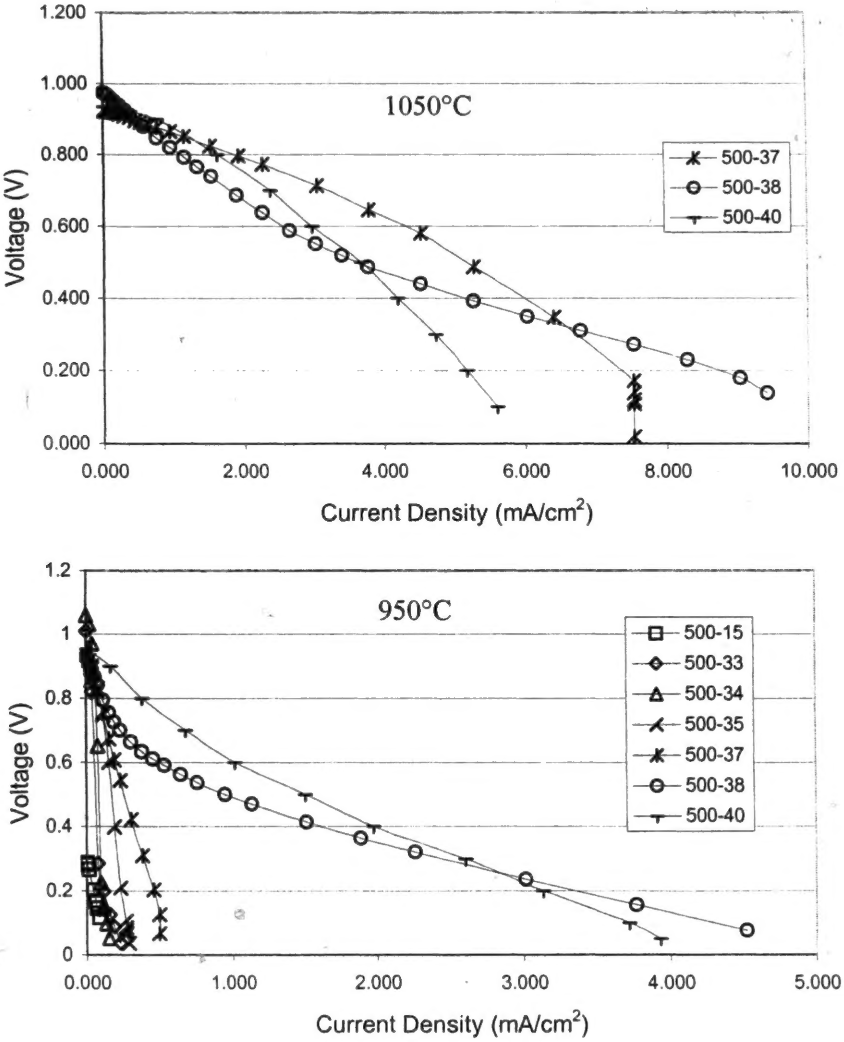

Figure 38: I-V curves for cells deposited at less than 1050°C

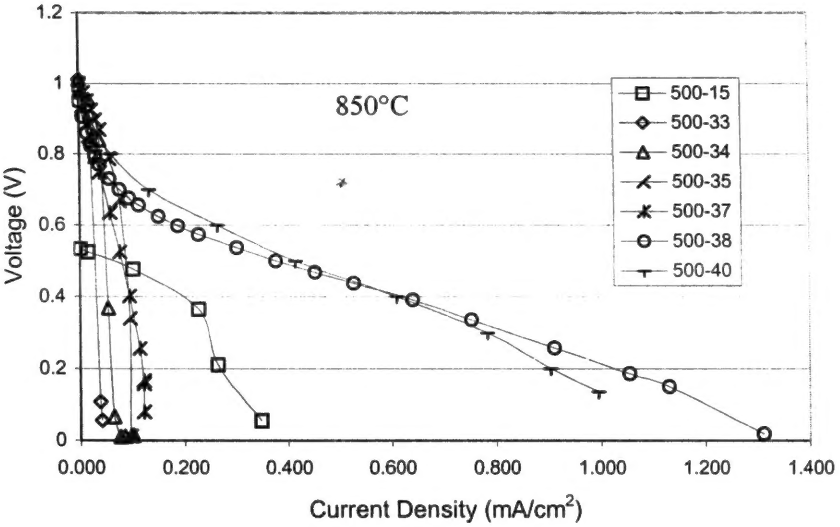

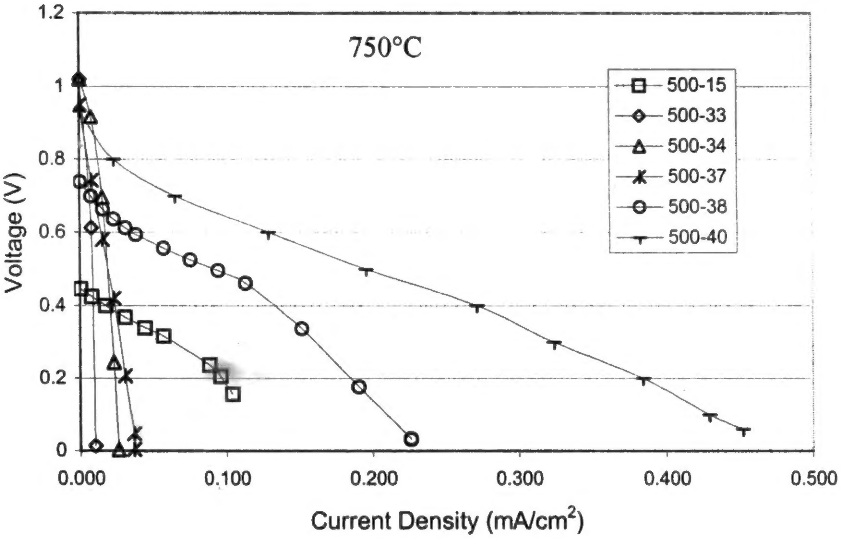

Figure 38 (cont): I-V curves for cells deposited at less than 1050°C

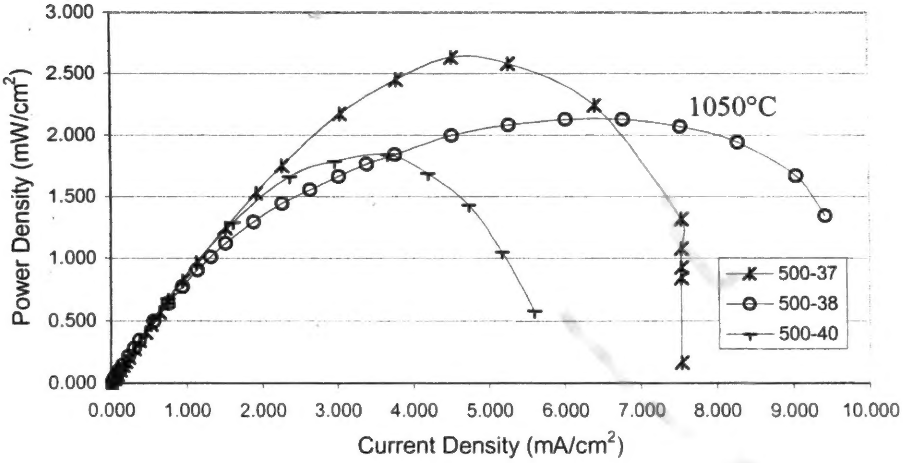

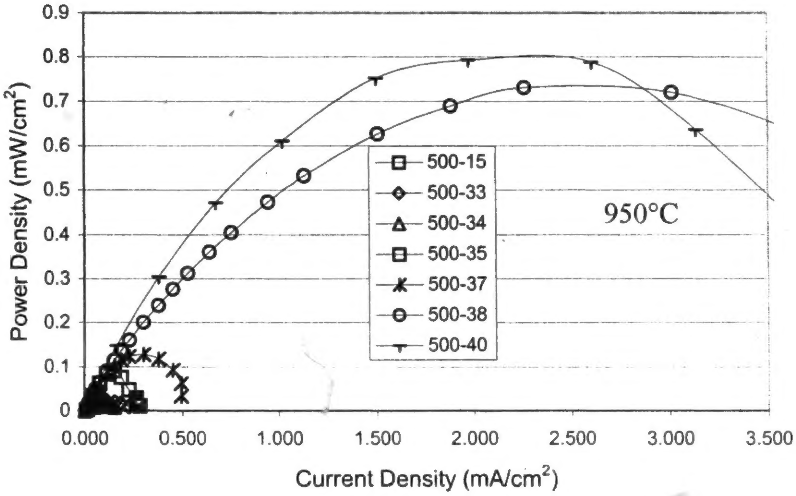

Figure 39: Power density for cells deposited at less than 1050°C

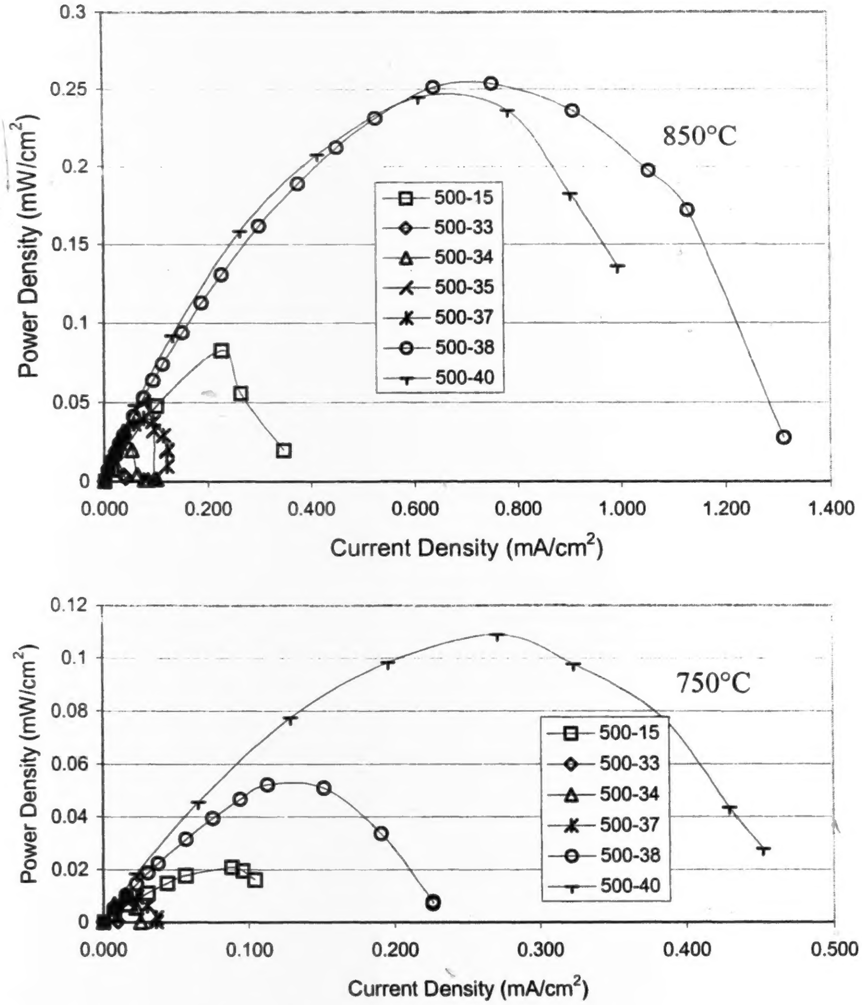

Figure 39 (cont): Power density for cells deposited at less than 1050°C

Not all of these cells were tested at 1050°C, since this was above their deposition temperatures; however, those that were showed similar performance at this temperature. The maximum power density achieved here is slightly more than 2.5 mW/cm^2, which is well below that for cells deposited at 1050°C and -300mV. Compared with the other cells deposited at 1050°C, these three do outperform those that were deposited at -200 mV, 0 mV and +300mV. Deposition for both cells 500-37 and 38 was carried out at -400mV, while cell 40 was deposited at -500 mV.

Below 1050°C, cell 500-38 and 40 well outperform the other cells in this group in terms of power density and, with the possible exception of 500-15, in polarization behaviour as well. At 750°C cell 500-15, which was deposited at 950°C and -200mV, has similar polarization behaviour to 500-38 and 40; however, the OCV is much smaller for 500-15. Cell 500-15, although not competitive with cells 38 and 40, stands out from the rest of the cells at 850°C, while at 950°C its OCV is so low that it is difficult to compare the cell with other ones in the group. This general trend indicates that cell performance improves not only as the deposition voltage becomes more negative, but also as the deposition temperature is raised.

A possible exception is seen for cells 38 and 40, which were deposited at low temperature, yet have very good performance, particularly at 750°C. In fact cell 40 gives the highest power density of all the cells tested at 750°C regardless of deposition conditions. Similarly cell 38 gives the third highest power density, after only cell 26. Comparison of the I-V curves of these cells (figure 40) reveals that the initial activation polarization of cells 38 and 40 is quite similar and less than that of cell 500-26. Where the difference is made up is in the second portion of the curve, the cell resistance, where cell 26 has a much shallower slope. The reason why the performance of cell 38 is so much less than that of cell 40 is a sharp drop off in voltage after about 0.1 mA. This is reminiscent of the drop off seen when concentration polarization becomes rate limiting, and is not surprising in this cell given its dense structure (figure 41 to appear). Why this is not seen in cell 500-26, which has a similar dense structure (figure 21), is not immediately clear. It is possible that the improvement is due to the coating, as it would have more of an effect at lower temperature due to lower overall electrode activity.

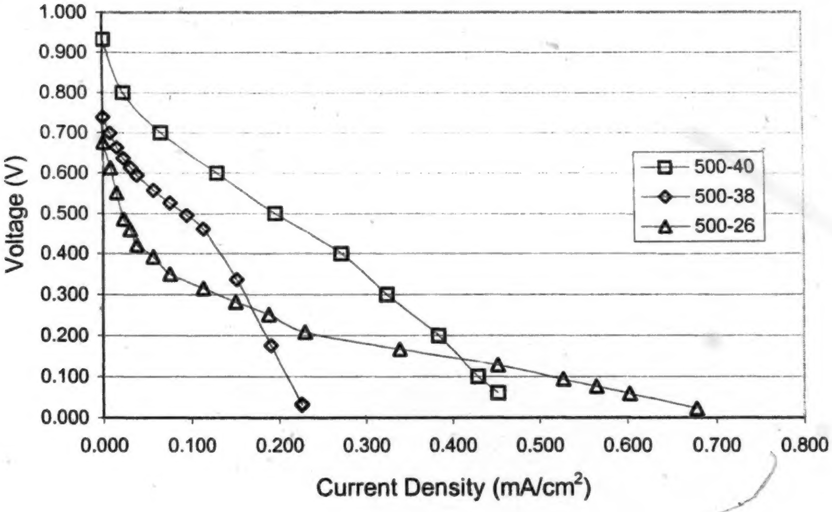

Figure 40: I-V curves for three best performing cells at 750°C

Figures 41 and 42 show SE images of the electrodes in this series in plan view (figure 41) and cross section (figure 42). No cross sectional image is available for cell 500-15. Also of note in the cross sectional images is that while sample 500-33 was prepared by mounting, sectioning and polishing, as were previous samples, cells 34, 35, 37 and 38 were all prepared by cleavage of the sample. This was done to eliminate smearing of the microstructure during polishing and sectioning, which was believed to obscure porosity. Examination of these cross sections shows that the apparent porosity of the sample is indeed affected by polishing; however, polishing gives a much flatter surface, which is beneficial for EDX analysis.

From figure 41 it is clear that only 500-38 shows the kind of electrode densification that was seen in some of the cells deposited at 1050°C. This is attributable to a lessening of diffusion of the electrode material during deposition, since the sample was not exposed for long periods at 1050°C. Densification of 500-38 is likely due to a combination of very long deposition time, close to four days, and sintering at the testing temperature of 1050°C. All of the electrodes in this series exhibit the same low atomic number coating seen in previous samples and, as before, the deposit contains increased amounts of silicon, magnesium and phosphorous. EDX analyses of the cross sections of these samples were also similar to previous results. Zirconium K_α peaks were visible for all the samples, while yttrium peaks were visible in some areas of some samples. A close up of cell 500-33 in BSE mode is shown in figure 43, while figure 44 shows the EDX spectrum for one of the points denoted in the BSE image. Clearly there is some zirconium present, as well as some magnesium and silicon. There also appears to be a very small peak for yttrium at 15 keV. Results obtained for other cells were similar to this, sometimes with a more pronounced yttrium peak, and sometimes with none at all.

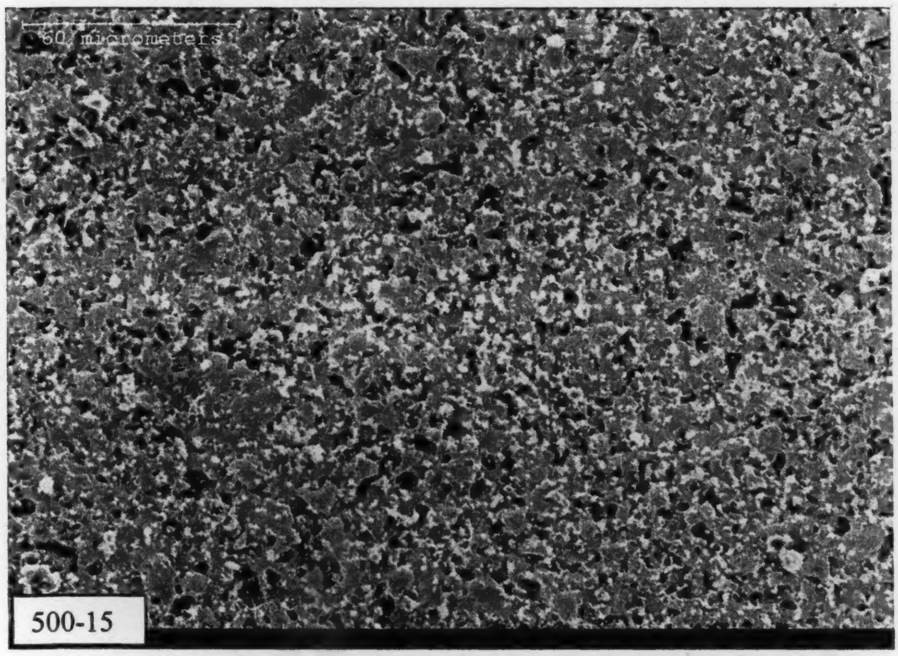

Figure 41: Plan view of anodes of cells deposited at less than 1050°C.

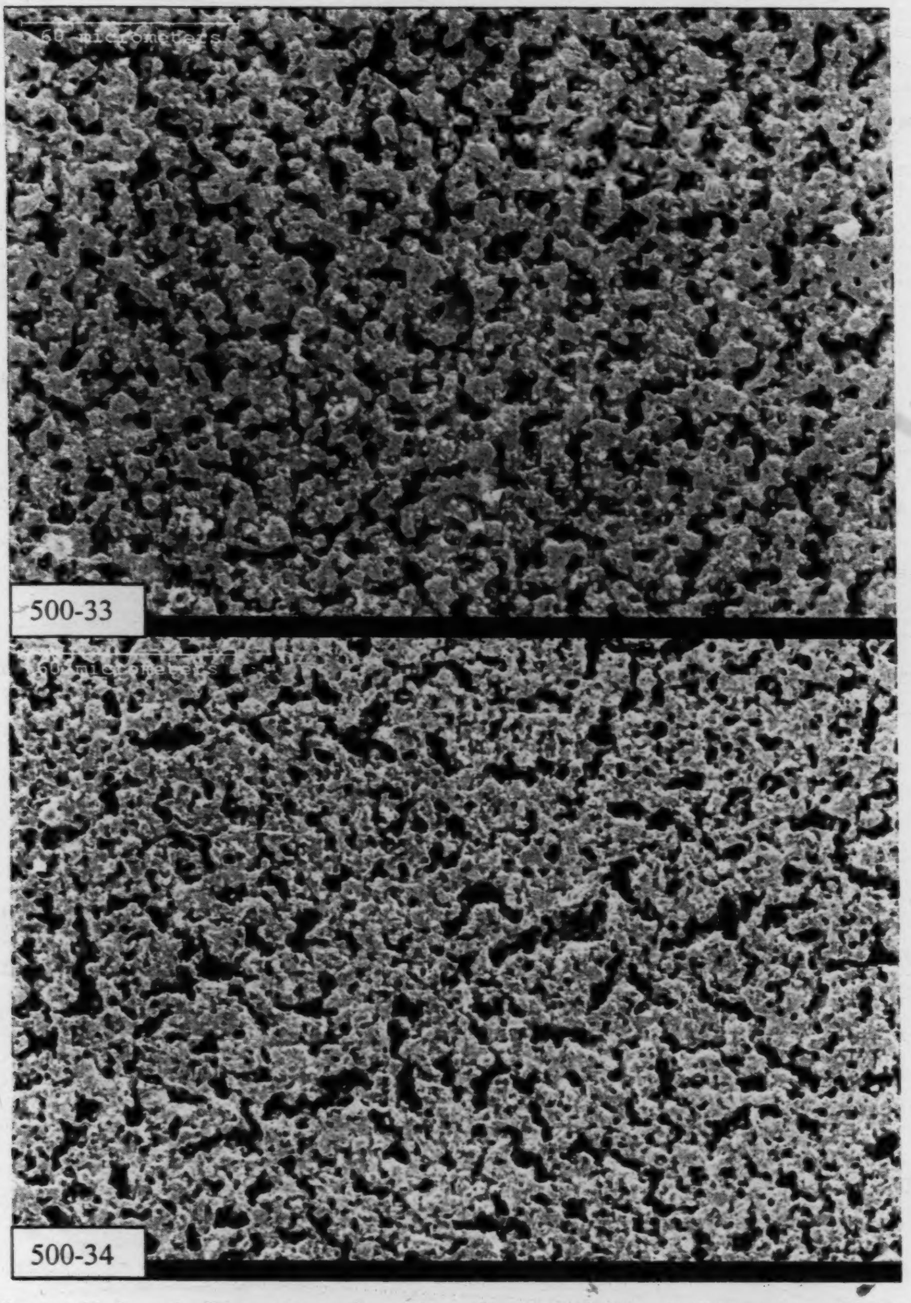
60 micrometers
500-33
60 micrometers
500-34

Figure 41 (cont): Plan view of anodes of cells deposited at less than 1050°C.

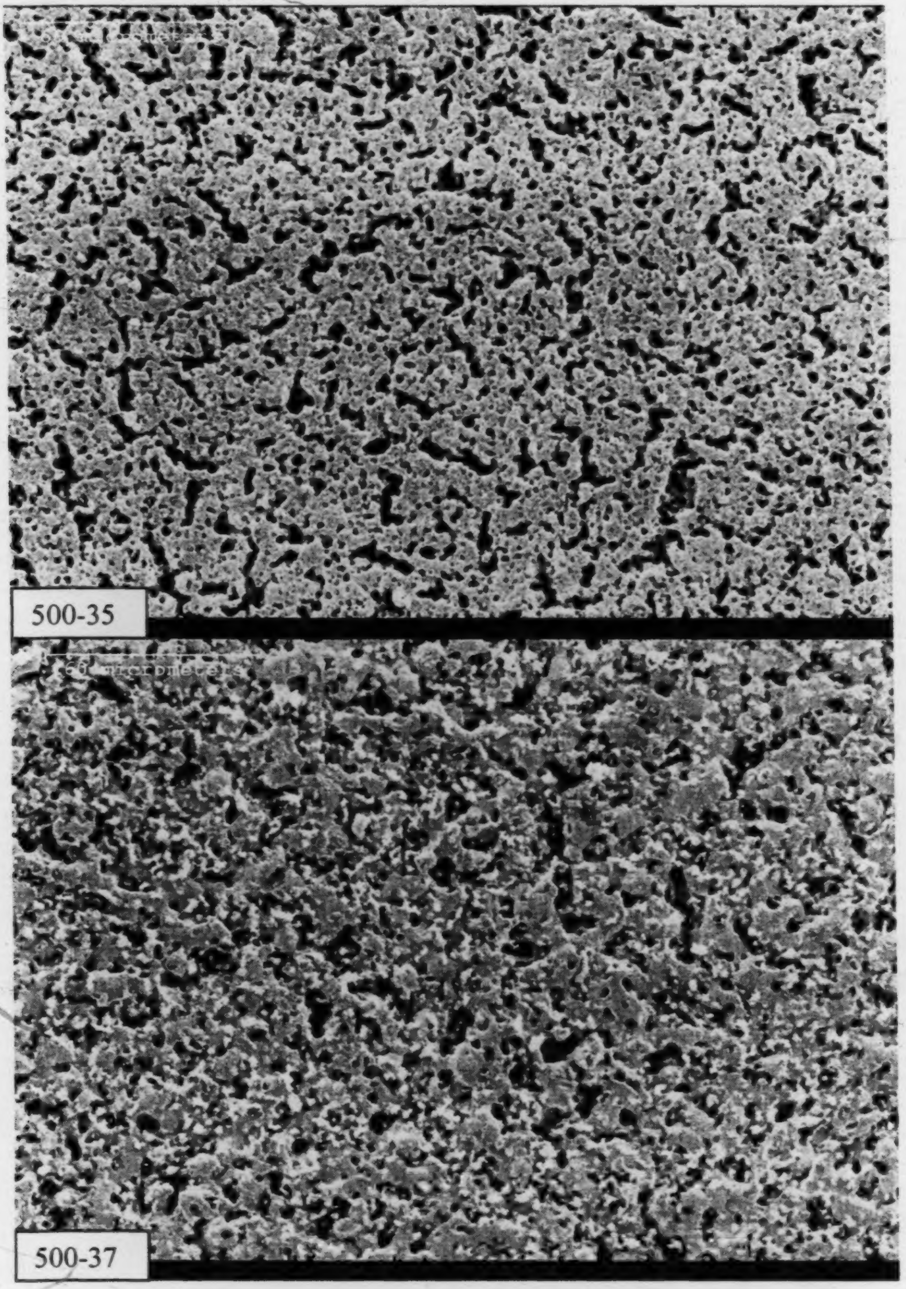
500-35
60 micrometers
500-37

Figure 41 (cont): Plan view of anodes of cells deposited at less than 1050°C.

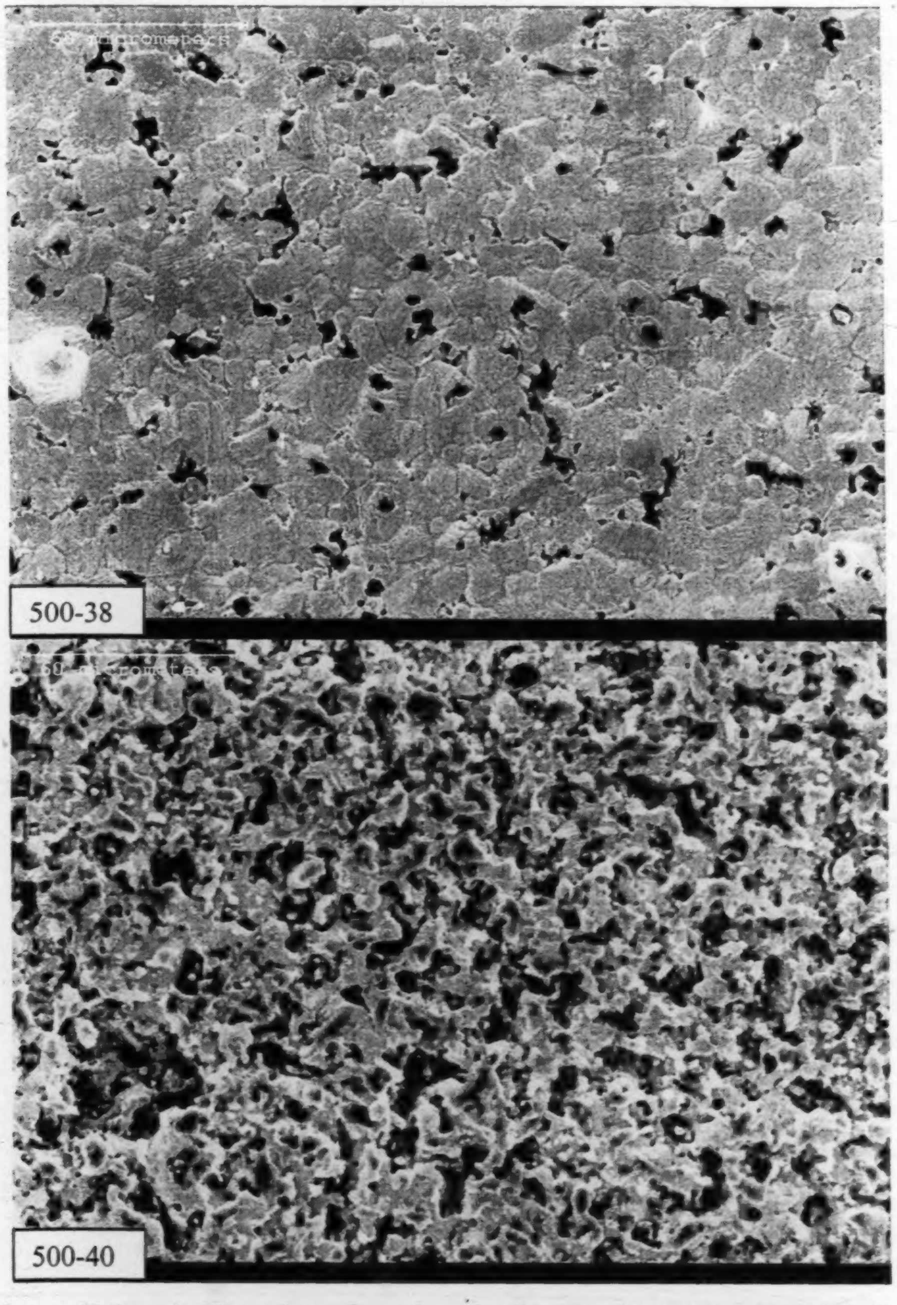
50 micrometers
500-38
50 micrometers
500-40

Figure 41 (cont): Plan view of anodes of cells deposited at less than 1050°C.

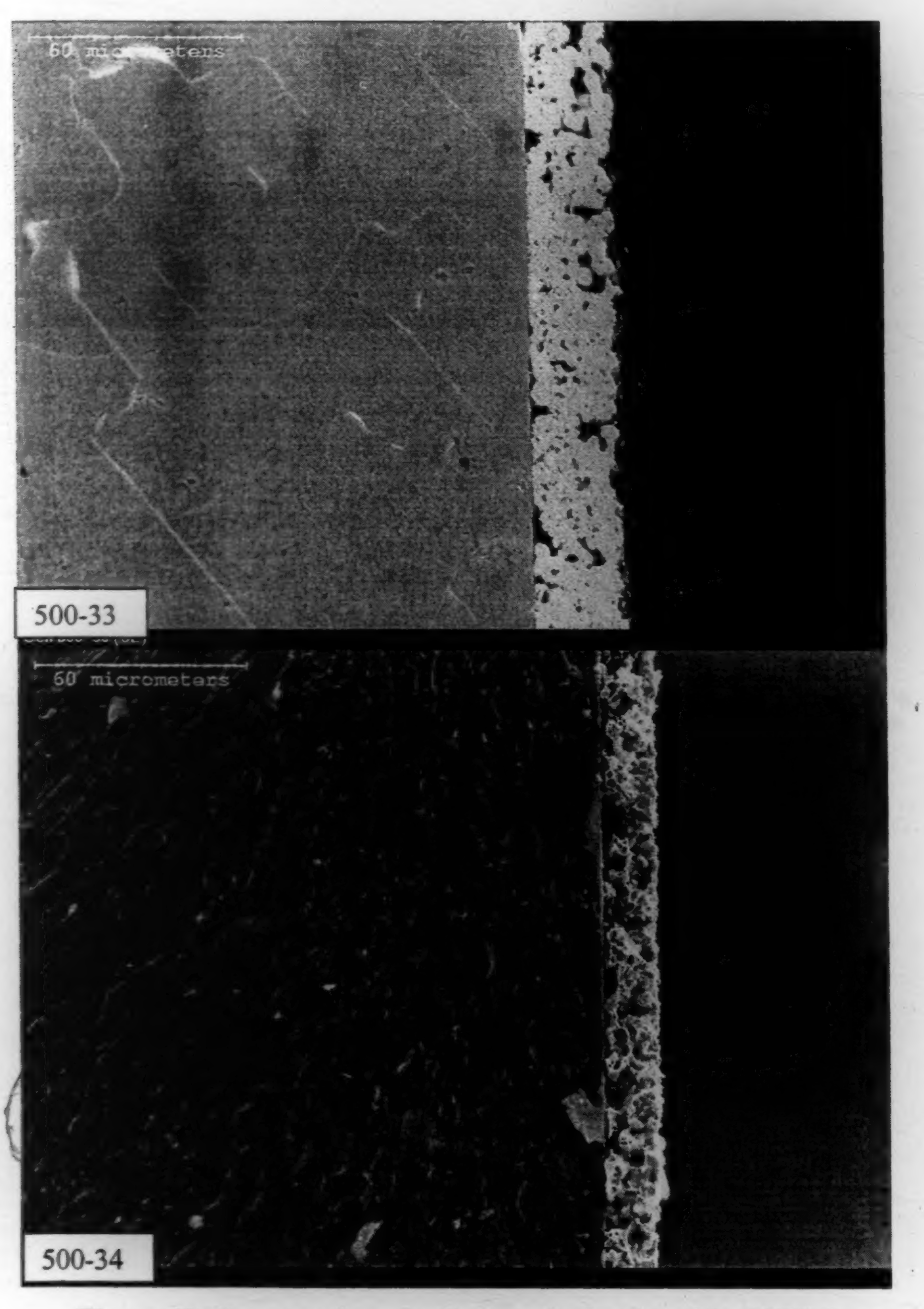
60 micrometers
500-33
60 micrometers
500-34

Figure 42: Cross section of cells deposited at less than 1050°C

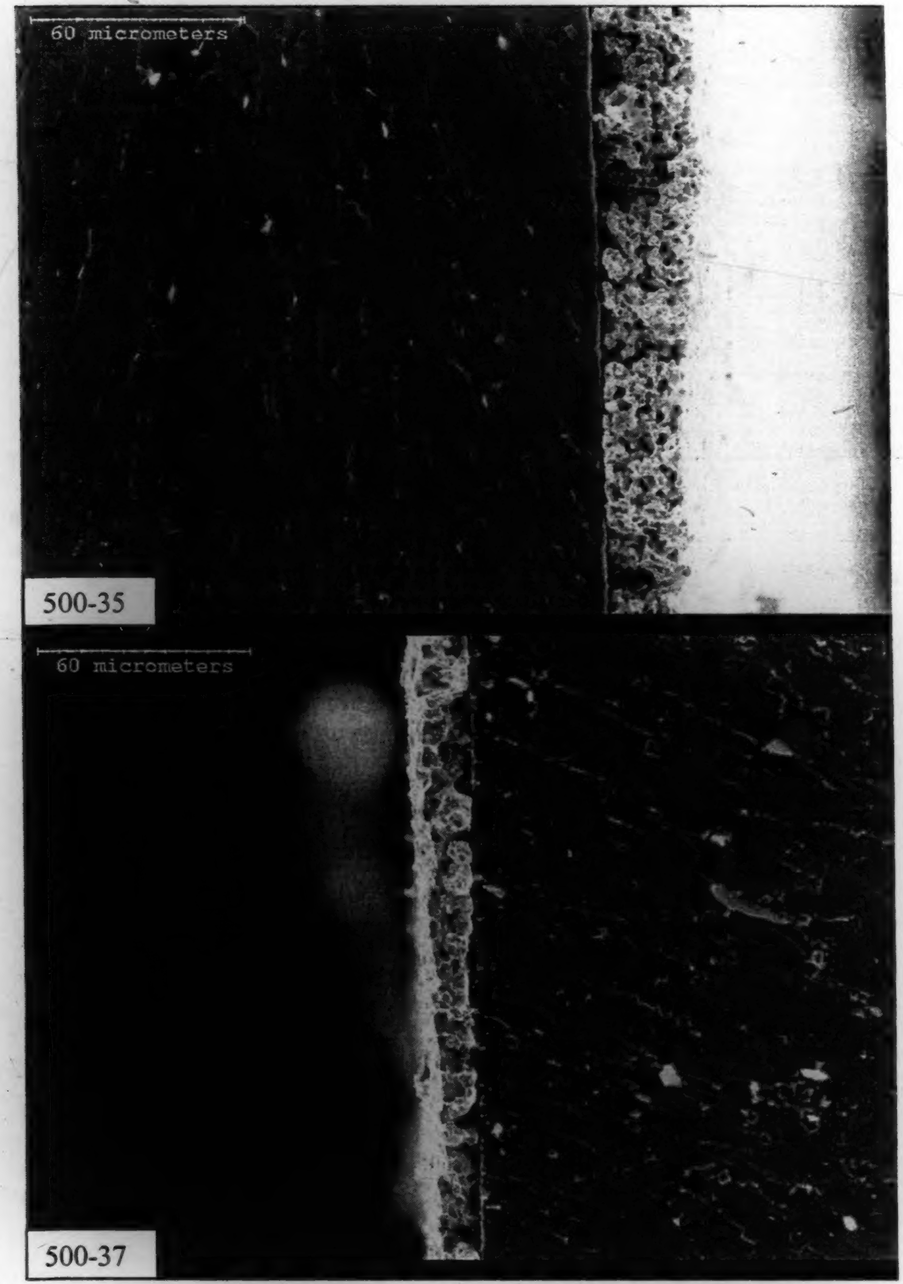
60 micrometers
500-35
60 micrometers
500-37

Figure 42 (cont): Cross section of cells deposited at less than 1050°C

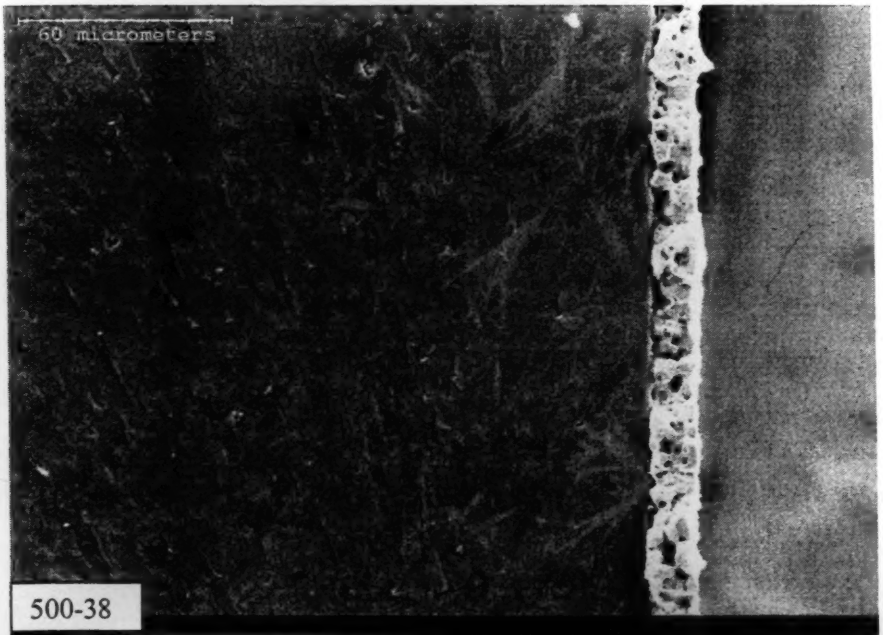
60 micrometers

500-38

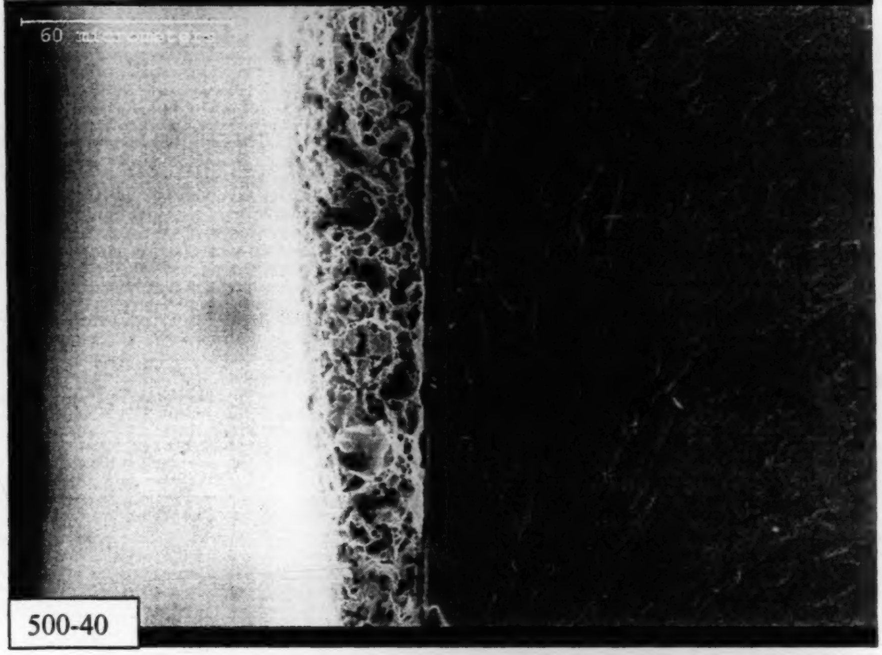
60 micrometers

500-40

Figure 42 (cont): Cross section of cells deposited at less than 1050°C

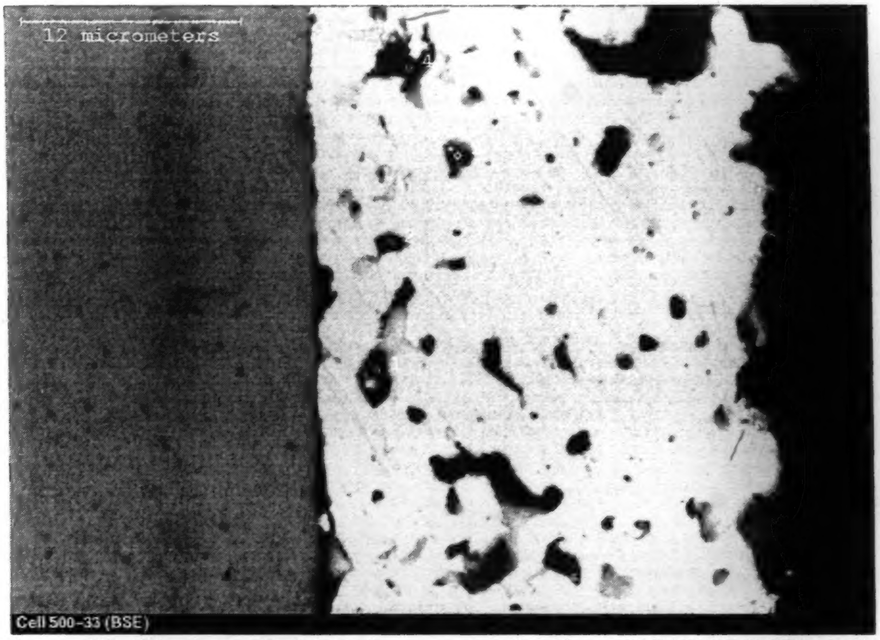

Figure 43: Close up of electrode cross section for cell 500-33 (BSE mode)

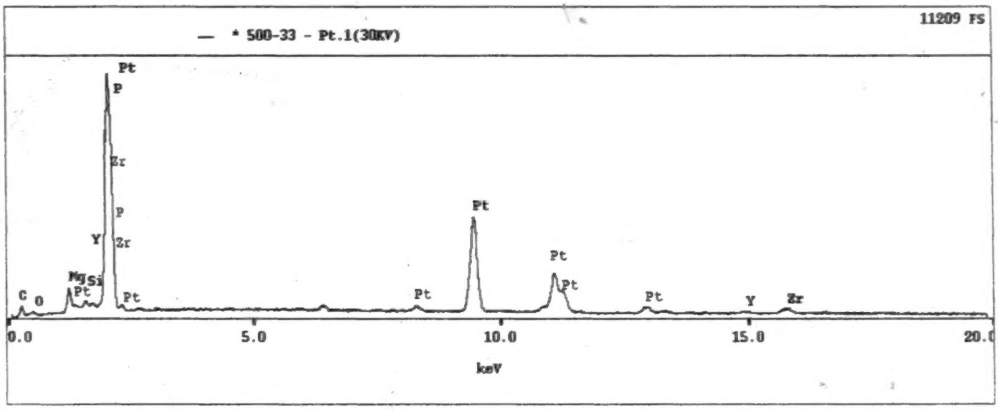

Figure 44: EDX spectrum for point 1 in figure 43

Of the cells in this grouping the worst polarization is exhibited by 500-33; however, microstructural examination reveals it to have a very open pore structure and good electrode-electrolyte adherence. This cell also had an OCV of nearly one volt for all the tests, so sealing was not the problem. From the available information, no conclusion can be drawn as to the root cause of the poor polarization behaviour.

Thin film EDX analysis of these samples was also conducted; however, the results shed little information on the nature of the deposit. An anode, onto which no deposition had been done, only showed the diffraction peaks for platinum. Similarly the XRD pattern for 500-15, which did have a deposit, showed only the peaks for platinum.

Sample 500-34 was also analyzed, and it showed additional diffraction peaks, which correspond to those for yttria-stabilized zirconia (figure 45). This pattern was a lot noisier than the other patterns; however, all of the major peaks seem to indicate either platinum or YSZ. This is perhaps due to the deposit, but may also be due to the substrate. Since 500-34 was sectioned for the SEM examination it did not have the same geometry as the standard, so diffraction peaks from the substrate cannot be discounted. Additionally no peaks were identified that belong to either silicon or magnesium compounds, while both these elements were detected in the deposit by EDX. Therefore two possibilities exist: Firstly the deposit does not contain a significant amount of Mg or Si when compared to YSZ, and the EDX analysis was wrong, or secondly the YSZ peaks in figure 45 are due to the substrate. Analysis of the surface by WDX showed that this sample did indeed have more zirconium in the sample than did cell 15. This is shown in figure 46, where zirconium appears as a shoulder on the large platinum peak. It still seems unlikely though that this zirconium is responsible for the YSZ peaks seen in figure 45, since the zirconium from the deposit is a very small percentage of the total electrode, and XRD is very insensitive to minor elements.

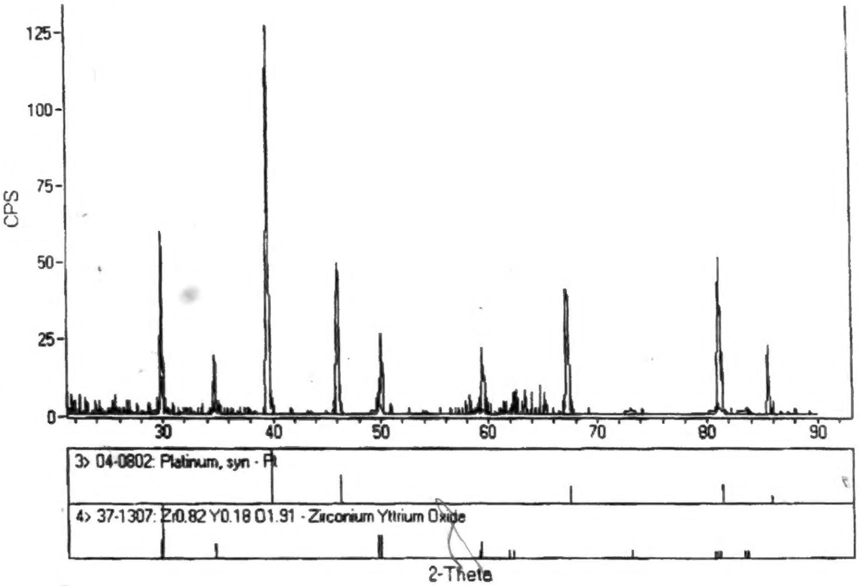

Figure 45: XRD pattern for anode of cell 500-34

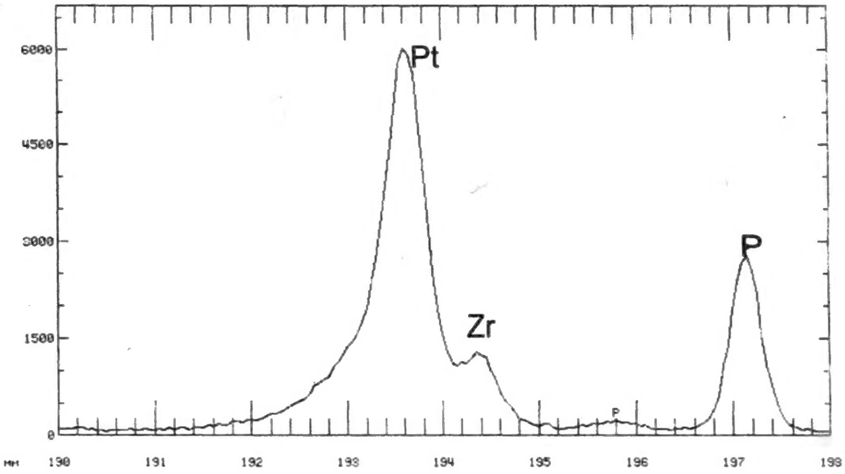

Figure 46: WDX spectrum for cell 500-34

A close up of the cross section of cell 500-38, which had good polarization behaviour, is shown in figure 47. Here, thin, semitransparent layers of YSZ are seen coating the platinum electrode, particularly near the electrolyte surface. This leads to better contact between the electrode and electrolyte. Also it prevents sintering of the electrode near the electrolyte surface, as evidenced by the increased porosity near the electrolyte, as compared to the surface porosity seen in figure 41. The combined effect of these two features is improved polarization behaviour and increased power density, as seen earlier. Complete coating of the electrode surface should further impede densification of the electrode due to sintering. In order to achieve this a balance must be obtained between high deposition rate and low sintering rate. Because deposition rate seems to increase with temperature, as does the diffusion rate, this may not be easy. Perhaps the best way to achieve this is with long deposition times at reduced temperature and high deposition voltages. Some evidence to support this theory was obtained from cell 500-40, which was deposited at a high negative voltage and reduced temperature, and gave the best performance of any cell tested at 750°C .In any event the results seen here clearly show that there are advantages in modifying the structure via PEVD. Despite the low porosity of the electrode surface, the improvements that resulted from a good PEVD deposit were enough to give this cell a performance comparable to any of the others at low operating temperature.

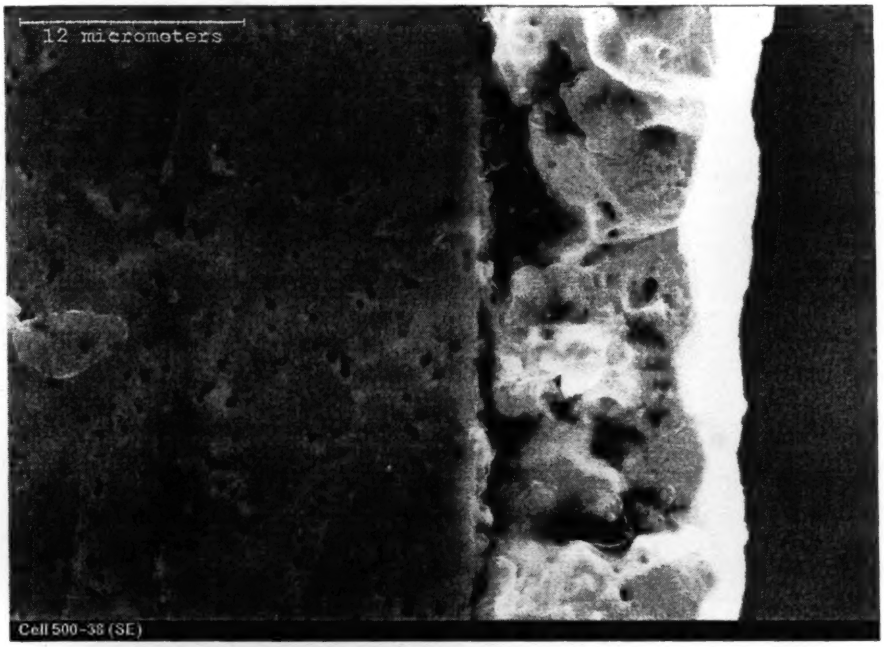

Figure 47: Cross section of cell 500-38

Further evidence of the improvement of electrode performance with deposition can be gained from impedance measurements on the cells before and after deposition. Figure 48 shows the effect of deposition on the cell impedance in the deposition environment. The reason why the final point on the before deposition plot is so far removed from the rest of the arc is not known, but whatever caused it is eliminated after deposition. Also, the portion of the graph below the x-axis is thought to be due to inductance in the lead wires and will be ignored, as it does not appear to be affected by deposition. Note that the scales on the two graphs are different, so the total impedance of the cell after deposition is about half that of the main arc of the cell before deposition. Additionally two distinct processes become apparent after deposition, whereas before deposition the arc appears to be due to a single process. Overall though, the deposition process is shown to improve electrode performance significantly when done under conditions of low deposition temperature.

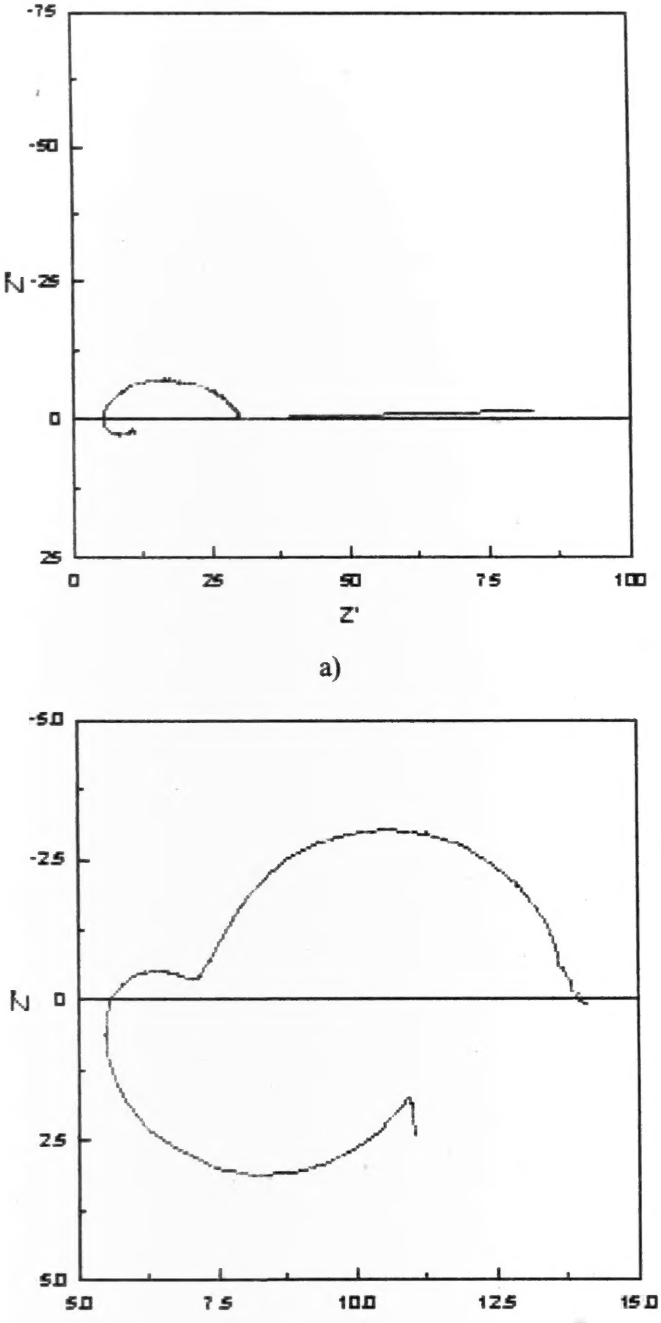

a)

b)

Figure 48: Complex impedance plots before (a) and after (b) deposition

5.5 Effect of Deposition Time and Temperature

As was done with cell 500-39 at 1050°C and -300 mV, cell 500-40 was deposited in stages at 900°C and an applied bias of -500 mV. The effect this had on the polarization and power generation characteristics of the cell is shown in figures 49 and 50, respectively. Upon comparison of these curves with those for cell 39 (figure 28), a significant change is noticed. For cell 39 the performance of the cell degraded with time, then reached a plateau. For cell 40 the performance also decreases with time up until 1307 minutes of deposition. The final curve, however, shows higher performance than was observed before deposition. This suggests that the changes in the electrode during deposition under these conditions (900°C, -500 mV) are different from those for cell 39 (1050°C, -300 mV). The most likely difference would be in the sintering of the platinum, which should be significantly less at 900°C than at 1050°C. This is confirmed in figures 41 and 42.

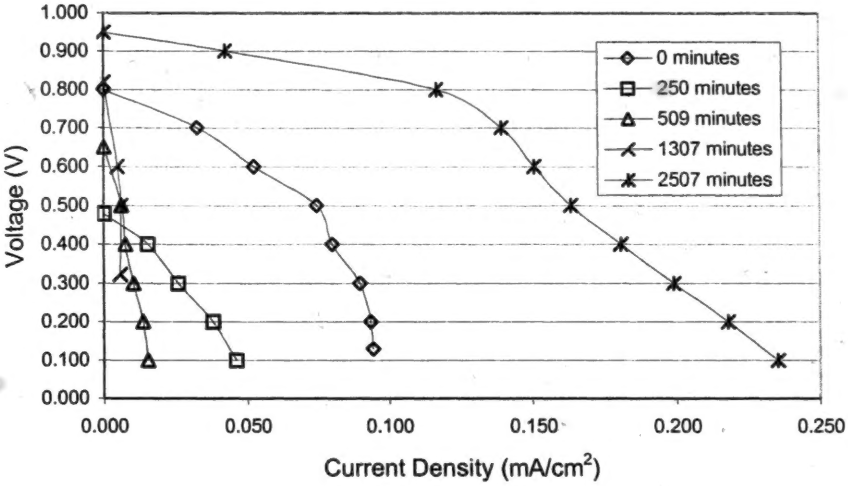

Figure 49: I-V curves during deposition for cell 500-40

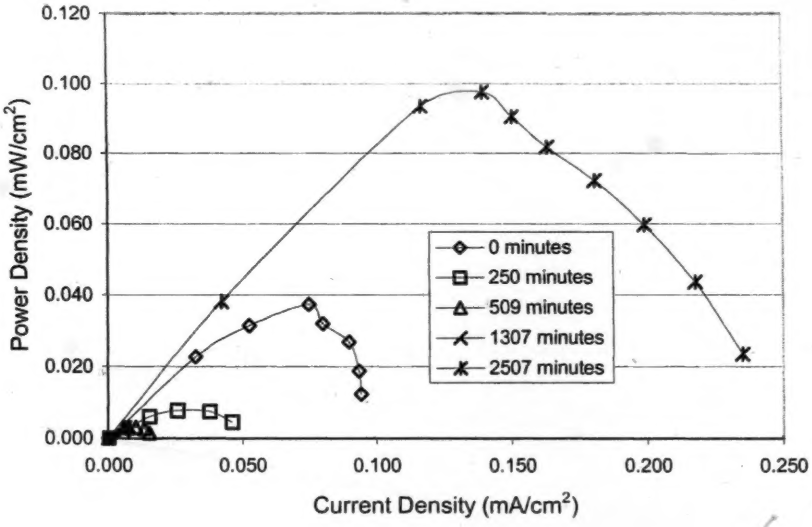

Figure 50: Power density of cell 500-40 during deposition

A comparison of close-ups of the plan view of these two cells shown in figure 51 shows more significant differences in the cell morphology. The texture seen on the surface of cell 39 indicates significant motion of the platinum, perhaps even melting during the course of cell deposition and testing. Cell 40 on the other hand has a smooth surface. This indicates that although 1050 °C is well below the melting temperature of platinum, it is too high a temperature for repeatable deposition by PEVD. Cross sections of these cells are shown in figure 52.

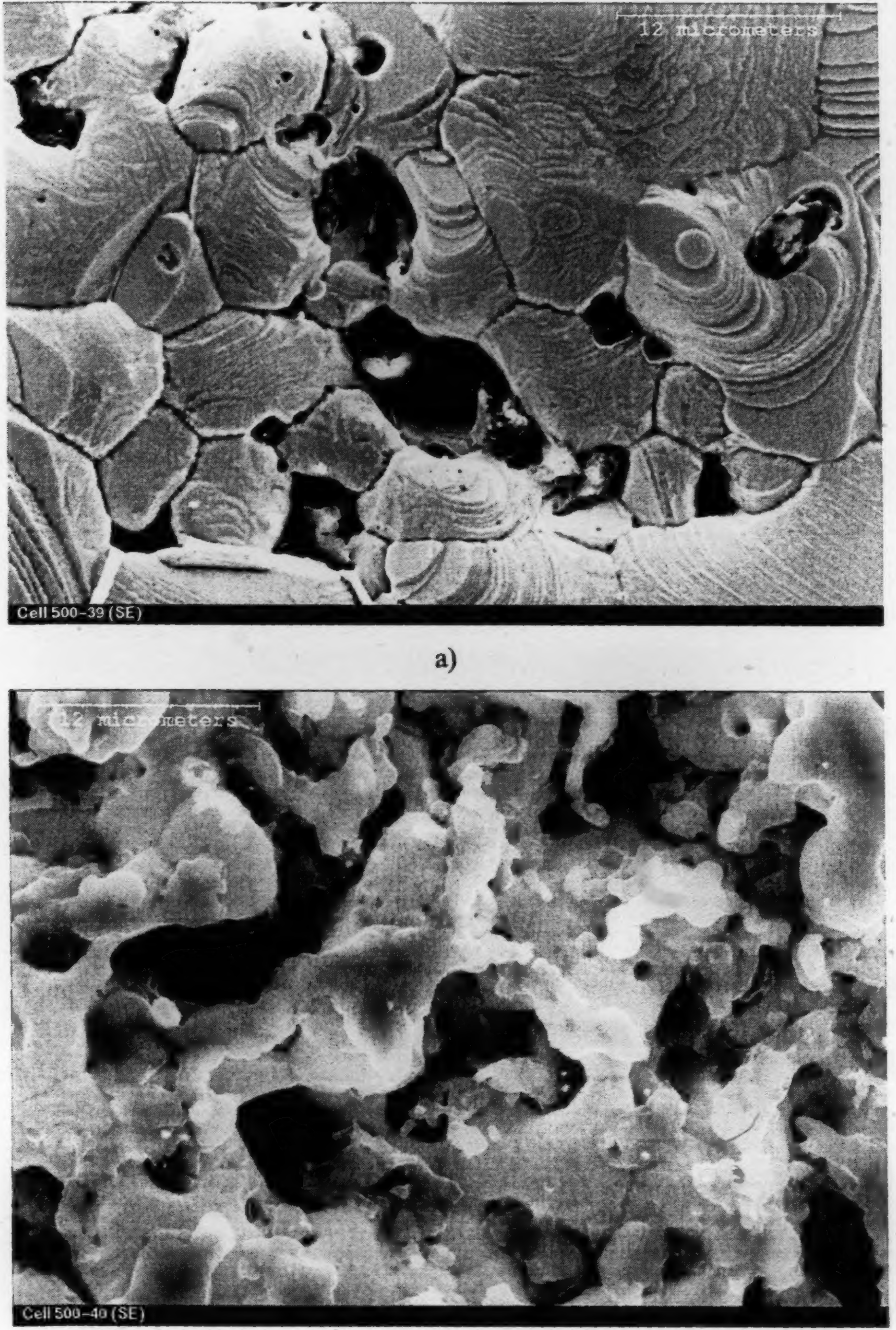
12 micrometers
Cell 500-39 (SE)
12 micrometers
Cell 500-40 (SE)

a)

b)

Figure 51: a) cell 500-39 b) cell 500-40

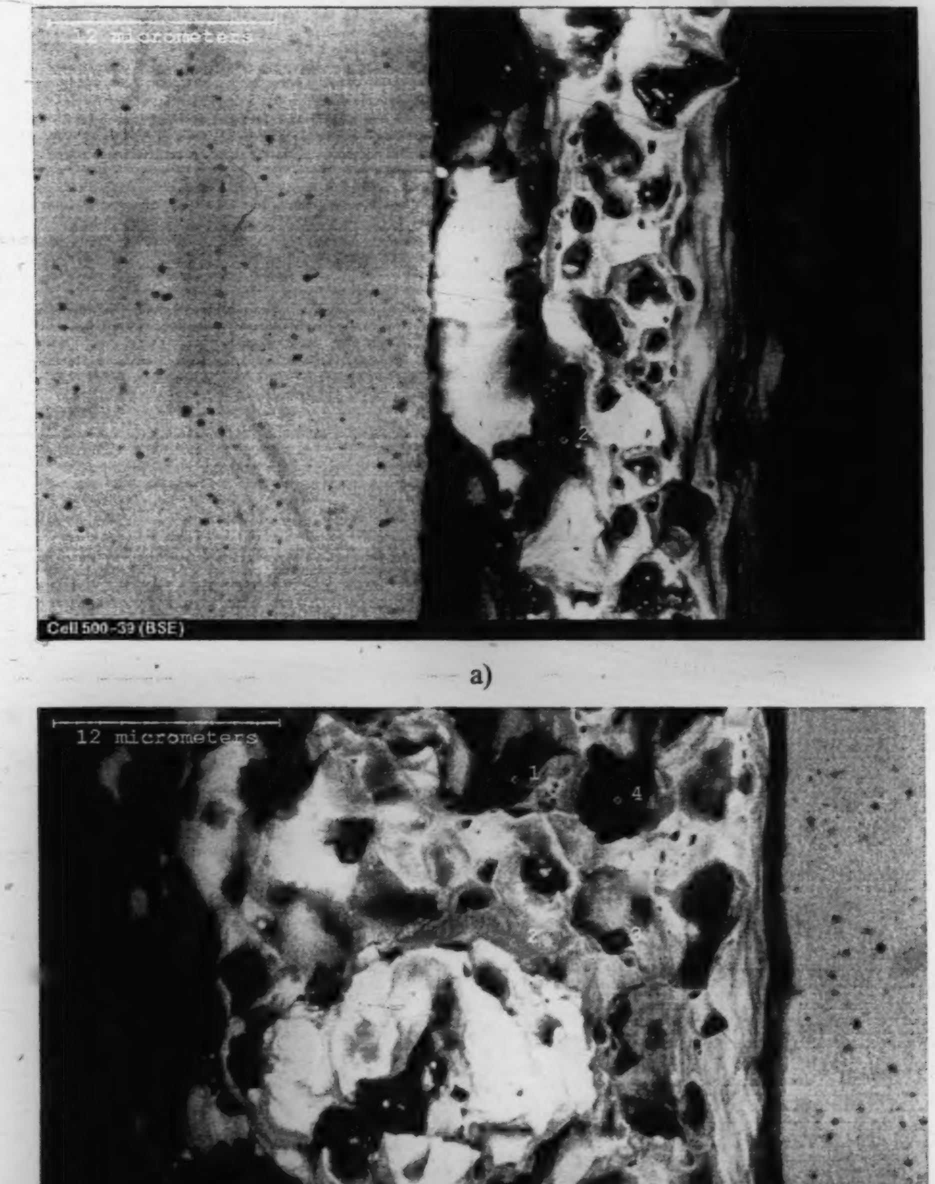
12 micrometers
Cell 500-39 (BSE)
2
12 micrometers
1
4
2
3
Cell 500-40 (BSE)

a)

b)

Figure 52: a) BSE cross section of cell 500-39 b) BSE cross section of cell 500-40

From these BSE images it is clear that the dark deposit phase, which has been shown to contain YSZ by EDX, is more pervasive in cell 40. This leads to larger 3PB length, and increased active area. The net result of this is that this cell gives excellent performance at low temperatures where the number of active sites is most important. These results show that, if the deposition temperature is not kept low, then sintering of the electrode can occur faster than the deposition reaction. This leads to a net loss of active sites. By keeping the deposition temperature low, densification can be limited and the number of active sites increased.

5.6 Pore Forming Agent Samples

Conductivity measurements on the samples made by the coated pore forming agent technique showed very low conductivities after reduction for the most part. This is not overly surprising considering the relatively low nickel concentrations (less than 15 vol%). Some samples however showed appreciable conductivity through the anode. These cells, designated HC 226 and HC 227, showed a conductivity of 0.6 S/cm, and were used for electrochemical testing. The outputs of these cells at 700°C are shown in figure 53. It is difficult to compare the performance of these cells to those used for PEVD since the testing temperature, electrolyte thickness and materials of construction are all different. However it is clear that this level of performance is not sufficient for use in commercial systems.

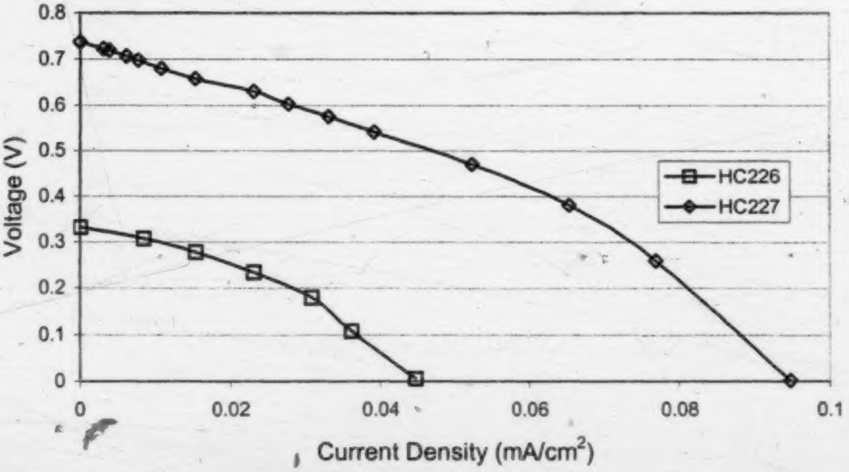

Figure 53: I-V curve for cells made by coated pore forming agent process.

In order to improve the performance of these cells it is recommended that the nickel content of the anode be increased to at least 30 vol% to ensure a continuous path through the nickel, and increase the catalytic surface area. The combination of this technique with PEVD is an interesting prospect because with the PFA technique it may be possible to engineer an electrode with a pore structure ideally suited for coating by PEVD; however, there is much work to be done before this can happen.

Chapter 6 Conclusions

From the results presented in the previous chapter we see that the deposition conditions have a significant effect on the nature of the PEVD coating and the cell performance. Although the film protects the metallic electrode from sintering once in place, care must be taken to avoid sintering of the anode during deposition. With the materials used, deposition at 1050°C more often than not leads to sintering of the anode before deposition is complete. Cross sectional examination of cells deposited at this temperature reveal that the deposit does indeed suppress sintering of the metal, but because film growth is so slow, the outer surface of the electrode densifies before it is coated. This leads to an overall loss of active sites and increased concentration polarization. The net result is a loss in cell output as the deposit is applied.

By increasing the applied bias that drives the PEVD reaction it is possible to improve the growth rate of the deposit. This is not enough though to overcome electrode diffusion at high deposition temperatures. When the deposition temperature is lowered to less than 1050°C, densification of the electrode surface is not normally observed over the course of deposition. Densification can still occur during cell testing at high temperature if the coating is not complete though. The best results for cell performance at low temperatures come from low deposition temperatures and high deposition voltages. This speeds up the deposition process somewhat and may be the cause of imperfect coatings. Imperfections in the coating, which is expected to be uniform, thin and dense cause the formation of active sites throughout the electrode wherever there is a hole in the coating.

Analysis of the films deposited is quite difficult due to the nature of the deposit and the materials chosen. Because the anode is a rough, porous surface it is difficult to get an accurate analysis of the composition of the thin deposit. Additionally, the overlap of the characteristic x-rays of platinum and zirconium make it impractical to use fluorescent x-rays to characterize the electrodes. This, in turn, makes it difficult to control the yttrium content of the film, which is crucial to the deposit's electrical characteristics. Because there are discrepancies in the literature for vapour pressures of yttrium chloride, it is not reasonable to assume that the yttria content of the film can be calculated directly using the Hertz-Knudsen relation. Therefore, with the current analytical techniques, it is possible only to estimate the yttria content of the film based on the appearance of the cell and the electrode performance.

It has also been shown that a deposit similar to the ones seen here does not significantly reduce the catalytic activity of the electrode. In fact, an increase in the tpb sites with a good deposit seems to play a larger role in determining electrode performance than does the loss of some catalyst surface. Additionally, the deposit does improve the resistance of the electrode to sintering. This should serve to improve cell lifetime at higher operating temperatures (1100°C), which may allow the SOFC to be connected directly to the exhaust of a coal gasifier.

The I-V tests done here also show that a very important factor in determining cell performance is the adhesion between the electrode and electrolyte. PEVD leads to good contact between these two cell components, leading to more stable performance.

Suggestions for Future Work

In order to fully evaluate the PEVD process and how it effects electrodes, it is important to have a good understanding of the effect of the yttria content of the film. This is important because it plays a major role in determining the electrical characteristics of the deposit. To simplify this task some changes should be made to the experimental setup. Firstly, the anode material should be changed from platinum to nickel, or another more common metal. This will not only make the results more applicable to commercial cells, but also simplify analysis of the film by its characteristic x-rays. Thus it will be much easier to determine the yttrium content of the film. Using, for example, nickel in place of platinum will increase diffusion during sintering though, giving at a deposition temperature of 950°C, a diffusion distance approximately twice that of platinum [168] making it more important to achieve high deposition rates.

Because the coating may have very high resistance to electronic charge carriers the increase in active area of the electrode due to PEVD may not have as large an effect on electrode performance as hoped. This is because electrons released on the anode surface need to pass through the coating to the electrode before being released to the external circuit. If the coating is thin enough, this may not be a problem, but if the coating is too thin, then it will have high resistance to the ionic current. If this is indeed a problem then two approaches can be taken to remedy the problem. Firstly a mixed conducting film can be grown. This would allow electrons to travel between the surface and the underlying electrode more easily, but as we have seen, mixed conducting deposits grow thicker than electrolytic ones, which could offset the benefits of having a mixed conducting deposit. The other alternative is to grow a porous coating. Thus the openings in the coating would expose the underlying metal to the surface so charge transfer at the pores will be more rapid. In order to grow such a film several possibilities exist. At low temperatures diffusion of adsorbed yttrium and zirconium chloride will be slower, and it may be possible to avoid forming a fully dense film. By increasing the deposition voltage the reaction rate can be increased, and if it can be made fast enough the film may not have time to densify during growth-the result being a porous film.

An alternative approach would be to start with a composite anode, already containing an ionic conducting phase. Thus there would already be 3pb sites throughout the electrode, so initial deposition would not necessarily be at the electrode/electrolyte interface. With the film growing from several active sites throughout the electrode, islands of the coating would form. If deposition were stopped before these islands could coalesce then, although the individual films would be dense, the overall effect would be a partial coating of the electrode, leaving some metal surface exposed.

Tests should also be done to determine how the film affects the response of the electrode to contaminants in the fuel. This is important for commercial application, where pipeline natural gas is a likely fuel of choice. It will also benefit SOFC development for use in conjunction with coal gasifiers, where there may be a large number of impurities in the fuel which would be too expensive to remove.

Some preliminary work was also done in which it was shown that it is possible make electrode pellets of a metal coated ceramic. This was done by a hydrometallurgical process in which nickel was precipitated onto YSZ powder using hydrogen in an autoclave. The resulting powders could then be pressed and sintered to make an electrode pellet with the reverse structure to that of PEVD electrodes - a thin metal coating over YSZ. These anodes still require much investigation in order to determine key properties such as conductivity. If the thin metallic coating provides sufficient electronic conductivity through the electrode, then they could be tested in fuel cells. These anodes would have the benefits of near perfect TEC match with the YSZ electrolyte, and a very large surface area for the nickel, which acts as a catalyst. Because the coating on the YSZ powders was not perfect it is expected that contact between YSZ particles would exist and there would be pinholes in the nickel coating so ions can reach the surface to react. The effect of long periods at operating temperature would need to be investigated though as the nickel would likely sinter, since the nickel coating does not adhere perfectly to the YSZ. These types of electrodes could have interesting properties, but there is much work to be done on them still.

References

[1] Grove, Philos. Mag., 141 (1839), p.127

[2] Yamamoto, Electrochimica Acta, 45 (2000), p.2423

[3] Steele, Journal of Materials Science, 36 (2001), p.1053

[4] Primdahl, Mogensen, Journal of Applied Electrochemistry, 30 (2000), p.247

[5] Eds. Heuer, Hobbs, *Science and Technology of Zirconia*, American Ceramic Society, Columbus, 1981

[6] Yang, Tu, Lu, Yong, Wen, Journal of the Australasian Ceramic Society, 34 (1998), p.210

[7] Mori, Yamamoto, Itoh, Abe, Yamamoto, Takeda, Yamamoto, First European Solid Oxide fuel cell Forum Oct. 3-7 1994, Lucerne, Switzerland, v.1, p.465

[8] Donelson, Amarasinghe, Goble, Hickey, Jiang, Love, Quach, Third European Solid Oxide Fuel Cell Forum, 2-5 June 1998, Nantes, France, p.151

[9] Xia, Liu, Solid State Ionics,144 (2001), p.249

[10] Huijsmans, van Berkel, Christie, Journal of Power Sources, 71 (1998), p.107

[11] Maric, Ohara, Fukui, Yoshida, Nishimura, Inagaki, Miura, Journal of the Electrochemical Society, 146 (1999), p.2006

[12] Lobachyov, Richter, Energy Conversion Management, 38 (1997), p.1693

[13] Bradford, *Corrosion Control*, Van Norstrand Reinhold, 1993

[14] Feduska, Isenberg, Journal of Power Sources,10 (1983), p.89

[15] Endo, Fukunaga, Wen, Yamada, Solid State Ionics, 135 (2000), p.353

[16] Steele, Solid State Ionics, 94 (1998), p.239

[17] Fukunaga, Ihara, Sakaki, Yamada, Solid State Ionics, 86-88 (1996), p.1179

[18] Abudala, Ihara, Komiyama, Yamada, Solid State Ionics, 86-88 (1996), p.1203

[19] Tang, Etsell, Ivey, Electrochemical society proceedings, 96-19 (1996), p.71

[20] Itoh, Yamamoto, Mori, Abe, Proceedings of the 4th International Symposium on Solid Oxide Fuel Cells, 1995, p.639

[21] Bawal, Solid State Ionics, 143 (2001), p.39

[22] Brylewski, Nanko, Maruyama, Przybylski, Solid State Ionics, 143 (2001), p.131

[23] Minh, Journal of the American Ceramic Society, 76 (1993), p.563

[24] Kim, Virkar, Fung, Mehta, Singhal, Journal of the Electrochemical Society, 146 (1999), p.69

[25] Siemens Westinghouse website:
http://www.siemenswestinghouse.com/en/fuelcells/sofc/tubular/index.cfm

[26] Fragmund, Charpentier, Schleich, Lunot, De France, New materials for fuel cells and modern battery systems II Proceedings of the 2nd international symposium, 1998, p.119

[27] Godickemeier, Sasaki, Gauckler, Riess, Solid State Ionics, 86-88 (1997), p.691

[28] Feng, Goodenough, European Journal of Solid State Inorganic Chemistry, 31 (1994), p.663

[29] Pasciak, Prociow, Mielcarek, Gornicka, Mazurek, Journal of the European Ceramic Society, 21 (2001), p.1867

[30] Ed.: Tallan, *Electrical conductivity in ceramics and glasses Part B*, Marcel Dekker inc. New York, 1974

[31] Ed.:Subbarao, *Solid Electrolytes and their Applications*, Plenum Press, New York, 1980

[32] Eds.: Claussen, Ruhle, Heuer, *Science and Technology of Zirconia II*, American Ceramic Society, Columbus Ohio, 1984

[33] Kondoh, Kawashima, Kikuchi, Tomii, Ito, Journal of the Electrochemical Society, 145 (1998), p.1527

[34] Barsoum, *Fundamentals of Ceramics*, Mcgraw Hill, 1997

[35] Minh, Takahashi, *Science and Technology of Ceramic Fuel Cells*, Elsevier Science, New York, 1995

[36] Virkar, Chen, Tanner, Kim, Solid State Ionics, 131 (2000), p.189

[37] Kondoh, Kikuchi, Tomii, Ito, Journal of the Electrochemical Society, 145 (1998), p.1536

[38] Kondoh, Kikuchi, Tomii, Ito, Journal of the Electrochemical Society, 145 (1998), p.1550

[39] Yahiro, Eguchi, Eguchi, Arai, Journal of Applied Electrochemistry, 18 (1988), p.527

[40] Tuller, Nowick, Journal of the Electrochemical Society, 122 (1975), p.255

[41] Kudo, Obayashi, Journal of the Electrochemical Society, 123 (1976), p.415

?

[42] Eguchi, Setoguchi, Inoue, Arai, Solid State Ionics, 52 (1992), p.165

[43] Kuseer, Ahmed-khanlou, Hrovat, Holc, Bernik, Kolar, Naoumidis, Tietz, Third European Solid Oxide Fuel Cell Forum, Nantes, France 2-5 June, 1998, p.145

[44] Ed.: Bauccio, *ASM Metals Reference Book Third Edition*, ASM international, Materials Park Ohio, 1993

[45] Godickemeier, Gauckler, Journal of the Electrochemical Society, 145 (1998), p.414

[46] Ishihara, Matsuda, Takita, Journal of the American Chemical Society, 116 (1994), p.3801

[47] Feng, Goodenough, Huang, Milliken, Journal of Power Sources, 63 (1996), p.47

[48] Yamaji, Horita, Ishikawa, Sakai, Yokokawa, Solid State Ionics, 108 (1998), p.415

[49] Yamaji, Negishi, Horita, Sakai, Yokokawa, Solid State Ionics, 135 (2000), p.389

[50] Ed.: van Gool, *Fast Ion Transport in Solids Solid State Batteries and Devices*, North Holland/American Elsevier, 1973

[51] Kim, Virkar, Fung, Mehta, Singhal, Journal of the Electrochemical Society, 146 (1999), p.69

[52] Sasaki, Wurth, Gschwend, Godickemeier, Gauckler, Journal of the Electrochemical Society, 143 (1996), p.530

[53] Yamamoto, Takeda, Kanno, Noda, Solid State Ionics, 22 (1987), p.241

[54] Tsai, Barnett, Solid State Ionics, 93 (1997), p.207

[55] Sasaki, Gauckler, Key Engineering Materials, 169-170 (1999), p.201

[56] Fleig, Journal of Power Sources, 105 (2002), p.228

[57] Kleitz, Petitbon, Solid State Ionics, 92 (1996), p.65

[58] Kenjo, Nishiya, Solid State Ionics, 57 (1992), p.295

[59] Ostergard, Clausen, Bagger, Mogensen, Electrochimica Acta, 40 (1995), p.1971

[60] Juhl, Primdahl, Manon, Mogensen, Journal of Power Sources, 61 (1996), p.173

[61] Van Herle, Ravindranathan Thampi, Journal of Applied Electrochemisrty, 24 (1994), p.970

[62] Kertesz, Riess, Tannhauser, Journal of Solid State Chemisitry, 42 (1982), p.125

[63] Goodenough, Physical Revue, 100 (1955), p.564

[64] Endo, Ihara, Kamiyami, Yamada, Solid State Ionics, 86-88 (1996), p.1191

[65] Van Santen, Jonker, Physica, 16 (1950), p.599

[66] Mori, Hiei, Sammes, Tompsett, Journal of the Electrochemical Society, 147 (2000) p.1295

[67] Stochniol, Syskakis, Naoumidis, Journal of the American Ceramic Society, 78 (1995), p.929

[68] McEvoy, Solid State Ionics, 135 (2000), p.331

[69] Tsiakaras, Marnellos, Athanasion, Stoukides, ten Elshof, Bouwmeester, Verweij, Solid State Ionics, 86-88 (1996), p.1451

[70] Sasaki, Takeda, Kuto, Imanishi, Yamamoto, Hattori, Iio, Esaki, Solid State Ionics, 118 (1999), p.187

[71] Mizusaki, Tabuchi, Matsuura, Yamauchi, Fueki, Journal of the Electrochemical Society, 136 (1989), p.2082

[72] Ohno, Nagata, Sato, Solid State Ionics, 3/4 (1981), p.439

[73] Takeda, Kanno, Noda, Tomida, Yamamoto, Journal of the Electrochemical Society, 134 (1987), p.2656

[74] Ohno, Nagata, Sato, Solid State Ionics, 9/10 (1983), p.1001

[75] Echigoya, Hiratsuka, Suto, Materials Transactions JIM, 30 (1989), 789

[76] Van herle, Ihringer, Vasquez Cavieres, Constantin, Bucheli, Journal of the European Ceramic Society, 21 (2001), p.1855

[77] Uchida, Arisaka, Watanabe, Solid State Ionics, 135 (2000), p.347

[78] Tu, Takeda, Imanishi, Yamamoto, Solid State Ionics, 117 (1999), p.277

[79] Kostogloudis, Tsiniarakis, Ftikos, Solid State Ionics, 135 (2000), p.529

[80] Chen, Nasrallah, Anderson, Proceedings of the 3rd International Symposium on Solid Oxide Fuel Cells, v.4, 1993, p.252

[81] Doshi, Richards, Carter, Wang, Krumpelt, Journal of the Electrochemical Society, 146 (1999), p.1273

[82] Wang, Kato, Nagata, Honda, Kaneko, Iwashita, Dokiya, Solid State Ionics, 146 (2002), p.203

[83] Kim, Kim, Mon, Park, Lee, Kobayashi, Nagai, Kim, Solid State Ionics, 143 (2001), p.379

[84] Koide, Someya, Yoshida, Maruyama, Solid State Ionics, 132 (2000), p.253

[85] Lee, Lee, Lee, Oh, Solid State Ionics, 98 (1997), p.39

[86] Simwonis, Tietz, Stover, Solid State Ionics, 132 (2000), p.241

[87] Fukui, Ohara, Mukai, Electrochemical Solid State Letters, 1 (1998), p.120

[88] Callister, *Materials Science and Engineering an Introduction Third Edition*, John Wiley and Sons Inc., 1994

[89] Skarmoutsos, Tsoga, Naoumidis, Nikolopoulos, Solid State Ionics, 135 (2000), p.439

[90] Aruna, Mutharaman, Patil, Solid State Ionics, 111 (1998), p.45

[91] Setoguchi, Okamoto, Eguchi, Arai, Journal of the Electrochemical Society, 139 (1992), p.2875

[92] Wen, Kato, Fukunaga, Ishitani, Yamada, Journal of the Electrochemical Society, 147 (2000), p.2076

[93] Brown, Primdahl, Mogensen, Journal of the Electrochemical Society, 147 (2000), p.475

[94] Jiang, Ramprakash, Love, Journal of the Australasian Ceramic Society, 34 (1998), p.112

[95] Ringuede, Bronine, Frade, Solid State Ionics, 146 (2002), p.219

[96] Jiang, Badwal, Journal of the Electrochemical Society, 144 (1997), p.3777

[98] Ahmed, Krumpelt, International Journal of Hydrogen Energy, 26 (2001), p.291

[99] Flesch, Meusinger, Naoumidis, Stover, Materials Science Forum, 308-311 (1999), p.788

[100] Ihara, Yokoyama, Abudula, Kato, Komiyama, Yamada, Journal of the Electrochemical Society, 146 (1999), p.2481

[101] Park, Cracium, Vohs, Gorte, Journal of the Electrochemical Society, 146 (1999), p.3603

[102] Hiei, Ishihara, Takita, Solid State Ionics, 86-88 (1998), p.1267

[102] Perry Murray, Tsai, Barnett, Nature, 400 (1999), p.649

[103] Suzuki, Sasaki, Otoshi, Kajimura, Ippomatsu, Solid State Ionics, 62 (1993), p.125

[104] Maric, Ohara, Fukui, Inagaki, Miura, Fujita, Electrochemical and Solid State Letters, 1 (1998), p.201

[105] Mori, Yamamura, Saito, Journal of the American Ceramic Society, 79 (1996), p.3309

[106] Sfeir, Van herle, McEvoy, Third European Solid Oxide Fuel Cell Forum, 2-5 June 1998, Nantes, France, p.267

[107] Pudmich, Boukamp, Gonzalez-Cuenca, Jungen, Zipp, Solid State Ionics, 135 (2000), p.433

[108] Doshi, Alcock, Gunadekaran, Carberry, Journal of Catalysis, 140 (1993), p.557

[109] Wang, Jiang, Zhang, Li, Yan, Lu, Solid State Ionics, 120 (1999), p.75

[110] Primdahl, Hansen, Grahl-Madsen, Larsen, Journal of the Electrochemical Society, 148 (2001), p.A74

[111] Vernoux, Guillodo, Fouletier, Hammou, Solid State Ionics, 135 (2000), p.425

[112] Huang, Feng, Goodenough, Milliken, Journal of the Electrochemical Society, 144 (1997), p. 3620

[113] Ishihara, Shibiyama, Nishiguchi, Takita, Solid State Ionics, 132 (2000), p.209

[114] Huang, Wan, Goodenough, Journal of the Electrochemical Society, 148 (2001), p.A788

[115] Godickemeier, Sasaki, Gauckler, Proceedings of the 4th International Symposium on Solid Oxide Fuel Cells, 1995, p.1072

[116] Shimada, Kumagai, Nagamoto, New Materials for Fuel Cells and Modern Battery Systems II Proceedings of the 2nd International Symposium, 1997, p.783

[117] Yamamoto, Itoh, Mori, Mori, Watanabe, Imanishi, Takeda, Yamamoto, Journal of power sources, 61 (1996), p.219

[118] Kindl, Proceedings of the 17th Riso Interantional Symposium, 1996, p.307

[119] Mori, Itoh, Mori, Abe, Proceedings of the 3rd International Symposium on Solid Oxide Fuel Cells, 1993, p.325

[120] Linderoth, Larsen, Third European Solid Oxide Fuel Cell Forum, 2-5 June 1998, Nantes, France, p.323

[121] Quadakkers, Greiner, Kock, Proceedings of the 1st European Solid Oxide Fuel Cell Forum, 1994, p.525

[122] Quadakkers, Greiner, Hansel, Puttanaik, Khanna, Mallener, Solid State Ionics, 91 (1996), p.55

[123] Kadowaki, Shiomitsu, Matsuda, Nakagawa, Tsuneizumi, Maruyama, Solid State Ionics, 67 (1993), p.65

[124] Dulieu, Cotton, Greiner, Honegger, Schotten, Christie, Seguelong, Third European Solid Oxide Fuel Cell Forum, 2-5 June 1998, Nantes, France, p.447

[125] Stacey, Badwal, Foger, Journal of the Australasian ceramic society, 34 (1998), p.7

[126] Boersma, Sammes, Zhang, Journal of the Australasian Ceramic Society, 34 (1998), p.242

[128] Simner, Stevenson, Journal of Power Sources, 102 (2001), p.310

[129] Pierson, Handbook of Chemical Vapor Deposition, Noyes Publication, New York, 1999

[130] Bryant, Journal of Materials Science, 12 (1977), p.1285

[131] Carlsson, *Advanced Surface Coatings: a Handbook of Surface Engineering*, Blackie & Son Limited, 1991

[132] Jensen, Kern, Thin Film Process II 1991, p.283

[133] Kim, Marzouk, Reucroft, Elevated Temperature Coatings: Science and Technology I, 1995, p.53

[134] de Vries, Lin, de Haart, Burggraaf, Conference on Ceramics in Energy Applications, Sheffield, April, 1990, p.195

[135] Maissel, Glang, *Handbook of Thin Film Technology*, McGraw-Hill, N.Y., 1970

[136] Minet, Langlais, Naslain, Bernard, 6th European Conference on Chemical Vapour Deposition, Jerusalem, Israel, 29 March-3 April, 1987, p.68

[137] Isenberg, Proceedings of the Symposium on Electrode Materials and Processes for Energy Conversion and Storage, Electrochemical Society Proceedings v.77-6 Princeton NJ, 1997, p.572

[138] Meixner, Cutler, Solid State Ionics, 146 (2002), p.273

[139] Hobien, Tietz, Stover, Cekada, Panjan, Journal of the European Ceramic Society, 21 (2001), p.1843

[140] Phillips, Datta, Conference on Ceramics in Energy Applications, Sheffield, April, 1990, p.183

[141] Brinker, Scherer, *Sol-gel Science: The Physics and Chemistry of Sol-gel Processing*, Academic Press, 1990

[142] C.J. Brinker, Ceramic Science and Engineering Proceedings, vol.9, no. 9-10, 1988, p.1103

[143] C.Brinker, A.Hurd, P.Schunk, G.Frye, C.Ashley, Journal of Non-Crystalline Solids, 147-148 (1992), p.424

[144] Nagamoto, Ikewaki, Materials Research Society Symposium Proceedings, v.547 II, 1999, p.333

[145] Xi, Yang, Journal of Materials Science, 31 (1996), p.2697

[146] Martin, Hruschka, Gubler, Gauckler, Journal of the American Ceramic Society, 84 (2001), p.328

[147] Ishihara, Sato, Takita, Journal of the American Ceramic Society, 79 (1996), p.913

[148] Yan, Jiang, Dong, Yu, Li, Journal of the Electrochemical Society, 149 (2002), p.A1132

[149] Mathews, Rabu, Sellar, Muddle, Solid State Ionics, 128 (2000), p.111

[150] Marinsek, Degen, Macek, Key Engineering Materials, 132-136 (1997), p.1365

[151] Simwonis, Thulen, Dias, Naoumidis, Stover, Journal of Materials Processing Technology, 92-93 (1999), p.107

[152] Buchkremer, Diekmann, de Haart, Kabs, Stimming, Stover, Electrochemical Proceedings, 97-18 (1997), p.160

[153] Corbin, Apte, Journal of the American Ceramic Society, 82 (1999), p.1693

[154] Corbin, Zhao-jie, Henein, Apte, Materials science and Engineering A, 262 (1999), p.192

[155] Third, Corbin, Apte, US patent 5,592,686 1997

[156] Reed, *Introduction to the Principles of Ceramic Processing*, John Wiley and Sons, Toronto, 1988

[157] Jiang, Callus, Badwal, Solid State Ionics, 132 (2000), p.1

[158] Wilkenhoner, Mallener, Buchkremer, Hauber, Stimming, 2nd European Solid Oxide Fuel Cell Forum, Orberrohrdorf, Switzerland, 1996, p.279

[159] Wilkenhoner, de Haart, Mallener, Buchkremer, 1996 Fuel Cell Seminar, Nov.17-20, Orlando, Florida, 1996, p.202

[160] Buchkremer, Diekmann, de Haart, Kabs, Nabielek, Stover, Vinke, Journal of the Australasian Ceramic Society, 34 (1998), p.136

[161] Tang, Etsell, Solid State Ionics, 91 (1996), p.213

[162] Tang, Etsell, Ivey, Journal of the American Ceramic Society, 83 (2000), p.1626

[163] Tang, Ivey, Etsell, Materials Research Society Symposium Proceedings v.527, 1998, p.539

[164] Young, Etsell, Solid State Ionics, 135 (2000), p.457

[165] Brown, *Halides of the Transition Metal Elements Halides of the Lanthanides and Actinides*, John Wiley and Sons, New York, 1968

[166] Shalayaev, Yelokhina, Kurkin, Physics of Metals and Metallography, 67 (1989), p.179

[167] Melmed, Journal of Applied Physics, 38 (19670, p.1885

[168] Smithells, *Metals Reference Book 5th Edition*, Butterworths, 1976